ASSESSMENT OF LAND USE LAND COVER CHANGE IN A HIMALAYAN REGION THROUGH INTEGRATED USE OF REMOTE SENSING AND GIS

Thesis Submitted for the Award of the Degree of

DOCTOR OF PHILOSOPHY

in

CIVIL ENGINEERING

By

Nishant Mehra
Registration Number: 41900213

Supervised By

Dr. Janaki Ballav Swain (22747)

Assistant Professor

School of Civil Engineering

Lovely Professional University- Jalandhar

LOVELY PROFESSIONAL UNIVERSITY, PUNJAB
2025

DECLARATION

I, hereby declared that the presented work in the thesis entitled "ASSESSMENT OF LAND USE LAND COVER CHANGE IN A HIMALAYAN REGION THROUGH INTEGRATED USE OF REMOTE SENSING AND GIS" in fulfilment of degree of **Doctor of Philosophy (Ph. D.)** is outcome of research work carried out by me under the supervision of Dr. Janaki Ballav Swain, working as Assistant Professor, in the School of Civil Engineering of Lovely Professional University, Punjab, India. In keeping with general practice of reporting scientific observations, due acknowledgements have been made whenever work described here has been based on findings of other investigator. This work has not been submitted in part or full to any other University or Institute for the award of any degree.

(Signature of Scholar)

Name of the scholar: Nishant Mehra

Registration No.: 41900213

Department/school: School of Civil Engineering

Lovely Professional University,

Punjab, India

CERTIFICATE

This is to certify that the work reported in the Ph. D. thesis entitled "ASSESSMENT OF LAND USE LAND COVER CHANGE IN A HIMALAYAN REGION THROUGH INTEGRATED USE OF REMOTE SENSING AND GIS" submitted in fulfilment of the requirement for the award of the degree of **Doctor of Philosophy (Ph.D.)** in the School of Civil Engineering, is a research work carried out by Nishant Mehra, Registration No. 41900213, is a bonafide record of his original work carried out under my supervision and that no part of thesis has been submitted for any other degree, diploma or equivalent course.

(Signature of Supervisor)

Name of supervisor: Dr Janaki Ballav Swain

Designation: Assistant Professor

Department/School: School of Civil Engineering

University: Lovely Professional University, Punjab, India

ACKNOWLEDGEMENT

At this moment of completion of my Ph.D. dissertation work, I want to thank the Almighty "**LORD SHIVA**", whose divine blessings empowered me to complete this challenging task efficiently.

1 express my most sincere gratitude to my proficient and dynamic Guide, Dr. Janaki Ballav Swain, Assistant Professor, School of Civil Engineering, LPU, Jalandhar, for his affectionate guidance, stupendous support and encouragement. His vast experience and deep understanding of the field proved to be of immense help to me.

I express my heartfelt gratitude to all the faculty members of the School of Civil Engineering, LPU, and Jalandhar for their insightful comments and suggestions in the end-term presentations and for improving the overall technical quality of this thesis.

I want to thank my parents, wife, son and relatives for always being there to encourage and inspire me throughout this journey. Their love, care and motivation gave me the strength to complete the thesis work.

I further extend my deepest regards towards Prof. Krishna Raj, Institute for Social and Economic Change, Bengaluru, India, Dr. Vivek Chauhan, Assistant Professor, NIT, Srinagar and Dr. Harish Kumar Nirala, Assistant Professor, Rajiv Gandhi Government Engineering College, Kangra at Nagrota Bagwan, HP for providing timely suggestions and directions related to the intricacies of Research Methodology. I sincerely thank Mr Sunil Kumar, Research Scholar, CSIR-IHBT, Palampur, HP, for providing the necessary details and information about Remote sensing and GIS. I also extend my sincere thanks to Department of Technical Eductation, Govt. of H.P., for giving me an opportunity to execute this research work.

Finally, I am thankful to all the PhD scholars of my Batch and all those who directly or indirectly helped me during this study.

ABSTRACT

The Himalayan region's cities will grow exponentially in the next two decades. The situation could be challenging owing to seismo-geographical complexities and limited resources in these regions. Population growth and popularity as tourist destinations have led to dispersed, inefficient, and haphazard urban development. Implementing monitoring systems for urban expansion can facilitate the adoption of sustainable development approaches that consider societal and environmental factors equally. The region chosen for the research study is the city of Dharamshala, located in the Western Himalayas and an important tourist and administrative centre of the state of Himachal Pradesh. The city has witnessed notable transformations in the past few decades, especially in the built-up areas. It requires immediate and proactive attention and intervention strategies to address the evolving landscape changes. The research aims to quantify the land cover changes occurring in the region and suggest effective intervention measures to manage and foster resilient and inclusive urban development while preserving the region's natural and cultural assets.

Leveraging geospatial data within a Geographic Information System (GIS) interface holds substantial potential for effectively tracking and quantifying Land Use and Land Cover (LULC) changes, facilitating the formulation of necessary interventions and strategies to achieve a sustainable ecosystem. The integrated use of remote sensing and GIS in the past few decades has increased substantially and has been instrumental in understanding the dynamic changes occurring in land use at a regional or global scale. Remote sensing (RS) and GIS have helped generate LULC thematic maps, which have proven immensely valuable in resource and land-use management, facilitating sustainable development by balancing developmental interests and conservation measures. This has helped to frame the interventions and management strategies to ensure sustainable development.

The availability of free satellite data coupled with open-source GIS platforms has significantly contributed to the progress in LULC change studies. Various studies have focussed on choosing a proper classification algorithm suited for a particular purpose, but choosing proper satellite data has not received attention. The satellite's spatial, temporal, and, most importantly, spectral configuration could have severe implications

for the Land cover classification of a region. The research study utilized three satellite imageries, Sentinel 2, Landsat 8 OLI (Operational Land Imager), and Landsat 7 ETM+ (Enhanced Thematic Mapper) for the research, and the performance of all the satellite imageries was judged based on accuracy metrics. The overall accuracy for Sentinel 2, Landsat 8 OLI, and Landsat 7 ETM+ was 83.40%, 80.06%, and 74.32%, respectively, while Kappa hat was 0.72, 0.65, and 0.53, respectively. The significant variations in the satellite performance show the importance of choosing a proper satellite source for LULC classification studies. The performance of Landsat 8 OLI demonstrated parity to Sentinel 2 with the added advantage of having historical satellite imageries from 2013, enhancing its suitability for remote sensing applications within this context.

The spatio-temporal changes occurring in the region are essential in understanding the complex interactions between the causative factors and/or driving change. A temporal scale of three years was chosen, and LULC maps were obtained for 2016, 2019, and 2022. Traditionally, classification algorithms, such as supervised, unsupervised, hybrid, or machine learning, have been used for land cover classification. The geographical and topographical complexities in Himalayan regions may contribute to the erroneous classification of the land cover, especially when working with satellite data. A simple classification approach could not yield the desired results and necessitates the use of post-classification correction measures. The research utilized an innovative approach involving the use of the Digital Elevation Model (DEM) and the use of Spectral Vegetation indices, like Enhanced Vegetation Index (EVI), Modified Normalized Difference Water Index (MNDWI), and Normalized Difference Built-up index (NDBI) as post classification correction measure. The river drainage network was extracted using the Strahler Order Algorithm. The Maximum Likelihood Classifier (MLC), a Supervised Classification technique, was performed on the three Landsat 8 OLI images for 2016, 2019, and 2022. Five land cover classes, viz. Protected areas, Agricultural areas, built-up areas, barren land, and water bodies were created using the Classification technique. The results indicate that the accuracy of the classified map increased from 75.90% to 93.48%, and kappa khat improved from 0.64 to 0.89 after the post-classification corrections were incorporated. The Producer Accuracy of the agricultural areas and built-up areas increased by 15.3% and 85.8%, respectively, while the User

Accuracy increased by 29.2% and 68.8%, respectively. The findings substantiate the necessity of post-classification correction measures in LULC studies.

The spatio-temporal analysis after adopting post-classification correction measures found that the built-up dynamic index had increased to 23.3% from 2016 to 2022. The built-up growth rate for the study period was found to be 145% for elevations less than and equal to 1000m, 143% for elevations ranging from 1000-1500m, and 119% for elevations greater than 1500m. The built-up growth rate for a distance up to 100 m from the streams was 119% from the year 2016 to 2022. The geospatial risk assessment highlights potential threats in the region due to increased built-up activities, emphasizing the need for prompt intervention by policy-makers, administrators, and environmentalists to advocate for a sustainable development model. The area at an altitude of less than 1500 m remained the most critical, with maximum changes in land use and land cover classes witnessed there. The built-up, agricultural, and protected areas exhibited the highest degree of transition in this region. This transformation can be attributed to improved transportation infrastructure, enhanced road networks, favourable climatic conditions conducive to habitation and agricultural pursuits, burgeoning commercial enterprises, and heightened population density within this geographical expanse.

The modelling and accurate prediction of land cover classes help to understand the complex linkages between spatial patterns and processes responsible for change. The research utilized socio-economic and spatial variables such as slope, elevation, distance from streams, distance from roads, distance from built-up areas, and distance from the centre of town to predict the future land cover classes. The research integrates Artificial Neural Networks with Cellular Automata to forecast and establish potential Land Use changes for 2025 and 2040. Comparison between the predicted and actual Land Use Land cover maps of 2022 indicates high agreement with kappa hat of 0.77 and a percentage of correctness of 86.83%. The study demonstrates that the built-up area will increase by 8.37 km^2 by 2040, reducing 7.08 km^2 and 1.16 km^2 in protected and agricultural areas, respectively. This signifies the impact of anthropogenic and socio-economic activities in the city and the rapid conversion of this hill station into a concrete jungle. The results also indicate widespread encroachments and abeyance of legislation.

TABLE OF CONTENTS

LIST OF TABLES

LIST OF FIGURES

LIST OF ABBREVIATIONS

AA ..... Agricultural areas

ALOS ……Advanced Land Observing Satellite

ANN ..... Artificial Neural Network

ASTER ……. Advanced Spaceborne Thermal Emission and Reflection Radiometer

BA ..... Built-up areas

BL .....Barren Land

CA..... Cellular Automata

CGIAR Consultative Group on International Agricultural Research

DAA. Distance from Agricultural areas

DBA ..... Distance from built-up areas

DEM .....Digital Elevation Model

DOS ..... Dark Object Subtraction

DR .....Distance from roads

DST ..... Distance from streams

DTC .... Distance from the town centre

EL ..... Elevation

ERTS ……... Earth Resource TechnologySatellite

ESA ..... European Space Agency

ETM ..... Enhanced Thematic Mapper

EVI ..... Enhanced Vegetation Index

FCC .....False Color Composite

GCP ..... Ground Control Point

GIS ... Geographic Information System

GLCF ..... Global Land cover Facility

GPS..... Global Positioning System

IRS ....Indian Remote Sensing Satellite

LAC .....Land Absorption Coefficient

LC .....Land Cover

LCR .....Land consumption rate

LIDAR .....Light detection and ranging

LISS Linear Imaging and Self-Scanning Sensor

LST..... Land surface temperature

LU ..... Land use

LULC .....Land use Land cover

MCA ..... Markov Chain Analysis

ML…….....Machine Learning

MLC .Maximum Likelihood Classifier

MLP ..... Multi-layer perceptron

MNDWI …… Modified Normalised Difference Water Index

MSS ..... Multi-Spectral Scanner

NDBI …….....Normalised Difference Built-up index

NDVI……...Normalised Difference Vegetation Index

NDWI……...Normalized Difference Water Index

NRMS…… National Resources Management system

NRSC.National Remote Sensing Centre

OA .....Overall Accuracy

OLI ..... Operational Land Imager

PA .....Protected Areas

PALSAR……. Phased Array Type L-Band Synthetic Aperture Radar

PCA ....Principal Component Analysis

PIF .....Pseudo-invariant features

PrA ..... Producer Accuracy

RS .....Remote Sensing

SCP .... Semi- Automatic classification

SDG ... Sustainable Development Goal

SEM .....Spatially Explicit Models

SL ..... Slope

SOI ..... Survey of India

SRTM …….Shuttle Radar Topographic Mission

TCP ..... Town and Country Planning

TIRS .....Thermal Infra-red sensor

TM .....Thematic Mapper

UA ..... User Accuracy

USGS ……..United States Geological Survey

WB..... Water bodies

CHAPTER 1
INTRODUCTION

1.1 Introduction to LULC change

The development of a region is a continuous and dynamic process. Information about various activities or the factors responsible for change must be available for the region's sustainable development, which may help in the decision-making and implementation of intervention strategies. The socio-economic growth of a region in any developing region has witnessed an increased demand for built-up areas, which in turn has come at the cost of vegetated and barren lands [1]. The various features present on the earth's surface, such as crops, water, barren land, built-up areas, etc., are known as "Land Cover (LC)", and their use by humans for various purposes, be it social, economic, recreational etc. is known as "Land use (LU)"[2]. The unorganised, unsystematic and uncontrolled construction, accompanied by the destruction of wetlands, loss of agricultural land, degrading air quality, and changes in wildlife habitat, are some of the problems witnessed in developing regions, which requires a holistic approach and knowledge of Land use Land cover (LULC) change. For better land management, information about the current land use patterns and the changes happening temporally must be available [3]. The remote sensing data can help understand the environmental process, especially when studying the patterns and changes occurring in the regions [4]. However, for a detailed analysis, it is also necessary to use a modern tool that can deal with spatio-temporal data and help analyse them so that the information can be used to implement land management practices better [5]. A Geographic Information System (GIS) is a platform that can help analyse spatio-temporal changes. The thematic information derived from Remote Sensing (RS) data, usually LULC classification, can be used as an input in the GIS for further analysis. The LC change has modified the micro and macro ecosystems and contributed significantly to climate change. The use of Remote sensing and GIS has proven to be a robust, efficient, and cost-effective solution for understanding the complex interactions between factors affecting these changes and the physical environment [6–8], which can lead to framing of the management/ intervention strategies promptly [9–11].

The quality of thematic maps should be good such that the actual LC on the ground is represented and accurate information on the transitions can be obtained [3]. Urban sprawl has become a significant challenge and concern for developing countries, and Himalayan regions pose more complexities because of the geographical, topographical, and seismic constraints [12–14]. Landscape heterogeneity and similar spatial characteristics of LULC classes are other significant challenges typical of Himalayan regions [15–18]. The classification approach applicable to one region can't be used as such in a different region because of the spatial heterogeneity in areas [19,20]. Each region is different in terms of geographical, topographical or soil conditions. The complexities are increasing in Himalayan regions as the issues of seismicity, landslides, and topography also become essential for land use management [21,22]. The rapid urbanisation and growing population have been a cause of concern in the cities of the Himalayan regions. The anthropogenic activities have resulted in increased built-up activities and a rapid decrease in vegetated or forested areas [17,18,23,24]. The call for sustainable development is getting more and more louder.

The availability of free data sets from various satellites has allowed the researchers to study the changes from a remote place, provided they have the necessary resources in the form of hardware and software. Landsat data is entirely free and can be downloaded from **https://earthexplorer.usgs.gov/**. Sentinel data is also free and is one of the most widely used data sources. However, any particular satellite data usage depends on many factors, not just limited to spectral, spatial, temporal and radiometric resolution [25,26]. The remote sensing data allows one to remotely interpret the phenomenon or changes/ transformations occurring in a particular area or region [2]. Free Landsat satellite data has been available since 1972, when a Multi-Spectral Scanner (MSS) was used, and four bands were available, which provided a relative advantage over other satellite data products for extensive temporal studies. There have been many improvements in the sensors thereafter. Finer spatial, temporal, spectral, and radiometric resolutions are available, improving the observation, interpretation, and analysis of changes occurring in the land masses. As per the information available from the United States Geological Survey (USGS), Landsat 1 satellite, launched in the year 1972, earlier known as the

Earth Resource Technology Satellite (ERTS) program, had only four bands (Red, green and 2 Infra-Red) and spatial resolution of 80m; while Landsat 8 launched in the year 2013 had nine bands and spatial resolution of 30m is available.

Landmasses generally show different spectral signatures when viewed through different Electromagnetic spectrum wavelengths. Typically, the Optical spectrum, which includes UV, visible, IR and thermal IR wavelengths, falling in the range of 0.3 to 14 μm, is commonly used for determining land features. Hyperspectral sensing, however, involves various bands in other regions of the Electromagnetic spectrum. But, before the images can be used for further image analysis, the related errors arising from atmospheric disturbances need to be corrected for atmospheric, topological and sun angle corrections. Such features are already available in the commonly used software for image classification, such as ERDAS Imagine, ENVI and Q-GIS. Also, to interpret the changes, it is equally essential that the images obtained from datasets are geo-referenced or converted into a geographic coordinate system from a geometric coordinate system, which requires accurate latitudes and longitudes of Ground control point (GCP). These ground control points must be easily distinguishable in the image, and the Global Positioning System (GPS) could be used to determine the latitude and longitude of the point in the actual site. It needs to be ensured that such GCPs are distributed throughout the image for accurate geographic registration of the images.

1.2 LULC Classification Scheme

The LULC change dynamics are essential for understanding the trend and direction of urban sprawl [27]. The increase in population coupled with anthropogenic activities [28,29] has resulted in urban sprawl, characterized by the rapid expansion of cities and towns into previously undeveloped areas [30–32]. The integrated use of Remote Sensing [RS] and GIS has helped researchers and policymakers identify urban expansion patterns, assess the impact of anthropogenic activities on the environment, and develop sustainable policies and strategies for the region [5,33–35].

The Anderson Land Use Land Cover Classification System, developed by the U.S. Geological Survey (USGS), is a widely applied framework for systematically

categorizing and mapping land cover and land use. It offers a standardized approach to delineate various land cover and land use types, serving diverse purposes, including environmental monitoring, urban planning, and natural resource management.

This classification system comprises multiple hierarchical levels, commencing with Level I, which encompasses overarching categories, and progressing to more refined levels with increased granularity up to Level IV. Level I encompasses significant land cover types such as water bodies, forests, agricultural land, and urban areas. Subsequent levels offer more detailed classifications within each broader category. **Fig. 1.1** shows the Anderson LULC system in the Level I and Level II categories, which is extensively used in remote sensing. The USGS classification system allows for more detailed land use and land cover categorisation at Levels III and IV, which are particularly useful for regional, county, or local planning purposes. While Levels I and II offer nationwide, interstate, or state-wide analysis, Levels III and IV provide finer resolution tailored to specific regions. Local users can design categories for Levels III and IV, ensuring they aggregate into higher-level categories. Mapping at these levels often requires additional supplemental information beyond imagery, with a resolution of 1 to 5 meters (Level III) or finer (Level IV) being suitable. Aerial photographs and high-resolution satellite data are commonly used for this purpose. For example, the Built-up area in Level I may be further classified into Residential, Commercial, Industrial, etc., in Level II and Residential may be further classified into Single-family, multi-family, group quarters, others, etc. in Level III. The urban sprawl analysis generally incorporates Level I Classification, while the vegetation studies usually incorporate Level II Classification.

The urban sprawl analysis generally incorporates Level I Classification, while the vegetation studies usually incorporate Level II Classification. Most of the LULC studies have been carried out by the researchers using Anderson Level-I classification.

Level I	Level II
1 Urban or built-up land	11 Residential
	12 Commercial and service
	13 Industrial
	14 Transportation, communications, and utilities
	15 Industrial and commercial complexes
	16 Mixed urban or built-up land
	17 Other urban or built-up land
2 Agricultural land	21 Cropland and pasture
	22 Orchards, groves, vineyards, nurseries, and ornamental horticultural areas
	23 Confined feeding operations
	24 Other agricultural land
3 Rangeland	31 Herbaceous rangeland
	32 Shrub and brush rangeland
	33 Mixed rangeland
4 Forest land	41 Deciduous forest land
	42 Evergreen forest land
	43 Mixed forest land
5 Water	51 Streams and canals
	52 Lakes
	53 Reservoirs
	54 Bays and estuaries
6 Wetland	61 Forested wetland
	62 Nonforested wetland
7 Barren land	71 Dry salt flats
	72 Beaches
	73 Sandy areas other than beaches
	74 Bare exposed rock
	75 Strip mines, quarries, and gravel pits
	76 Transitional areas
	77 Mixed barren land
8 Tundra	81 Shrub and brush tundra
	82 Herbaceous tundra
	83 Bare ground tundra
	84 Wet tundra
	85 Mixed tundra
9 Perennial snow or ice	91 Perennial snowfields
	92 Glaciers

Fig. 1.1 LULC classification Scheme for use with RS data [2]

1.3 LULC Classification Algorithm and Error Matrix

Image classification combines pre-installed algorithms with the expertise of the interpreter. Various techniques are employed, including those that compare spectral responses across different timeframes and others that assess the spatial proximity of

pixels [2]. However, different classification systems can yield diverse land classification outcomes, even with similar input data [36]. The effectiveness of any algorithm depends on the specific scope and objectives of the research study, as well as the available resources. LULC classification is thus a synergistic blend of artistic interpretation and scientific methodology.

Supervised and *unsupervised classification* methods have been widely used in RS and GIS. The difference between the classification procedure adopted lies in the fact that in supervised classification, the training sites are selected and land types identified *priori* to the classification of the test sites, while in unsupervised classification, the clusters are formed by the algorithm itself based on spectral characteristics and then land class types identified by the classifier.

Maximum Likelihood Classifier (MLC) has been widely used as a supervised classification algorithm for LULC identification and classification [6,17,30,33]. The algorithm works on the Bayes theorem and uses class mean vectors and covariance matrix as the inputs for classification, with the pixel being assigned to a particular class having the highest probability [37,38]. The MLC considers the variance-covariance in a specific land use class and assumes normally distributed data. The performance is better than other parametric classifiers [39,40].

On completion of the LULC classification, its accuracy must be judged. Accuracy assessment for a classified map is vital to substantiate the appropriateness and usefulness of the classified thematic map [2,3]. Error matrix and kappa-hat are widely used parameters for accurately assessing classified thematic maps [7,41]. Error matrix compares the classification of ground points (reference points) with the test points, and the results are presented in tabular form. The reference data is presented as columns and classification data as rows in the error matrix, with the total of columns under each class category showing the actual number of that class type while the total of rows showing the number of class types identified by the classifier. Error matrix is represented in the matrix form wherein the number of sample units assigned to a particular class in a classified map is expressed relative to the number of sample units assigned to a specific class in reference classification [2].

The overall accuracy (OA) is computed using diagonal elements of the error matrix, while the non-diagonal elements correspond to errors of omission and commission [2]. Accuracy metrics, Producer Accuracy (PrA), and User Accuracy (UA) can provide greater detail related to individual classified land cover by including these errors. PA represents the errors of omission and states how well the test pixels are classified in a land cover map. UA represents the errors of commission and indicates the probability of whether a pixel being assigned a land cover type in a classified map is represented accurately on the ground.

However, the error matrix does not confirm the accuracy as it extracts the statistics from the results and tells the homogeneity of classes chosen (reference points) and identified by the classifier [41]**.** To measure whether the accuracy is by chance or actual, Kappa-hat, also known as kappa statistics, is used, the value of which measures between 0 and 1. A higher value denotes a true agreement, and a value approaching 0 represents chance agreement.

Kappa-hat is a good indicator for measuring the percentage of correct values of an error matrix due to a "true" agreement versus a "chance" agreement [1]. [7] used **Table 1.1** for rating the Kappa-hat according to their values.

Table 1.1 Rating Criteria of Kappa- hat

S. No	Kappa-hat	Strength of agreement
1	0.41 - 0.60	Moderate
2	0.61 - 0.80	Substantial
3	0.81 - 1.00	Almost perfect

The sample design is an essential aspect of accuracy assessment [41,42]. The following formula (i) was used to determine the sample size.

$$n = \frac{[\sum Wi\ Si]^2}{[S[\hat{o}]]^2 + (1/N)\sum Wi\ Si^2} \qquad \text{.....(i)}$$

n= number of pixels in the study area, S[ô] is the standard error of estimated overall accuracy that is supposed to be achieved

i = number of class types, 4 in this case.

W_i is the mapped proportion of the area of each of the four classes, and Si is the standard deviation of each of the four classes. Si = $\sqrt{U\text{i}\,[1 - Ui]}$

1.4 Post-Classification correction approaches

The RS data embedded in the GIS interface offers a reliable and cost-effective approach in Himalayan regions, especially the inaccessible and far-flung areas [43]. However, the automatic digital classification techniques provide more challenges in the hilly areas characterized by rugged topography, cloud cover, narrow valleys, mixed spectral characteristics, and shadows [24,44]. All these factors limit the accuracy of the thematic map and, thus, restrict its applicability. Therefore, it becomes imperative that data from multiple sources be included in the classification approach. The mountainous regions offer more complexities in decoding the thematic features using the remote sensing data [13,18,44,45] in digital image analysis, as streams, built-up areas and rocky mountains may be classified as a single land cover type. Further, the shadow areas also pose a challenge to the classifiers, and thus, the use of ancillary data like the Digital Elevation Model (DEM) becomes all-important in Himalayan regions [43,46].

Post-classification accuracy measures are essential in improving the accuracy metrics. Ancillary data can support the post-classification correction measures [47,48]. The performance of MLC is not satisfactory with the data, which is not normally distributed [40]. However, research has shown that using ancillary data to support MLC can improve classification accuracy [30,47,49,50]. [51] performed MLC on satellite images and assisted with Survey of India topo-sheets to classify seven land cover classes, achieving higher accuracy. Ancillary data in the form of Digital (DEM has also been integrated with the classification algorithm to improve the classification accuracy [18,32,52,53]. [46] in his research in Nepal found that including DEM as one of the component bands during image classification substantially improves accuracy.

The spatial information, like slope, aspect, elevation, etc., can be used to create a conditional raster for better land cover classification. The river networks in Himalayan regions are generally characterized by the presence of boulders, rocks, and cobbles

[54,55], and thus, their misclassification with built-up areas is very probable [47]. DEM can also be used for drainage network generation through Strahler Stream order in GIS [56,57]. [58] devised a system assigning orders to a stream network while moving from the catchment boundary towards the outlet. Strahler's stream order in GIS has been efficiently used to derive the drainage networks of streams [59–61].

The Himalayan regions offer more complexity than other flat regions of India. The spectral characteristics of non-vegetated areas, rivers, and built-up areas may overlap in these regions, and thus, the simple classification algorithms may not be suited for this purpose. Post-classification correction measures involving creating a mask for each land cover type can be constructive in the accurate land cover classifications [62]. Due to the overlapping spectral characteristics of built-up areas and streams, the Strahler order algorithm available in SAGA was used to delineate the rivers accurately.

Spectral vegetation indices and the Digital Elevation model greatly help classify the areas more accurately. Enhanced Vegetation Index (EVI) is more robust as compared to the Normalised Difference Vegetation Index (NDVI) in minimizing the biases resulting from canopy background and aerosol variations [63–65]. The satellite images were chosen for November, and they were characterised by crops of low height in agricultural areas. By carefully selecting threshold values for EVI, it is possible to generate a forest mask that effectively distinguishes densely vegetated areas from those with lower vegetation density and is used to separate Protected Areas from Agricultural Areas. Modified Normalised Difference Water Index (MNDWI) is handy in removing built-up noises [66] when applied to open water areas and can be used advantageously to mask built-up areas. [67] proposed the Normalised Difference Built-up Index (NDBI) while studying the built-up areas in Nanjing, China and achieved an accuracy of 92.6% in classifying built-up areas. Three spectral vegetation indices, EVI, NDBI, and MNDWI, were used to improve the overall accuracy of the classified map resulting from unsupervised classification. These parameters were calculated using eq (ii), (iii), and (iv) respectively.

$$EVI = 2.5 * \frac{NIR - R}{L + NIR + C1 * R - C2 * B} \qquad \text{.....(ii)}$$

$$NDBI = \frac{MIR-NIR}{MIR+NIR} \quad \text{.....(iii)}$$

and

$$MNDWI = \frac{G-MIR}{G+MIR} \quad \text{.....(iv)}$$

NIR = Near Infrared Band

MIR = Mid Infrared Band

R = Red Band

B = Blue Band

G = Green Band

L is the soil adjustment factor, C1 and C2 are the aerosols resistance weights (L = 1, C1= 6, and C2 =7.5)

The field visits, Google Earth imagery, and knowledge of the study area were helpful in the validation of classified data products.

The drainage patterns of rivers remain camouflaged under the thick vegetation cover and represent a great challenge in identifying riverine sources [24]. Further, the morphological characteristics of high-altitude rivers, characterized by the presence of boulders and cobbles, closely resemble the built-up areas and increase the complexity of the classification algorithm to predict the class type accurately. Thus, using DEM to obtain stream networks can immensely help obtain the rivers' drainage patterns. The research done by [58], [61], [68] and [69] can give insights into the criteria used by algorithms to calculate drainage patterns. Different researchers have incorporated this method to derive the drainage networks of the rivers [14,61]. This approach can be beneficial for correctly classifying the water bodies in Himalayan regions.

Another challenge in Himalayan regions is the mixed spectral characteristics of built-up and agricultural areas. The band ratio method, MNDWI, can suppress built-up areas from a region [70]. Thus, with other band ratio methods, NDBI can separate built-up features and agricultural areas [67].

1.5 LULC prediction and intervention strategies

The Population projection indicates that Central and South Asia will likely become the world's most populous region by 2037 [71]. India has overtaken China to become the most populated country, and the demographic trend is anticipated to continue for several decades. The immediate developmental pressures accompanied by pressing built-up demand have increased the population, catapulting LULC changes [72–74].

The notable features of urban sprawl involve a decline in plantation areas [17,33], unsystematic and irregular expansion spatially [75,76], developmental pressures in higher elevations [18,77,78], change in agricultural practices [44,52,79,80], and upsurge in urban heat island [81–83]. The urban sprawl has resulted in socioeconomic and cultural challenges [76]. The spatio-temporal changes in the hilly areas require special attention due to the landscape, geological, and seismic factors [17,18,43,84]. Thus, monitoring and precise prognostication of LULC transformations is vital for implementing safe and sustainable development practices in the Himalayan cities [85]. The integrated use of RS and GIS has helped immensely in developing a framework of sustainable management practices and understanding the intricacies between patterns and the processes driving the changes [17,47,86,87]. The simulation and development of future maps have been gaining the attention of the research community [88,89]. Modern Self-Learning algorithms have further improved the accuracy of these simulation models [34,90–92]. Understanding dynamic changes occurring in the region and incorporating driving factors can help in simulation capabilities [89].

Cellular Automata (CA) based models are spatially explicit models (SEM) in which the future state of a LULC category relies on the past local interactions between LULC categories [85,89]. The model's popularity in GIS grew immensely in the 1980s, catalyzed by pivotal contributions from [93], [94] and [95]. The model's accuracy depended upon the spatio-temporal data, the LULC category in the adjacent cells, and transition rules [96,97]. [95], [98] and [99] demonstrated their application as a robust spatial dynamic model. The open structure, simplicity, good spatial resolution, and integration feature render it suitable for urban sprawl studies [85,89,96,100]. Since the model only considers spatial attributes, it has an inherent disadvantage of not including socio-economic variables, limiting the simulation and prediction capabilities [85,89].

The non-uniform cell space, dynamic neighbourhood classes, and non-stationary transition rules present avenues for adapting the original CA framework to facilitate real-time investigations into complex urban sprawl dynamics [85,96]. Consequently, integrating CA with other models becomes imperative to capture the nuanced dynamics of urban sprawl effectively.

To mitigate the limitations inherent in stand-alone models, researchers have adopted hybrid approaches, like the CA-Markov Model [101] and the CA-ANN model [102] to synergise the strength of different models. Incorporating spatial patterns with the mechanisms inducing changes in LULC categories is vital for precise simulation and forecasting of LULC maps [87]. Artificial Neural Network (ANN) possess the ability to discern and analyze the intricate interplay among driving factors and induced changes [89,103]. ANN's architecture simulates and behaves similarly to the human brain and nervous system [104–106]. ANN can deal with incomplete data, does not assume input data distribution, and can detect interlinkages between spatial and socio-economic variables [107,108]. Multi-layer perceptron (MLP)- ANN, comprising input, hidden and output layers, is among the prevalent models in ANN due to its rapidity, precision and capability to predict outcomes from stochastic events. Thus, it exhibits the fidelity and realism of modelling for precise forecasting and assessment of LULC transitions [109]. Researchers have utilized CA-ANN models to tackle spatial-dynamic changes and incorporated the driving factors responsible for these changes, enabling precise prediction and assessment of LULC changes [8,82,100,103,110].

The study endeavours to employ MLP-ANN and CA simulation methodologies to simulate LULC changes in Dharamshala, an expeditiously expanding city in Himachal Pradesh, India. Anticipated outcomes are poised to assist urban planners and policy-makers in implementing a strategic framework built on a sustainable development model. Utilizing LULC maps from 2016 and 2019, the model seeks to simulate and validate the LULC map for 2022, subsequently extrapolating projections for future LULC maps of 2025 and 2040.

1.6 Motivation

The city of Dharamshala has been designated as a renowned hill station. It serves as the state's winter capital and headquarters of the Central Tibetan Administration, attracting

domestic and international visitors. Additionally, it functions as the administrative seat of Kangra district, housing various governmental offices. Following its declaration as a Municipal Corporation in 2015, Dharamshala underwent rapid urbanization, facilitated by the amalgamation of nine adjacent villages. Notably, it was selected as one of the 100 cities in India and the sole representative from Himachal Pradesh for development under the National Smart Cities Mission initiated by the Government of India in 2016.

A notable surge in urban expansion has been observed within the city since 2016, prompting a compelling need to scrutinize the recent transformations within this geographical region through a scientific framework. The selection of 2016 as the study's baseline year symbolizes the onset and manifestation of socio-economic shifts within the city, attributed to the establishment of Municipal Limits, the hosting of international cricket matches, and its significance as the residence of His Holiness the Dalai Lama.

Being a popular tourist destination, the city has witnessed remarkable changes in the areal extent (urban sprawl) and land cover changes, especially in built-up areas [23]. The unplanned development in the region [45], mixed with rugged topography, seismicity, and increasing population, offers a complex problem to urban planners, which requires immediate attention and the adoption of management strategies. The research study is aimed at addressing these concerns.

1.7 Contribution of the study

Comparison of satellite imagery on a global/regional scale with the coarser spatial resolution is well-documented [111–115]. The results have shown inconsistent classification results since they were produced from different satellite sources and/or the researchers adopted different class definitions. [116] compared the results of Digital Elevation Models from three different sources of different resolutions, finding the maximum basin delineation error in a finer spatial resolution data source. For the comparison of classified products, the aggregation of different data products (having different spatial resolutions) into a uniform spatial scale may involve the use of statistical measures, which may cause inconsistencies in classifying land cover types [117,118]. [36], [80] and [119–123] discussed various classification algorithms and change detection analysis techniques adeptly used in optical remote sensing. Due to the

availability of free remotely sensed data products, the suitability of remote sensing data from different satellites also needs to be compared, and the best-performing satellite data need to be chosen for further analysis, be it change detection studies or simulation of future land cover types. Thus, the study contributes to the existing knowledge by providing insight into the importance of satellite data-products before LULC classification. This adds to the existing knowledge and shall contribute to the research community.

The study also tries to measure the trend and direction of LULC transitions occurring in Dharamshala city and predict the future LULC classes. The same will help to understand the complex spatio-temporal dynamics occurring in the region and propose intervention strategies for optimum utilisation of resources based on the Sustainable development model. This will be the contribution of the proposed research work on society and nature.

1.8 Research Objectives

The research aimed to identify LULC changes in Dharamshala, as shown in **Fig. 1.2**, located in Himachal Pradesh, India. The study area is a part of the Lesser Western Himalayan range, covering an area of 42.5 km^2. The research locale lies between latitudes 32°9’52” N to 32°15’58” N and longitudes 76°17’22” E to 76°23’09” E. The topographic relief exhibits substantial variation, spanning from an altitude of 790 meters in the southwestern sector to 2130 meters above mean sea level (AMSL) in the northern expanse of the territory. During winter, the northern part of the region experiences moderate to heavy snowfall.

The city encounters a moderate mean annual temperature of approximately 19.1 ± 0.5°C. June emerges as the warmest month, registering a peak average temperature of 32°C, while January represents the coldest month, recording a minimum average temperature of 10°C [21] — furthermore, the annual precipitation averages around 2900 mm, contributing to its relatively wet climate.

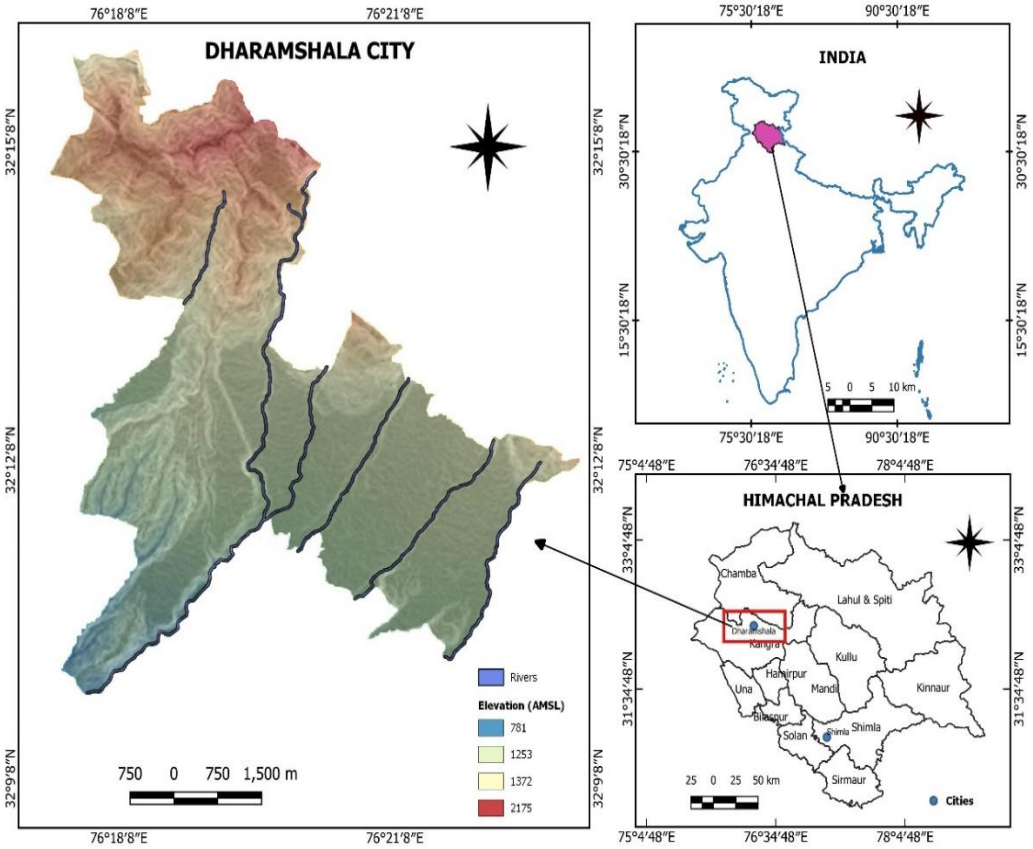

Fig. 1.2 Study area, the city of Dharamshala

Land use records from 2016 reveal that more than half of the area is covered under forests. The dominant soil order, as per USDA soil taxonomy, is Alfisols, primarily due to the extensive forest cover in the region. The city of Dharamshala exhibits diverse topographical and climatic characteristics, with significant variations in elevation, temperature, and precipitation. Its substantial forest coverage and prevalence of Alfisols highlight the importance of understanding the ecological dynamics and implications for land management and environmental conservation in this region.

The city serves as the winter capital of Himachal Pradesh and hosts the Central Tibetan Administration. Renowned as a sought-after hill station, it attracts tourists from across the nation and around the globe. Additionally, it acts as the administrative centre for Kangra district of the sate of Himachal Pradesh. In 2015, the city attained Municipal Corporation status through the amalgamation of nine adjacent villages, marking the

onset of rapid urbanization. Selected in 2016 as the sole representative from Himachal Pradesh, it joined the National Smart Cities Mission initiated by the Indian Government. However, the region faces challenges stemming from haphazard development, compounded by its rugged terrain, seismic activity, and burgeoning population. Addressing these issues necessitates urgent attention and the implementation of effective intervention strategies [45].

Since 2016, the city has experienced a significant surge in urban development, prompting a pressing need to analyze recent changes in the area from a scientific perspective. The study's chosen time-frame of 2016 aligns with a period marked by substantial socio-economic transformations, including the establishment of Municipal Limits, an international cricket ground, and the presence of His Holiness the Dalai Lama's residence.

The objectives of the research study are summarized below:-

1. To analyse the accuracy of land use land cover classification using Multi-temporal and Multi–sensor satellite images for urban land use mapping.
2. To quantify the dynamics of ‘change detection’ at the spatio-temporal scale in a non-stationary set up.
3. To predict the impact of land use change in future along with the identification and quantification of driving factors responsible for it.

1.9 Organisation of the Thesis

The research study covers three crucial aspects signifying the three objectives of the proposed work.

a) Comparison of satellite data products.

b) Spatio-temporal LULC transitions from 2016 to 2022.

c) Modelling and simulation of LULC maps.

The entire thesis has been organised into six Chapters. The first Chapter is the Introduction, as elucidated above. The organisation of the thesis into the other five chapters is mentioned below in the following sub-sections.

1.9.1 Chapter 2: Review of Literature

The review of literature has been divided into four distinct sections that depict the design and workflow of the proposed work. Section 2.1 covers Digital Image analysis and geo-spatial data, 2.2 LULC change studies and assessment of driving factors, 2.3 Post-classification corrections and integration of remote sensing data, and 2.4 Modelling and simulation of LULC change. Based on the review of the Literature, three research objectives were identified for the research area.

1.9.2 Chapter 3: Methods and Materials

Chapter 3 includes the design methodology for the proposed research work. The design methodology for the three objectives chosen for the study has been elucidated in the sub-sections of this Chapter. 3.2.1 incorporates Objective 1, i.e. comparison of satellite data products. 3.2.2 includes Spatio-temporal LULC transitions from 2016 to 2022, and 3.2.3 includes Modelling and simulation of future LULC maps for 2025 and 2040.

1.9.3 Chapter 4: Results and Discussion

Chapter 4 covers the results from the three objectives. A detailed discussion of the findings from the three objectives has been summarised in the three sections of Chapter 4. The suitability of satellite data for a particular research study has been justified in Section 4.1. The LULC transitions and geo-spatial analysis of the region under study from 2016 to 2022 have been performed in Section 4.2. The LULC maps for 2025 and 2040 were predicted, and the trend of further city expansion has been discussed in Section 4.3.

1.9.4 Chapter 5: Conclusion

Sections 5.1, 5.2 and 5.3 present the conclusion from the three objectives chosen for the research study. Section 5.4 presents the proposed intervention strategies that will help environmentalists, policy-makers, and administrators balance the needs and conservation of resources in alignment with the Sustainable Development Goals (SDG).

CHAPTER 2
REVIEW OF LITERATURE

The literature review is essential in establishing the contextual framework, identifying research gaps, and presenting the research design. It serves as the foundation upon which new research is built, ensuring scientific rigour and relevance. It helps the researchers to synthesize existing findings, validate hypotheses, and refine research questions. Additionally, it enables the identification of methodologies, theoretical frameworks, and analytical techniques employed in similar studies, facilitating informed decision-making during the research process.

A comprehensive literature review demonstrates scholarly competence and contributes to the advancement of scientific knowledge by situating the research within the broader academic discourse. Thus, integrating a thorough literature review is imperative for the thesis's credibility, validity, and scholarly impact.

In the thesis, the literature review has been presented in tabulated form. The review has been organised into four Sections: **2.1** Digital image analysis and geo-spatial data, **2.2** LULC change studies and assessment of driving factors, **2.3** Post Classification corrections and integration of remote sensing data, and **2.4** Modelling and Simulation of LULC changes.

2.1 Digital image analysis and geo-spatial data

S. No.	Name of author (s) & Year	Data source/ Data inventory	Instrument used	Abstract/ Findings
2.1.1	John F. O Callaghan (1984)	- United States Geological Survey (USGS)	- Gestalt Photomapper II	- [124] presented a methodology, D-8, for extracting drainage network from digital elevation data, working on the premises of movement of water from higher to lower elevation. - The algorithm consisted of a series of steps, including identifying the outlet points, delineating the catchment areas, and determining the stream network - Useful for studying hydrology, erosion, and other related fields. Three test areas were used in the study to represent different terrain types. - The authors noted that the proposed method is computationally efficient and produced accurate results, making it suitable for large-scale studies

2.1.2	Ashbindu Singh (1989)	- USGS	- Landsat Multi-Spectral Scanner (MSS)	- [36] reviewed various change detection techniques and suggested that registering images and selecting threshold values were essential for accurately classifying images. - Pre-processing of the image, such as edge enhancement or image soothing, didn't improve classification accuracy. - The researcher opined developing those techniques that don't require image registration.
2.1.3	Yong Du et al. (2002)	- USGS	- Landsat 5 Thematic Mapper (TM)	- [125] selected three Landsat images from 1986, 1987, and 1991 and performed relative radiometric correction using Pseudo-invariant features (PIF). Quality control measures improved their accuracy. - Quality control measures for the selection of PIFs included removal of cloudy pixels, threshold values or a range defined based on PCA and removal of PIFs breaching those selected / defined ranges.

				- After radiometric correction, NDVI was calculated for the chosen periods, wherein a patch of fire could be easily discerned, and the recovery of the same in different time-period could also be observed.
2.1.4	Sumira Nazir Zaz and Shakil Ahmad Romshoo (2012)	- USGS - Geological Map of India - Earthdata - Soil field data	- Landsat TM and Landsat ETM (Enchanced Thematic Mapper) - Shuttle Radar Topographic Mission (SRTM) - DEM	- [126] studied land degradation in the Kashmir valley from 1992 to 2001. and 80 Ground Control Points (GCPs) were chosen, and Root mean squared error (RMSE) was achieved equal to one pixel. - MLC was used for classification into five land use land cover classes based on National Resources Management system (NRMS) standards. - Slope classified as flat 0-3%, gentle 3–15 %, moderate 15–25 %, steep 25–35 % and very steep >35. - NDVI was used for assessing the amount of vegetation in the region, and Kappa was used for accuracy assessment.

2.1.5	Brijesh Kumar et al. (2017)	- Consultative Group on International Agricultural Research (CGIAR) - Intergraph - USGS -Ganga Flood Control Commission - Google Earth	- SRTM 90m - SRTM 30m -Advanced Spaceborne Thermal Emission and Reflection Radiometer (ASTER) 30m	- [116] evaluated the acceptability and the significance of adequate resolution of datasets from different satellites. - The results were compared with the digitized river network derived from Google Earth and basin boundary digitized using Ganga Flood Control Commission map. - It was concluded that the automatic delineation model overestimated the basin area in flat slopes while underestimating the area in steep slopes. - The performance of lesser spatial resolution of SRTM 90m was found to be the best, and the delineation error was found to be significant for the high spatial resolution DEMs.
2.1.6	Cláudia M. Viana et al. (2019)	- USGS	- Landsat 5 TM - Landsat 8 OLI	- [127] demonstrated a methodology to use RS and GIS to study urban sprawl in Beja, south-eastern Portugal, covering an area of 12 km^2 using spectral indices.

				- The study demonstrated monitoring, measuring and simulating urban sprawl and identifying biophysical and socio-economic factors. - The research study found that Ecosystem function and structure had been disturbed based on the demands and satisfaction of humans, resulting in vulnerability associated with places, people, economic dynamics and climate.
2.1.7	Naghmeh Nazarnia et al. (2019)	- Geospatial data used for the creation of buffer zones, six in number.	- NIL	- [128] described urban sprawl as a phenomenon visually perceived in the landscape. - Reasoned that urban sprawl has three dimensions: built-up area (amount), its dispersion in the landscape (spatial configuration) and the utilization of area per inhabitant or job. - The choice of the city's urban centre holds considerable ramifications for accurate quantification of urban transformations.

2.1.8	Prabuddh Kumar Mishra et al. (2019)	- Copernicus (European Space Agency, ESA) - USGS - Topographical Map (Survey of India, SOI)	- Sentinel 2A - Landsat 5 TM - ASTER DEM	- [23] conducted the study in the Rani Khola watershed of Sikkim state lying in Eastern Himalayas using Landsat imagery for 1988, 1996 and 2008 and Sentinel imagery for 2017. - Image pre-processing achieved using the SCP plugin in QGIS - Re-sampling of 10 m Sentinel imagery into 30m satellite imagery. MLC was used for classification, and accuracy was assessed using 3.9 m spatial resolution Planet Scope with 300 stratified random points. - Found that the dense forests had increased in the study area due to massive afforestation programmes and stringent law enforcement in the hill state.
2.1.9	K. Dhanaraj and Dasharatha P. Angadi (2020)	- USGS -Topographical Map (SOI)	- Landsat MSS, TM, ETM^{+} and Operational Land Imager (OLI)-	- [129] studied the urban growth dynamics in Mangaluru, Karnataka, using change detection and spatial trend analysis.

		- Demographic data from the Census of India Handbook - Field observation	Thermal Infra-red sensor (TIRS)	- RS images chosen depended upon availability, cloud-free conditions, and the season the features were exposed to maximum. - The radiometric correction was performed using the SCP plugin in QGIS to convert digital numbers into reflectance values using Dark Object Subtraction. - Anderson Level-1 classification was used for land cover classification. - Dynamic degree was calculated for each land cover type and was found to be maximum for the built-up areas, especially along highways.
2.1.10	Sandipta Das and Dasharatha P Angadi (2020)	- USGS - Topographical sheet maps (SOI) - Census of India Handbook	- Landsat MSS, TM and ETM^{+}	- [48] described the utility of Remote Sensing and GIS in understanding land cover transformations in data-scarce regions. - Landsat images were used in the study area, and MLC was used for LULC classification.

				-Anderson LULC classification scheme adopted in the study. - A positive correlation between population and urban expansion was found. Elucidated the negative impact of urban expansion, including increased slum environment degradation in water and air quality. - The study suggested sustainable town development focusing on vertical rather than horizontal expansion.
2.1.11	Nguyen Thanh Son, Nguyen Thi Thu Trang, Xuan Thanh Bui & Chau Thi Da (2021)	- USGS - LULC maps from the World Bank and Asian Disaster Preparedness Centre - Flood map from United Nations Institute for Training and Research	- Landsat TM -ASTER DEM	- [130] used satellite imageries and geospatial data for the spatio-temporal evaluation of the decadal urban sprawl and flood risk assessment. - 30 GCPs were used for image registration in 1986 and 2001 by achieving RMSE of less than 15m. - Ancillary data included in the form of LULC maps, flood maps, DEM, shapefiles of rivers and canals, and demographic density. 20% of the area was found to be very vulnerable to floods.

2.2 LULC change studies and assessment of driving factors

S. No.	Name of author(s) & Year	Data source/ Data inventory	Instrument used	Abstract/ Findings
2.2.1	S Ghosh et al. (1996)	- Indian Remote Sensing Satellite (IRS) - Topographical Map (SOI) - Field data related to roads, soil, administrative boundaries, vegetation, altitude, settlements	- IRS-1B	- [77] carried out the study in the Pranmati watershed, a part of the Ganga river catchment, in Chamoli district, Uttarakhand. - Found out that the forests and pasture lands were converted into agricultural land. Also, a small portion of agricultural land was converted into forests. - The extension of agriculture was more near settlements, possibly due to the encroachment of nearby land. -The extension of agriculture was maximum at an altitude of 2200 m – 2400 m and slope between 20^o – 30^o, with potato being grown as a cash crop.Forest regeneration was observed to be maximum at elevations between 1600 m – 2000 m and slopes

				between 20^o – 30^o and was concentrated in southern parts of the watershed.
2.2.2	Muh Dimyati et al. (1996)	- USGS	- Landsat MSS	- [131] studied LULC changes in Yogyakarta, located on Java island of Indonesia. The effect of road accessibility in the settlement was also investigated. - The settlement was increasing and had occupied the areas from paddy fields and open/barren land. - A good correlation existed between road accessibility and settlement, with new settlements coming around areas near roads. - For the years 1972 to 1984, a large portion of paddy fields were converted into roads, while for the years 1984 to 1990, a large portion of open barren land was converted to settlements. Land changes observed were from paddy fields to open barren land and to settlement.

2.2.3	J.F. Mas (1999)	- USGS	- Landsat MSS	- [122] compared Change detection techniques in Mexico by using the North American Landscape Characterization Project and comparing from different times of the year. - The region had witnessed changes due to cattle rearing, rice farming, aquaculture and petroleum exploration and the six change detection techniques were compared with aerial photographs - Found the Post-classification Method to be the optimal approach to detect LULC changes captured at different times and for radiometric corrections.
2.2.4	Shahab Fazal (2012)	- USGS - NASA Earthdata - Topographical sheet (SOI)	- Landsat - ASTER -DEM	- [75] found that vacant land, commercial area, unplanned residential area and planned residential area increased considerably at the cost of agricultural land. - An increase in vacant land observed due to subsidence in land rates and expectations of the owners for land price hikes.

				- An increase in plantation (tree crops) was also observed because of the availability of reasonable prices in the near market. - Around 40% loss in food-grain production was expected due to a decrease in agricultural area. Around 35% of agricultural land is non-recoverable.
2.2.5	B S Bisht and B P Kothyari (2001)	- USGS - Topographical Sheet (SOI)	- Landsat 5 TM	- [78] studied LULC changes for the years 1963-1986 and 1986-1996 in the Garur Ganga watershed of Bagheswar district in Uttarakhand using the satellite data of LANDSAT TM accompanied by ground verification and interpretation of images in GIS. - The agricultural area and settlement increased from 1963-1986 and 1986-1996, while the forests were converted into open forests; barren land also decreased mainly due to encroachments. - The maximum agricultural area witnessed in elevations of 1200-1800 m and slopes of 7-21%.

2.2.6	Rao and Pant (2001)	- USGS - Topographical Sheet (SOI) - Slope inclination maps and Land use maps from the World Bank-funded Integrated Watershed Development Programme	- Landsat 5 TM	- [32] prepared DEM to study the disturbances slope-wise; field interviews and workshops were conducted to determine the factors responsible for LULCC. - Forest cover had been reduced dramatically in the region, and half of the forests had been eliminated at slopes less than 15º. Agriculture expansion was found to be 75% at slopes of 10º -15º. - Population growth in the region was found to be a primary reason for change in the study area. The demand for wood, manure, and grazing pastures had put the region's forest resources under stress, as well as those of humans and the government.
2.2.7	Civco et al. (2002)	- USGS	- Landsat TM and ETM^{+}	- [119] compared four LULCC detection methods. Chose two sites within the Stoney Brook Millstone watershed in New Jersey for study. - Cluster busting technique was used in Traditional post classification, Z – statistics in cross-correlational

				analysis, NIPS (NAUTILUS Image Processing system) & Neural SIM Program used for Neural network and e-Cognition was used in Image Segmentation & Object Oriented Classification. - All the methods, except neural networks, could detect changes in urban growth. The neural network better-detected changes from barren to urban areas than others. Image segmentation and object-oriented classification results were overall promising.
2.2.8	H. Alphan (2003)	- USGS	- Landsat TM and ETM^{+}	- [132] used satellite data (Landsat TM, Landsat ETM+) from 1984 to 2000 to study the effects of urbanisation and migration on the agricultural and built-up areas in the city of Adana, Turkey. -Geo-referencing and supervised classification were performed while ERDAS IMAGINE was used for image processing.

				- Found that the urban area almost doubled, whereas agricultural areas and semi-natural areas had decreased. - The agricultural land was converted into urban areas while semi-natural areas into agricultural areas.
2.2.9	Nagendra et al. (2004)	-	-	- [87] gave the rationale to integrate spatial patterns with the underlying processes driving landform alterations. - The tropical countries faced significant issues related to the transition of forest land into agricultural land, whereas, in Western developed countries, issues of urban sprawl and city planning were dominant. - Suggested that the bio-physical factors, such as wildlife, biodiversity, etc and socio-economic factors both need to be considered while studying the impact of landscape fragmentation.

				- Edge density for urban areas was a valuable criterion for studying the extent of urban sprawl, and private land use management practices were needed in Western countries.
2.2.10	Dwivedi et al. (2005)	- USGS - Topographical Sheet (SOI)	- Landsat TM	- [49] used ancillary data such as topographical maps, published reports and maps for geo-referencing in ERDAS Imagine. - Unsupervised classification was performed, and spectral clusters were formed and converted into class ts using separability analysis. - The grass area, scrub lands, and croplands had increased while a decrease was noticed in barren land. - Soil and water conservation measures, thereby improving the vegetation cover, were the main driving forces of changes.

2.2.11	Li et al. (2006)	- USGS - Soil data from RS Application Institute of Chinese Academy of Sciences - Topographical map - Climatological data from the Chinese Academy of Agricultural Sciences	- Landsat MSS and TM	- [133] SPCA was used to determine the Environment Vulnerability Index for the region, and five levels were defined. - It was found in the study that overall, the region is medial in terms of vulnerability, but there had been an increase in the percentage of area under medial and heavy vulnerability from 1972 to 2000. - The region at elevations greater than 3500 was more vulnerable, and vulnerability was more in the Northern region than the Southern region. - Socio-economic impact on the region was considered to be the primary driver of change.
2.2.12	Xiao et al. (2006)	- NASA - Maps of the city by the Department of Defence, China	- Landsat 5 TM and Landsat 7 ETM^{+}	- [134] found that the urban area expanded from 6.31 km^2 in the year 1934 to 165.5 km^2 in the year 2001 at an average rate of expansion of 2.4 km^2 / year. High-speed expansion in terms of urban growth rate was observed from the period 1991 to 2001.

		- Bureau of Land Resources, Survey and Cartography, China		- Urban area, vegetable field, water and grass had increased from 1987 to 2001. Socio-economic factors, higher returns for crops, better land use policies, and better parks were the primary reasons for this. - Further, residential, crop fields, trees, orchards, and sandy/bare soil had decreased, with the increasing population being a major driving factor. - An increase in urbanised areas showed a strong correlation between population growth and improvement in traffic conditions, while a complex relation was found between gross industrial products and investment in urban infrastructure.
2.2.13	Yu et al. (2007)	- NASA (USGS) - IRS - Land use patterns and socio-economic	- Landsat MS and TM	- [28] found a surge in dense forests and agricultural areas with decreased open forests and grasslands. SPCA was performed to evaluate vulnerability, which was higher in warm areas, steep slopes and lower elevations.

		data through questionnaire	- LISS (Linear Imaging and Self Scanning Sensor) -III	- Human activities showed a positive correlation to environment vulnerability.
2.2.14	Dong et al. (2007)	- NASA (USGS)	- Landsat TM and ETM^{+}	- [19] studied the changes at Modoi County in the Qinghai-Tibetean Plateau, China, from 1990-2000. - The study found a decrease in grasslands, marshy areas, and water bodies. At the same time, an upsurge was witnessed in Sand-Gobi and barren land, indicating the region's deteriorating geo-climate and the need for proper management strategies. - Climatic factors, frozen soil changes, hydrological changes, and anthropogenic activities, such as rats, insects, and pests, were the main contributing factors in the study.
2.2.15	Berberoglu and Akin (2009)	- NASA (USGS)	- Landsat TM	- [80] used four different change detection techniques, and their suitability was checked in terms of accuracy in one of the coastal regions of Turkey, and accuracy

		- Topographical and agricultural maps, Turkey		assessment was made using Khap statistics and an error matrix. - Before applying Change Detection techniques, NDVI was derived, and 12 LULC classes were identified for the study; and high-resolution imagery, aerial photographs and field surveys were conducted for corrections of classification results - Change Vector Analysis, which was time-consuming and computationally exhaustive, gave the best results for the Mediterranean region, while Image Rationing was the least accurate. - No detection technique could detect wetland and sand vegetation changes, as they had similar spectral signatures.
2.2.16	Onur et al. (2009)	- USGS - DEM	- Landsat MSS and TM	- [29] performed the pre-processing of images using image enhancement techniques like histogram equalisation, standard deviation stretch, brightness/

		- Digital Globe	- ASTER - IKONOS	contrast adjustment, and geo-referencing using topographic sheets. MLC was used as the change detection method. - Open spaces with little or no vegetation and the urban fabric had increased in the region, while forests, heterogeneous agricultural areas and permanent crops had decreased throughout the study period. - The population explosion and urbanisation were considered significant factors for LULC change.
2.2.17	Laxmikant et al. (2012)	- Global Land cover Facility (GLCF) - IRS- P5 and P-6 - Census data	- Landsat MSS and ETM^{+} - LISS- IV and Cartosat- I	- [135] used Land Absorption Coefficient (LAC) and Land consumption rate (LCR) to determine qualitative assessment change. - Ground truth points and GPS were used for location accuracy. Image segmentation approach to extract built-up areas. The built-up area in the region increased from 15.26 km^2 to 25.87 km^2

				- LCR (quantifying the variation in the utilization of urban territory for each incremental rise in population) was high in 1976, decreased from 1976-1999 and further increased from 1999-2008, with population growth and development activities being the significant contributors to land change. - LAC (a measure of the spatial extent of a city) decreased from 1976 to 1999 and then increased from 1999 to 2008, showing that the population that was earlier concentrated in the city showed signs of urban sprawl later on.
2.2.18	Mushtaq and Pandey (2013)	- NASA (USGS) - IRS - Topographical sheets (SOI)	- - Landsat TM and ETM^{+} - LISS- III	- [74] used the geo-spatial data to study LULC change at Wular Lake. False Color Composite (FCC) was used for visual inspection, supported by ground validation. Lake area decreased from 24 km^2 to 9 km^2, thus reducing the flood-resisting capacity of the lake.

				- The aquatic vegetation, built-up area, and scrubs increased during the study period, resulting in increased erosion, runoff, sedimentation, and a change in the lake from oligotrophic to eutrophic. - Anthropogenic activities (socio-economic pressure) were the primary factor for LULC change, supplemented by urbanisation, deforestation, increased demand for fuel wood and change of cropland to horticulture.
2.2.19	El-Asmar (2013)	-NASA (USGS) - French Space Agency CNES	- Landsat MSS, TM, ETM^{+} - SPOT +4	- [136] used six satellite images to investigate the extent of change for 38 years in Burullus Lagoon, Egypt, a site protected by the Ramsar Convention. - The water indices, NDWI and MNDWI were used. Due to the absence of an MIR band in MSS, NDWI was used to calculate the area of water bodies for the 1973 image, while MNDWI was used for the rest of the

				satellite images. Dark Object Subtraction (DOS) was performed for atmospheric correction - The construction of dams and better irrigation facilities resulted in increased sedimentation and further discharge of agricultural waste into the lagoon, which was the primary cause of the decrease in the lagoon area. Land conversion into agriculture & aquaculture and the construction of highways were also the driving forces of change.
2.2.20	Hegazy and Kaloop (2015)	- USGS - Topo sheets by Survey of Egypt	-	- [79] studied LULC changes from 1985 to 2010 and predicted LULC for 2035 using Markov Analysis. A large portion of agricultural land was transformed into a built-up area and barren land. The water also decreased during the period. - Urbanization was considered the primary factor for LULC change, and a large portion of cultivatable land was converted into infertile and barren land.

				- It was forecasted that in 2035, the same trend would follow, with decreased agricultural land and water and increased built-up areas and barren land.
2.2.21	Rawat & Kumar (2015)	- GLCF - Earthexplorer	- Landsat TM	- [17] used remotely sensed data for 1990 and 2010. MLC used for supervised classification in ERDAS 9.3NDVI, NDWI and NDBI were used to classify the images. - Accuracy assessment was found to be 90.29% and 92.13% for 1990 and 2010, respectively. - Quantitative and qualitative changes determined using cross-tabulation. Agriculture, barren land, and water bodies decreased while there was an increase in vegetation and built-up areas. - A large portion of agricultural land was transformed into vegetation, barren land, and built-up areas. The increase in vegetation was mainly due to afforestation programmes initiated in the region.

2.2.22	Meshesha et al. (2016)	- Earth explorer - DEM - LULC changes through informal interviews and focused discussions	- Landsat 5 and Landsat 8	- [52] used Landsat satellite imagery for 1984, 1999 and 2015 to study the changes in 31 years in the Beressa Watershed of Ethiopia. Supervised Classification followed. Histogram equalization was performed for image enhancement. DEM was prepared to study the slope, length, width, and stream network. - An increase in farmland, forest land, plantations, settlements, and water bodies was witnessed. Afforestation and awareness programmes at the regional level and better water harvesting techniques followed by farmers to conserve water for agriculture were the reasons for the increase in Farmland and Water Bodies. However, agriculture on steep slopes had increased erosion, and land cover degradation was anticipated.
2.2.23	Hassan et al. (2016)	- USGS	- Landsat 5	- [137] used Supervised classification and Stratified Random Method accompanied by the Kappa method

		- Space and Upper Atmosphere Research Commission, Pakistan - Aerial Photographs - Topographical maps	- SPOT 5	and obtained good accuracy. The barren area, which occupied 55% of the land area in 1992, was reduced to 1.87% in 2012. The built-up area showed the maximum increase, followed by agriculture and water. Decrease in forest area too. - Urbanization and economic development in the region were the significant causes of land change. A close relationship existed between the geometric centre of the city and the availability of substantial roads with urbanization.
2.2.24	D Kumar (2017)	- GLCF - Topographical sheets (SOI)	- Landsat MSS, TM and ETM^{+}	- [28] used Landsat Remotely sensed images to study LULC changes from 1977 to 2010 in Kamrup, Assam. Six LULC categories were used, which included open forests, dense forests, settlements, sand areas, agricultural land and water bodies. - Due to anthropogenic activities, a reduction in the dense forests and agricultural land and an increase in

				open forest and settlement were observed. In contrast, a slight change was observed in the sand and water bodies area.
2.2.25	Debnath et al. (2017)	- GLCF - SOI Topographical sheet	- Landsat MSS and TM	- [51] divided the river into five reaches, from Chakmaghat up to Khowai, and 23 reference sites were selected. Determination of LULC classes on ArcGIS and accuracy assessment made using Confusion Matrix by randomly selecting a minimum of 30 points for each class. - Cultivated land showed decreased area due to bank migration and increased barren land (210%) and dense forests (66%) observed, influenced by deposition of sand and afforestation policies, respectively. Around 60% of cultivated land and 59% of open forests remained unchanged, while 66% of water bodies were converted into cultivated land.

2.2.26	Mondal et al. (2019)	- GLCF	- Landsat MSS and OLI	- [73] used Landsat Remote sensing data to study LULC changes in Sagar Island located in Hooghly estuary, India. Overall accuracy was 79.53%, and Kappa hat was calculated to be 0.74. - Agriculture (mono-crop) land decreased by 5.67% and was mostly converted into agricultural land and settlements. Settlement in the region had increased by 9.8 %.
2.2.27	Deka et al. (2019)	- GLCF - IRS	- Landsat MSS - LISS – I and LISS-III	- [18] studied three districts of Arunachal Pradesh using the RS data from three satellites. Error matrix used for accuracy assessment. - Cultivated and built-up area gained from evergreen broad-leaf forest and mixed forest categories. Using DEM, it was found that cultivated land and built-up land gained maximum at 0-500 m elevation. The forests were stable at altitudes greater than 1500 m,

				while disturbances were witnessed in all types of forests at elevations less than 1500 m. - Forest depreciation, swift urbanization and agricultural expansion were supposedly the main drivers of LULC changes.
2.2.28	Chowdhury at al. (2020)	- USGS - GDEM	- Landsat MSS, TM and OLI -ASTER	- [33] used RS images and analyzed LULC changes for 40 years (1978-2017) for the watershed region of the Halda river in Bangladesh. MLC was used for LULC classification. - The accuracy assessment was found to be satisfactory, and a random sampling method along with Kappa Statistics was used. Quantification of classification performed using QGIS. Vegetation decreased by 35%, while the settlement and agricultural land rose by 182.5 % and 83.3%, showing increased anthropogenic activities in the region.

2.2.29	Negi & Irfan (2022)	- USGS - SOI Topo sheets DEM	- Landsat 5 TM, Landsat 7 ETM+ and Landsat 8 OLI/TIRS	- [138] observed LULC transformations occurring in upper Kullu valley, HP from 1990 to 2020. MLC used to classify the study area into eight classes and DEM to avoid misclassification of agricultural land. - Increase in barren land, agricultural land, built-up areas while decrease in forest cover and snow cover found. Horticulture, hydropower projects and tourism were the major driving factors. - Soil degradation, loss of water bodies, traditional houses either disappeared or rendered obsolete and expansion of fruit cultivation alongwith better road connectivity observed during this period.
2.2.30	Mehra and Swain (2023)	- USGS - Earthdata DEM - Google Earth imagery	- Landsat 8 OLI -Phased Array Type L-Band Synthetic Aperture Radar	- [65] demonstrated the use of EVI to create zonation of Dharmashala city into four land cover types: Stable zone, dynamic zone, rivers and lake. - Validation using Ground truth points and Google Earth imagery. Maximum percentage of dynamic class

			(PALSAR), 12.5m DEM	was at an altitude less than 1500m and at a slope less than 20^{o}. - The overall accuracy of the classified land cover using Landsat-EVI was found to be 88.51%, and kappa hat was 0.83.
2.2.31	Chowdhury Md. (2024)	- USGS - Google Earth 7.2.0	- Landsat 8 OLI	- [139] compared the accuracy of four algorithms for LULC calssfication of Dhaka city. Two were ML based algorithms, Random Forest and Support Vector Machine, one deep learning based ANN and the fourth being traditional MLC - The performance of ANN was found to be the best, however, the results of traditional MLC was also found to be satisfactory. - The overall accuracy and kappa hat of MLC found to be higher than SVM and the results showed slight variation as compared to other advanced alogirthm.

2.3 Post Classification corrections and Integration of remote sensing data

S. No.	Name of author(s) & Year	Data source/ Data inventory	Instrument used	Abstract/ Findings
2.3.1	Kumar and Lal (2007)	- IRS, National Remote Sensing Centre (NRSC), Hyderabad - SOI Toposheets	- LISS III	- [140] performed Digital Image Processing using ERDAS Imagine and forest density was calculated. - Forest density calculation cross-checked with NDVI analysis and showed a positive correlation. Overall accuracy was 88.17 % - The forest density was maximum in the central and western regions (Baroh) of Kangra, while it was least for the eastern region (Baijnath). - It was found that there was a 5.8% increase in forest as compared to the Forest Survey of India Report (1999), and this could be due to the reforestation programmes by the State Forest Department and awareness programmes for locals.

2.3.2	Thakkar et al. (2016)	- IRS NRSC, Hyderabad and BISAG, Gandhinagar - SOI Toposheets	- LISS-III and LISS-IV	- [47] used MLC to classify the images, and after that, post-classification corrections were adopted to improve the accuracy. - The ancillary data included texture imagery, NDWI and Drainage network used. Statistical analysis to compare MLC with post-classification corrections using the McNemar Test, a non-parametric test. - Agriculture, forest land, settlement, quarry, water bodies and barren land had increased in the region. Watershed development programmes by various agencies and the region's economic development due to the granite mines' location were the major reasons.
2.3.3	Shi et al. (2019)	- High resolution ZiY-3	- ZiYuan-3 - Landsat 8 OLI - Sentinel 1A	- [141] integrated multi-source remote sensing data from satellites with a social media platform (WeChat), which helped improve the accuracy of land cover classes.

				- Radiation and atmospheric correction was performed on the Landsat image to convert the digital numbers (DN) into spectral radiance values. The accuracy metrics were improved by the integration of multi-source data, with Landsat 8 being the most significant addition and resulting in the improvement of all land cover classes.
2.3.4	Xu et al. (2019)	- National Center for Air-borne Laser Mapping, University of Houston	- Multispectral-Light detection and ranging (LIDAR) - High-resolution imagery - Hyperspectral imagery	- [142] used post-classification measures and Neural Networks, which achieved more remarkable accuracy and was adopted by all the winning teams in the 2018 IEEE Geoscience and Remote Sensing Society (GRSS) Data Fusion contest. - Post-classification corrections can help improve unclassified/misclassified pixels.
2.3.5	Pech-May et al. (2022)	- European Space Agency	- Sentinel 2 - Landsat	- [143] used microwave sensors that operate at long wavelengths and are little affected by clouds and noise to produce high-resolution images, inferring that this

		- USGS - Google Earth Engine		required sophisticated and complex image processing mechanisms. - Optical sensors, although having inherent deficiencies related to noise, clouds but were abundantly used as the spectral data is highly correlated with earth and image analysis algorithms dependent on visual data and were generally preferred for land cover studies. EVI and NDWI were used to detect vegetation and water bodies. Sentinel 2 satellite imagery used, which has inherently cumulus clouds and thus restricts image usage
2.3.6	Mehra and Swain (2024)	- USGS - Earthdata DEM - Google Earth imagery	- Landsat 8 OLI - Advanced Land Observing Satellite (ALOS) PALSAR 12.5m DEM	- [62] used Spectral vegetation indices, ancillary data and DEM as post-classification correction measures. - MLC was performed initially, and four land cover categories were formed. Landsat satellite images were used, and Random stratified sampling was conducted.

				- Post-classification corrections resulted in improvement in overall accuracy and kappa hat
2.3.7	Kumar et al. (2023)	- ESA - USGS - SOI	- Sentinel – 2 - Landsat – 7 ETM+	- [144] used MLC to study ecological degradation in Sarbari Khad watershed of Kullu from 2000 to 2021. MLC used for LULC classification of the study area into seven classes and post-classifcation correction measures included class recoding and accuracy assessment through ground truth points. - Forest land degradation alongwith soil erosion was evident through the findings. The open forests and agricultural practices intensified during this period. - The expansion in tourist inflow, horticulture and population were the major driving factors. LULC transitions if not managed sustainably, could pose significant challenges for the locals in near future, in the form of Snow cover retreat induced climate

				change, water insecurity, Glacial lake outburst floods and landslide vulnerability.

2.4 Modelling and Simulation of LULC change

S. No.	Name of author(s) & Year	Data source/ Data inventory	Instrument used	Abstract/ Findings
2.4.1	Li and Yeh (2001)	-	-	- [145] described the CA approach as a neighbourhood based in which the state of the central cell depends upon the neighbourhood cells. - Compacted zones were created which are suitable for urban and agricultural areas based on temporal dynamics. - Compared to traditional methods, an integrated approach involving GIS, remote sensing, and CA was used for zoning. - The model was tested in the Pearl River Delta, China, and results indicated the model's better ability to

				explore alternatives and zoning patterns conveniently and quickly.
2.4.2	Myint and Wang (2006)	- USGS - Drainage and road layers from the GIS unit of Norman city.	- Landsat MSS, TM and ETM^{+}	- [146] demonstrated the integration of Markov Chain Analysis with the Cellular Automata technique for future prediction, resulting in the removal of the salt-pepper effect and better interpretation of future images. - Suitability criteria were used to construct areas using multi-criteria decision-making and fuzzy standardization approaches in IDRISI. - Classification accuracy was 86% for the projected map. - Errors in classifying temporally different images have a bearing on the overall accuracy of projected images.
2.4.3	Thota and Changalasetty (2013)	- National Institute of Diabetes and Digestive and	-	- [147] used MLP feed-forward type. - Reasoned that the meticulous selection of the learning rate parameter is imperative for optimizing the

		Kidney Diseases USA		percentage of correctly classified instances in any classification problem. The optimal learning rate gives the most negligible value for the root mean squared error. - Low learning rate, the network will take a longer time to converge, while for a high learning rate, the network will not converge. - 0.0001 to 0.02 was found to be a good range for selecting the LR as it gave Relative absolute error % and Root relative squared error % values increased correct pixel values.
2.4.4	Deep and Saklani (2014)	- NRSC, Hyderabad	- IRS-LISS-IV	- [148] used LISS-IV data to study Dehradun City, Uttarakhand, India. - Post-classification change analyses were performed using the CA-Markov Model, which facilitated the identification, measurement and examination of

				dynamic transformations. - Unsupervised classification was performed to create LULC of 2004 and 2009. - Clock tower, roads and railway line used as the spatial or driving factors in transitional potential modelling - Optimal outcomes were achieved by utilizing 12 iterations and 17*17 neighbourhood configuration.
2.4.5	Mohammady et al. (2014)	- USGS	- Landsat TM and ETM^{+}	- [149] explained that the increasing world population was responsible for urban sprawl, and the urban planners' task was to check and suggest measures to check urban growth. - Anderson Level I Classification system adopted. The model's performance was evaluated using various metrics, such as the mean absolute error and RMSE. - Six datasets in the study were related to proximity to roads, residential areas, green spaces, region centre, elevation, and slope.

2.4.6	Liping et al. (2018)	- USGS - Fujian Environmental Bulletin - Fujian Statistical Yearbook	- Landsat TM and OLI	- [44] used the CA–Markov Model and validated it by comparing the observed changes for the year 2014 with the forecasted, and Kappa hat of 0.81 was obtained. Barren land and construction land had increased at the cost of woodland, which occupied the maximum area, and the same trend is anticipated for 2025 and 2036, thus requiring attention to the conservation of ecology. - The changes in woodland were due to timber harvesting and urban expansion, whereas human activities were considered significant causes for the rise in construction land and barren land.
2.4.7	Das and Sarkar (2019)	- USGS - SOI Topo sheets - Google maps	- Landsat TM and ETM^{+}	- [150] used DOS in SCP plugin of QGIS for atmospheric correction and performed MLC for LULC classification using ERDAS. - The Markov Chain was used for future prediction, and the MMULT function in MS Excel was used for the transition probability matrix.

				- For validation of the model, a chi-square test was performed, and the simulated and actual values were checked to see whether or not the simulated values were significantly different.
2.4.8	Hakim et al. (2019)	- USGS	- Landsat 7 ETM^{+} and Landsat 8 OLI/TIRS	- [110] focussed on applying spatial dynamic modelling techniques to anticipate land use land cover change. MLC was used for LULC classification. - Images captured by the Landsat satellite in 2008, 2013, and 2018, and the analysis forecasted the future LULC change for the sub-district. - Spatial dynamic Modelling techniques, Markov Chain and CA were used. - Input data included land use maps, demographic data, and geospatial parameters like slope, aspect and proximity from roads.

2.4.9	Saputra and Lee (2019)	- USGS - Distance from the road by Ministry of Environment and Forestry, Indonesia - Soil type from the Food and Agriculture Organisation (FAO)	- ASTER DEM 30m	- [103] created future LULC maps by simulating and predicting them using an ANN-based CA model. - Five criteria were used as exploratory data, including altitude, slope, proximity to road, aspect and soil type. - The study found that altitude and distance from the road significantly impact LULC changes in the region. - A decrease in Forests and an increase in Plantations is anticipated in the years 2050 and 2070.
2.4.10	Buğday (2019)	- USGS	- Landsat 5 TM and Landsat 8 OLI/ TIRS	- [90] performed MLC and used Landsat imageries to model and simulate LULC changes occurring in the Sinop province of Turkey. - Months so chosen that the cloud rate was less than ten per cent. The MOLUSCE plugin was used for simulation, and MLC for the LULC classification.

				- Proximity to roads and streams was chosen as the input variable driving LULC changes, and zonation was done on the roads as 10m, 50m, and 100m. - Learning rate 0.001 and 0.050 momentum value used in the MLP for simulation purposes. Five iterations were selected for simulation.
2.4.11	Mzava et al. (2019)	- USGS - Toposheets - Google Earth images	- Landsat MSS, TM, OLI/TIRS	- [7] used Image correction measures as pre-processing of satellite images. The SCP plugin in QGIS used for LULC classification into five categories. - The histogram equalization technique was used to enhance the image and improve the perceptual capability of images. The elevation and slope input data chosen in the study were used as the independent variables, while LULC maps were used as the dependent variables.

				- MOLUSCE plugin used in QGIS 2.10.1. The analysis of LULC changes showed an increase in built-up areas fuelled by the increasing population in the study area. - The developmental pressures indicated by the improved economy had resulted in the transition from thick vegetation to urban areas.
2.4.12	Ramachandran et al. (2020)	- Socio-economic data from the Office of Census Commissioner - Roads, railways and rivers from Open Street Map - USGS - Soil data from the International Soil	- Landsat TM, ETM+ and OLI - SRTM DEM 30m	- [151] used LULC maps, DEM, soil data, plant species data and climate data used as exploratory maps. Compound growth rate used for population forecasting. - The MOLUSCE plugin was used for future LULC simulations. The Intergovernmental Panel on Climate Change-AR5 Representative Concentration Pathways used for climate simulation; Maximum Entropy Bioclimatic modelling technique used for plant species simulation.

		Reference and Information Centre (ISRIC)		- The study employed an integrated model to simulate future LULC maps, potential species distributions, and human population. A decrease in forest cover and an increase in agricultural land, built-up areas, and barren land were witnessed from 2005 to 2050.
2.4.13	Gharaibeh et al. (2020)	- USGS (Earth explorer)	- Landsat 7 ETM^{+}	- [85] included four spatial cum socio-economic variables comprising slope, proximity to roads and urban centres, and soil fertility responsible for LULC transformations. - The Anderson Level-I classification system was adopted for LULC classification. The learning rate was set at 0.0003, and the momentum factor was set at 0.5 in ANN architecture. - The CA model was used because of its simplicity, flexibility and integration with other models, but it had limitations in modelling the driving factors and was dependent only on spatial data. MCA model had the

				advantages of depending on spatio-temporal factors and working on transition matrices. - CA-MCA assumed a linear trend among the spatial-temporal process. The ANN model was incorporated to include driving factors, which could capture non-linear inter-relationships between the factors and complex patterns.
2.4.14	Tariq and Shu (2020)	- USGS - City boundary from Urban Unit RS, Faisalabad - Toposheets - Aerial Imagery	- Landsat TM, ETM+ and OLI	- [152] described that CA offered an economical approach to predict and analyse future LULC transformations. - Scan line errors in ETM^{+} corrected using triangular approach in ENVI. The months were chosen, so the cloud cover percentage was less than 10%. - The transition probability map was used as an input to CA, and CA could expose spatio-temporal shifts occurring in a landscape.

2.4.15	Kafy et al. (2021)	- USGS	- Landsat 5 TM and Landsat 8 OLI - SRTM DEM	- [34] used the Support Vector Machine algorithm to predict and analyse future LULC and Land surface temperature (LST) at Chattogram, Bangladesh. - Each satellite scene chosen had cloud coverage of less than 10%. MOLUSCE was used to simulate LST in the future. The area was divided into five classes based on LST with max LST at 36^{o} C and minimum set at 20^{o} C - Seven driving factors responsible for LULC transformations in the region chosen. Geographical variables derived from DEM. Spatial variables were calculated using Euclidean Distance, while LULC maps acted as independent variables.
2.4.16	Kamaraj and Rangarajan (2022)	- NRSC, Hyderabad - Roads from OpenStreetMap - Bhuvan, India	- Carto DEM	- [100] used the CA model for analysing land-use change dynamics in spatial and temporal contexts and provided insights for sustainable land management practices in the region.

				- The study was conducted in the Bhavani river basin and used the MOLUSCE tool, which leveraged various datasets such as DEM, distances from roads and built-up areas, and three LULC maps. The proximity spatial variables were created using Euclidean distance. -The investigation established criteria for simulating future LULC maps using ANN-CA Model, including a neighbourhood size of 1, 1000 iterations, ten hidden layers, a momentum value of 0.06, and a learning rate of 0.001.
2.4.17	Muhammad et al. (2022)	- USGS - Resources And Environment Science Data Centre, China - WorldClim DEM	- Landsat TM, ETM^{+} and OLI	- [82] analyzed spatiotemporal LULC changes in Linyi City, China, using Landsat data. Three spatial variables, DEM, slope, and distance from roads, were used. - Proximity factors calculated using Euclidean Distance. The ANN Model was set with 100 iterations, a neighbourhood value of 3 x 3 pixels, a learning rate

		- Roads from Socioeconomic Data and Application Centre , NASA - Administrative boundaries from Global Administrative Areas		of 0.001, and a momentum value of 0.05 and used for future LULC map for 2020. - The model validation showed satisfactory results, having a kappa value of 0.51, and it was used to forecast LULC maps for the years 2030, 2040, and 2050 after running iterations. A significant increase in impervious areas and a decline in forest areas was witnessed during the study period.
2.4.18	Atef et al. (2023)	- Satellite images from USGS - DEM from the Japanese Aerospace Exploration Agency, JAXA	- Landsat TM and OLI	- [101] included biophysical and socio-economic variables, including the use of Distance variables and DEM. Manipulation of RS images done using Google Earth Engine. - The findings assisted in the implementation of proper land management strategies based on a sustainable development model.

				- Used the CA-Markov Model for simulation and validation of the model, which was performed with the actual LULC map for 2020. Agriculture and built-up areas were found to have a greater tendency for transformation.
2.4.19	Phinzi et al. (2023)	- Satellite images from the South African National Space Agency	- SPOT 7	- [153] studied the importance of training pixels on Overall Accuracy (OA). -LULC classification was performed for 9 LULC classes on Level 1 and Level 2 using Anderson Classification-based USGS Level Classification. - The models which had more training samples outperformed those with smaller training samples in Random Forest Classification. The same trend was applicable to UA, but variability was observed for PrA.

2.4.20	Madhavi Jain (2024)	- Landsat - IRS -ASTER DEM - Socio-economic Data and Applications Center (SEDAC)	- Landsat MSS, TM and OLI - LISS-III - MOLUSCE 3.0.13	- [154] used CA based ANN to predict future LULC map of Delhi city for the year 2030. - Slope, elevation, aspect, distance from road/rail network and distance from built-up areas were taken as dependent variables. - Different number of iterations were tested in increments of 50 and, finally, 300 iterations were chosen as more than this no improvement was witnessed in ANN learning curve. - Structural similarity index used for quantitative assessment of pixel based similarity between the predicted and actual LULC map showed 0.83, with values close to 1 indicating perfect similarity.

2.5 Summary of the Literature Review

The synthesis of the literature survey is essential in deciding the further discourse of research and providing the road map for the study in focus. The summary of the Literature Survey has been shown in **Fig. 2.1**.

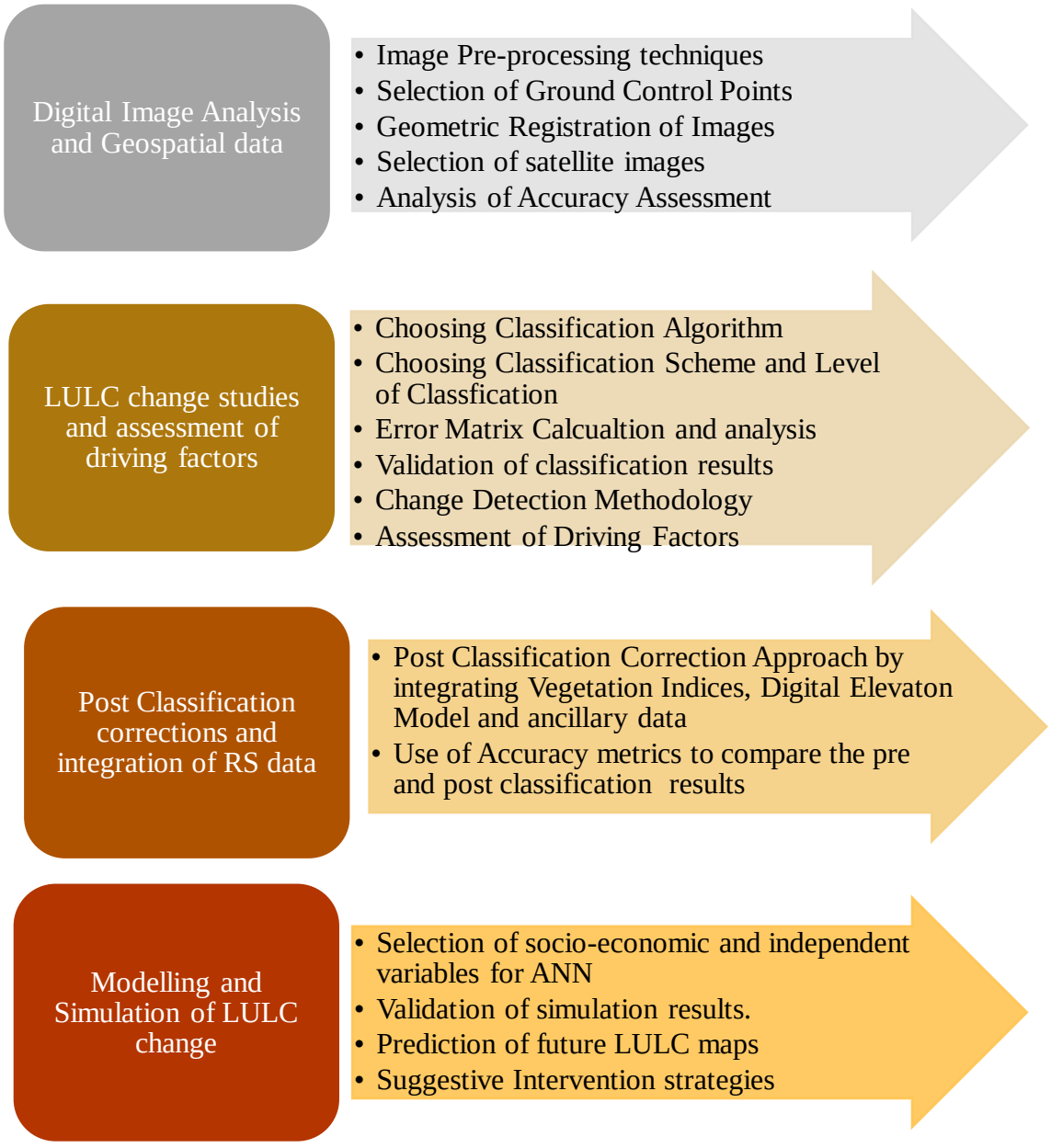

Fig. 2.1 Summary of Literature Survey

CHAPTER 3
METHODS AND MATERIALS

3.1 Overview

The research study involves three significant aspects;

a) To illustrate the difference in the classification results using three different satellite products.

b) Identify the trend and direction of LULC transitions.

c) Modelling and simulation of LULC maps.

The emphasis in a) is to check whether the results from different satellites are significantly different or using the different satellite data –product yield similar results. The results have been compared using the accuracy metrics prevalent in RS and GIS. This forms the core research gap identified in Chapter 2, Review of Literature.

In b), the focus is to understand the complex LULC transitions occurring in the research area by creating LULC maps for 2016, 2019 and 2022.

In c), the research incorporated the driving factors for predicting the future LULC maps for the years 2025 and 2040. Further, intervention strategies that will help policy-makers, administrators, and environmentalists have been proposed concerning the research area.

3.2 Methodology

The methodology and work-flow structure adopted in the research study have been demonstrated in **Fig. 3.1**. The methodology has been sub-divided into three sections covering the three aspects of the research study as mentioned above. In the succeeding sections, the break-up of the methodology covering these three aspects has been done as 1) Comparison of satellite data–products, 2) Spatio-temporal LULC transitions from 2016 to 2022, and 3) Modelling and simulation of LULC maps.

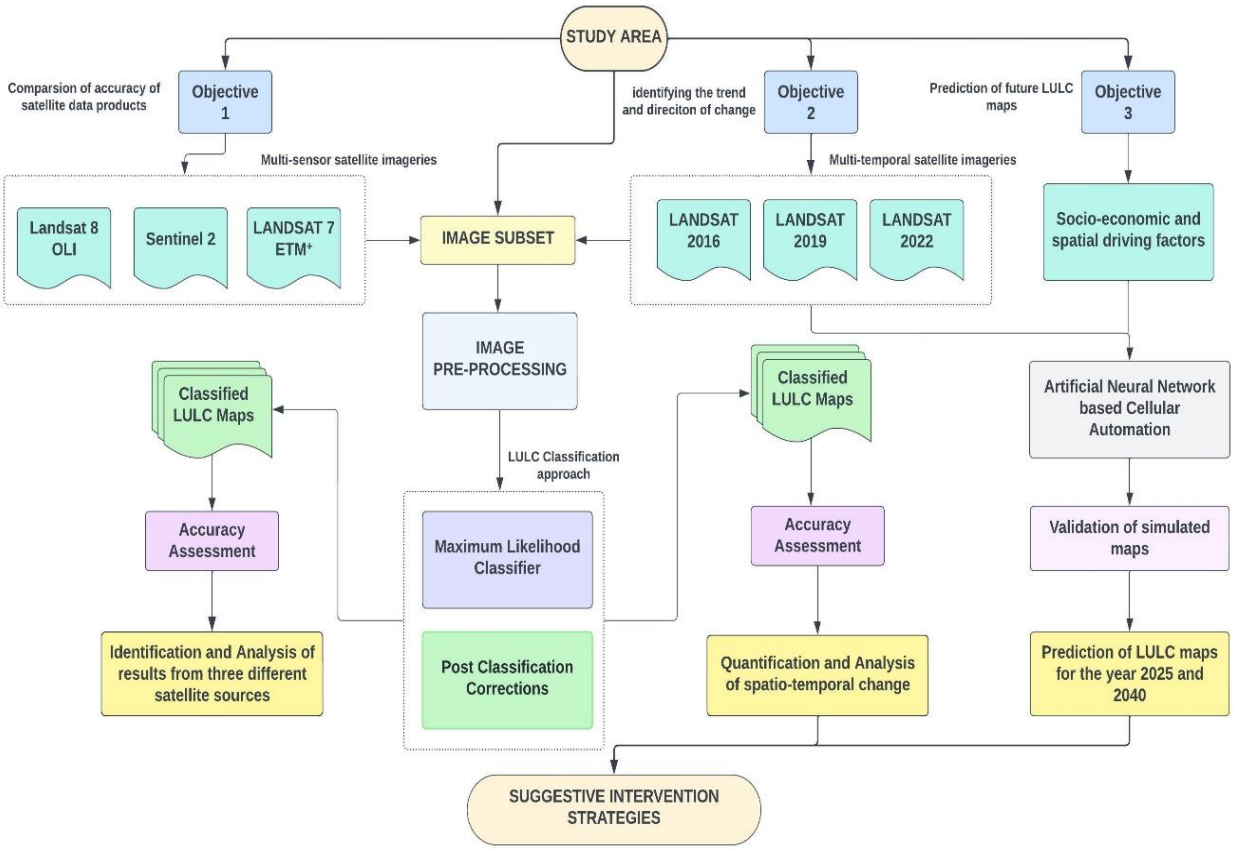

Fig. 3.1 Methodology and work-flow structure

3.2.1 Comparison of satellite data –products

This study integrated satellite and ancillary data to achieve a robust and accurate Classification procedure. The satellite data products of Sentinel 2, Landsat 8 OLI, and Landsat 7 ETM+ were downloaded from USGS (http://earthexplorer.usgs.gov/). The specifications of satellite imagery are given in **Table 3.1**. Further, three indices, EVI, MNDWI, and NDBI, were used to improve the classification. The ancillary data included the DEM, draft Town and Country Planning (TCP) Report of Dharamshala city, and remotely sensed images using Google Earth and Planet Scope for aid and support in image classification and analysis. The shapefile of the study area was generated using the TCP report, while the slope and aspect layers were generated using the DEM. The process followed in the creation of the shape file has been elucidated in **Fig. 3.2**.

October is characterized by less or no rainfall in the research locale, and the cloud cover percentage in each satellite image was less than 10%. The selection of a similar month in the three different remotely sensed data products is essential to reduce phenological effects [155].

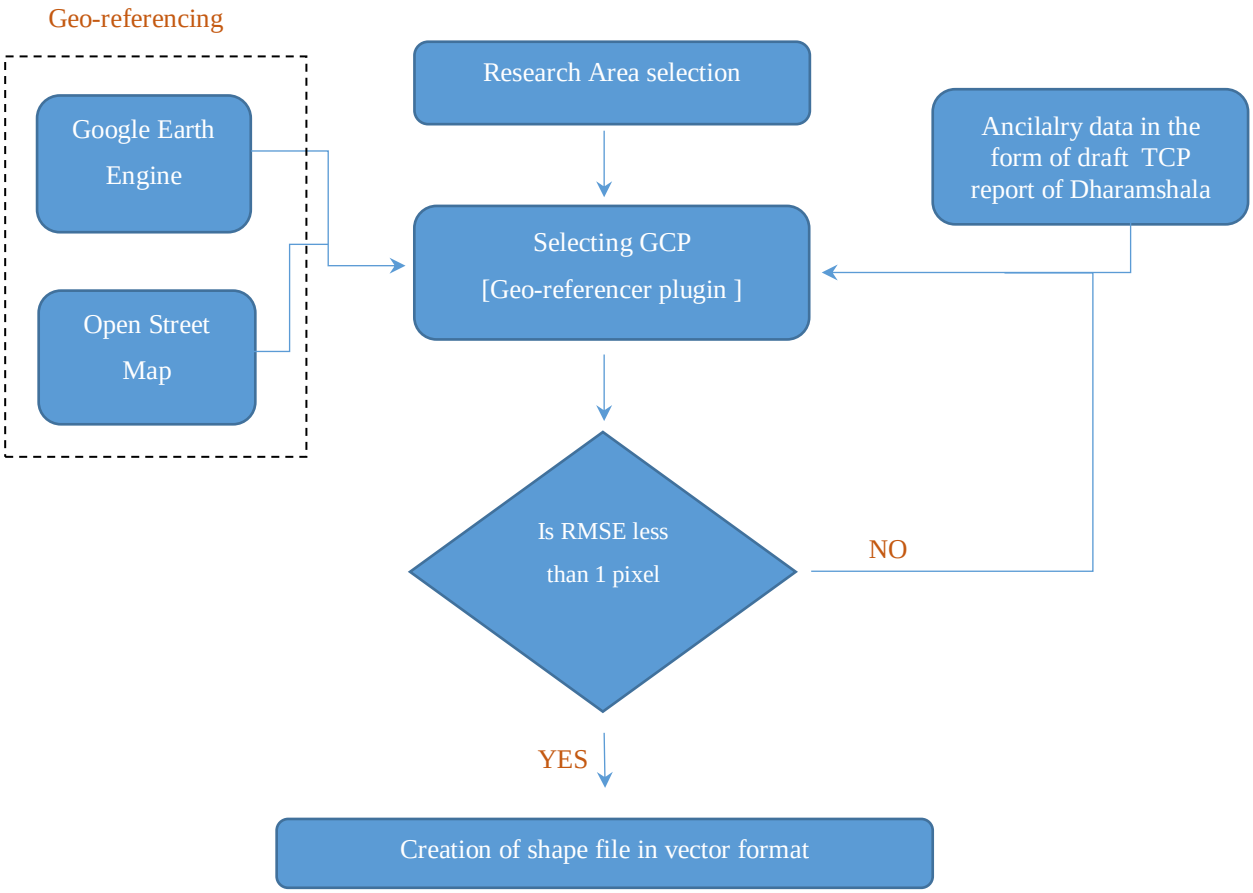

Fig. 3.2 Creation of shape file of the study area

3.2.1.1 Image Pre-processing

The scan line errors in ETM+ were corrected using the FillNoData module available in QGIS, which uses the Inverse Distance Weighting (IDW) Interpolation algorithm to find the no-data values. IDW is based upon a simple but promising technique that the similarity between two points is inversely related to their distances. In addition, weights are applied to model spatial interactions between the points [156].

Table 3.1 Satellite specifications (**Source:** USGS Earth Explorer)

Satellite	Sensor	Path/Row or Tile number	Date of Acquisition	Number of Spectral bands	Spatial Resolution	Cloud Cover Percentage
Landsat 7	ETM+	148/38	30.11.2020	8	30m (1,2,3,4,5,7)	3.00
Landsat 8	OLI/TIRS	148/38	06.11.2020	11	30 m (1,2,3,4,5,6,7,9)	1.41
Sentinel 2	Multi-Spectral Instrument	T43SFR	08.11.2020	12	10 m (B,G,R, NIR)	20.31

3.2.1.2 LULC Classification Scheme

Tea plantations are protected under Section 5 of the Himachal Pradesh Ceiling on Land Holdings Act, 1972 while forests are protected under Indian Forest Act, 1927, and thus both these land cover types were included in one category. There are several classification schemes available, such as IGBP, GLC2000, USGS, and others, that can be adapted to meet the specific requirements and objectives of a given project [43,157]. A modified Anderson Scheme was adopted to classify the study area into four major classes, viz., Protected areas, Built-up areas, agricultural areas, and water bodies, as shown in **Table 3.2**.

Table 3.2 Classes delineated based on unsupervised classification

Class Name	Description
Protected areas	Includes Forests and tea plantations
Agricultural areas	Croplands and pastures
Built-up areas	Isolated and clustered dwellings (residential, commercial, government, etc), roads.
Water bodies	Streams and lakes

Unsupervised K-means clustering was performed to work out LULC classification for the study area. Since the algorithm does not require the setting up of training areas before classification, and there's no requirement of masking or setting of thresholds [36,126], it was an appropriate approach to prepare the thematic maps with the slightest manipulation and ideally suited for comparison.

The Himalayan regions offer more complexity than other flat regions of India. The spectral characteristics of non-vegetated areas, rivers, and built-up areas may overlap in these regions, and thus, the simple classification algorithms may not be suited for this purpose. Post-classification correction measures involving creating a mask for each land cover type can be constructive in the accurate land cover classifications [62]. Due to the overlapping spectral characteristics of built-up areas and streams, which are primarily characterized by the presence of boulders and cobbles in this region, the Strahler order algorithm available in SAGA was used to accurately delineate the rivers

The use of spectral vegetation indices and the Digital Elevation model provides a great help in classifying the areas with more accuracy. EVI is more robust than NDVI in minimizing the biases resulting from canopy background and aerosol variations [63–65]. The satellite images were chosen for the month of November, characterised by crops of low height in agricultural areas. By carefully selecting threshold values for EVI, it is possible to generate a forest mask that effectively distinguishes densely vegetated areas from those with lower vegetation density. It was used to separate Protected Areas from Agricultural Areas. MNDWI is very useful in removing built-up noises [66] when applied to open water areas and can be used advantageously to mask built-up areas. [67] proposed the Normalised Difference Built-up indices while studying the built-up areas in Nanjing City of China and achieved an accuracy of 92.6% for classifying built-up areas. Three spectral vegetation indices, EVI, NDBI, and MNDWI, were used to improve the overall accuracy of the classified map resulting from unsupervised classification. These parameters were calculated using eq (i), (ii), and (iii) respectively.

$$EVI = 2.5 * \frac{NIR - R}{L + NIR + C1 * R - C2 * B} \quad \text{.....(i)}$$

NDBI = $\frac{MIR-NIR}{MIR+NIR}$ …….(ii)

and

MNDWI = $\frac{G-MIR}{G+MIR}$ …….(iii)

NIR = Near Infrared Band (Band 4 for ETM+, Band 5 for Landsat 8, and Band 8 for sentinel)

MIR = Mid Infrared Band (Band 5 for ETM+, Band 6 for Landsat 8, and Band 11 for sentinel)

R = Red Band (Band 3 for ETM+, Band 4 for Landsat 8, and Band 4 for sentinel)

B = Blue Band (Band 1 for ETM+, Band 2 for Landsat 8, and Band 2 for sentinel)

G = Green Band (Band 2 for ETM+, Band 3 for Landsat 8, and Band 3 for sentinel)

L is the soil adjustment factor, C1 and C2 are the aerosols resistance weights (L = 1, C1= 6, and C2 =7.5)

3.2.1.3 Accuracy Assessment

Accuracy assessment for a classified map is essential to substantiate the appropriateness and usefulness of the classified thematic map [2,3]. Error matrix and kappa-hat are widely used parameters for accurately assessing classified thematic maps [7,41]. Error matrix is represented in the matrix form wherein the number of pixels assigned to a particular class in a classified map is expressed corresponding to the number of pixels assigned to a specific class in actual classification (41].

The OA is computed using diagonal elements of the error matrix, while the other elements correspond to omission and commission errors [2]. Accuracy metrics, such as Producer Accuracy (PrA) and User Accuracy (UA), can provide greater detail related to individual classified land cover by including these errors. Producer accuracy represents the errors of omission and evaluates the effectiveness of classifying test pixels in a land cover map. User Accuracy represents the errors of commission and is

indicative of the probability of a pixel being assigned a land cover type in a classified map that is represented accurately on the ground.

The Kappa-hat statistic is a robust metric for assessing the proportion of correct values within an error matrix attributable to genuine agreement versus agreement occurring by chance. The sample design is also important for accuracy assessment [41,42]. The following formula (iv) was used for the determination of sample size [Cochran, 1977]

$$n = \frac{[\sum Wi\ Si]^2}{[S[\hat{o}]]^2 + \left({}^{1}/_{N}\right) \sum Wi\ Si^2} \qquad \text{.....(iv)}$$

where,

where N= number of pixels in the study area,

S[ô] is the standard error of estimated overall accuracy

i = number of class types, four here.

W_i is the proportional area of each class, and Si is the standard deviation of each class.

Si = $\sqrt{Ui\ [1 - Ui]}$

The sample allocation for each land cover type in the satellites is shown in **Table 3.3**.

Table 3.3 Sample allocation for the satellites

Land cover type	Sentinel-2	Landsat-8 OLI	Landsat-7 ETM+
Protected areas	247	250	286
Built-Up areas	67	48	55
Agricultural areas	78	78	52
Water Bodies	12	11	12
Total samples	404	387	405

Random stratified sampling was performed in QGIS, and the error matrix and kappa-hat statistic were calculated for each satellite.

3.2.2 Spatio-temporal LULC transitions from 2016 to 2022

Landsat 8 OLI remotely sensed images, clipped to the shapefile of the study area, for 2016, 2019, and 2022 used in the study. The description of the data used in the study is shown in **Table 3.4**.

Table 3.4 Description of satellite imageries used for spatiotemporal LULC transitions (**Source:** USGS Earth Explorer)

Satellite	Sensor	Path/ Row	Date of Acquisition
Landsat 8	OLI/TIRS	148/38	19-05-2016, 12-05-2019 and 20-05-2022

In addition to this, ALOS-PALSAR DEM was used to create a drainage network for the major streams in the area. May usually has little or no rainfall in the study area, and all temporal images were selected for May, with a cloud percentage of less than ten per cent. Ancillary data comprised a Town and Country Planning Report, DEM, and statistical data from the Department of Economics and Statistics, Government of Himachal Pradesh, aiding in image classification and accuracy validation stages. The methodological framework adopted for studying spatio-temporal LULC transitions from 2016 to 2022 has been elucidated in **Fig. 3.3**.

3.2.2.1 Image Pre-processing

The temporal remotely sensed images of three years underwent a conversion process to obtain spectral radiance values. Atmospheric correction was then carried out using DOS within the SCP plugin in QGIS software. Subsequently, the images were merged into a mosaic, and a subset was generated using the municipal corporation limits shapefile of Dharamshala City.

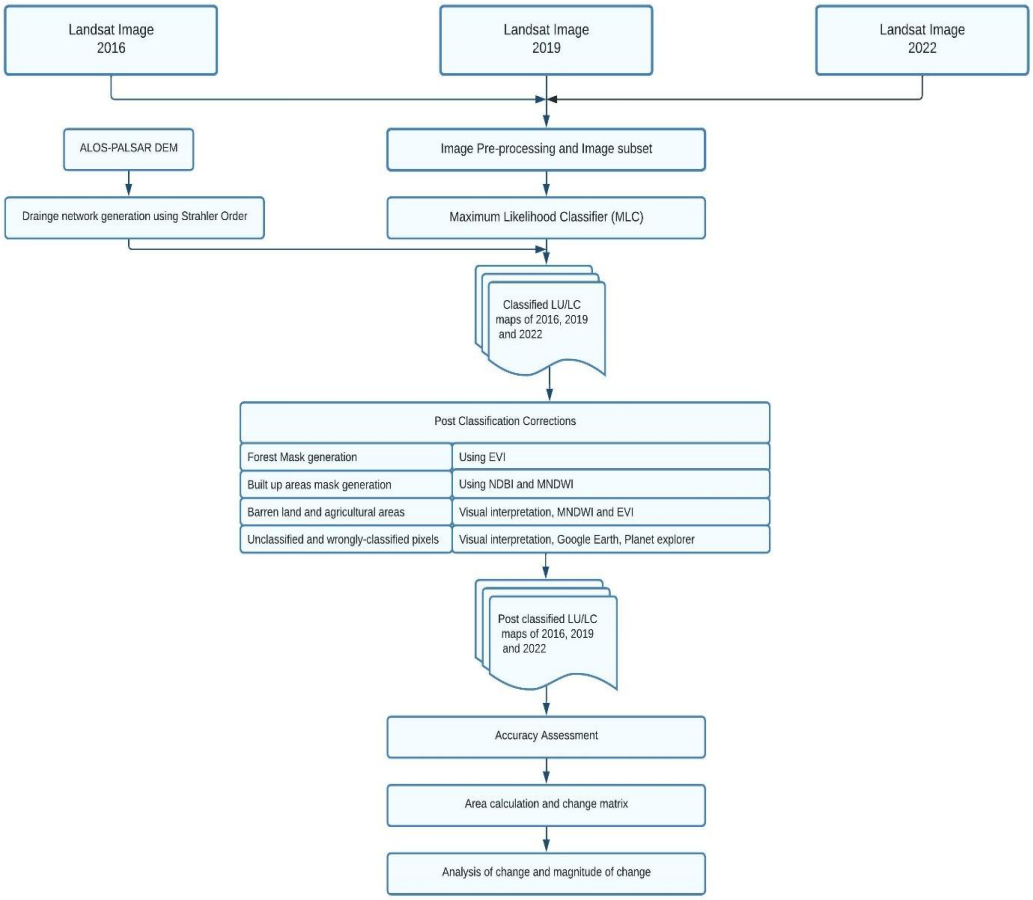

Fig. 3.3 Methodological workflow for LULC transitions

3.2.2.2 LULC classification

Various Land cover classification schemes are available, and a specific project's scope and demands govern the selection of land cover classes [18,43]. In this particular study, Modified Anderson's Land use land cover classification system was adopted to examine multi-temporal LULC changes in the region. [17], [24], [28], [43], and [126] used the Maximum Likelihood Classifier (MLC) for creating LULC maps in the Himalayan regions. The ancillary information from reliable sources and the author's acquaintance with the area under study were also helpful in classifying the area, Five LULC classes, viz. Protected Areas (PA), Agricultural areas (AA), Built-up areas (BA), Barren Land (BL), and water bodies (WB) were chosen, as shown in **Table 3.5**. The reason for including Forests and Tea plantations under the Category of Protected Areas was that both are protected entities under the legislation. The forests and tea plantations

were clubbed under PA due to legislative protection provided to them under Central and state rules, respectively.

Table 3.5 Delineation of LULC classes

LULC class	A broad description of the classes included
Protected areas (PA)	covers forest areas and tea plantations
Agricultural areas (AA)	Those areas represent crops
Built-up areas (BA)	Residential/ commercial establishments and roads
Barren land (BL)	Areas without vegetation, such as rocks, landslide zones, uncultivable area
Water bodies (WB)	Streams and lake

3.2.2.3 Post-classification corrections

The accuracy of MLC depends upon the training inputs and is a prerequisite for the normal distribution of data [37,158,159]. Thus, the post-classification accuracy improvement measures are imperative after the initial MLC [47]. Three spectral vegetation indices, namely, EVI, NDBI, and MNDWI, were used along with slope, aspect, and elevation raster layers generated from DEM. The image segmentation approach was also followed to improve the classification accuracy.

Most of the noises were in built-up areas and agricultural areas. The region's spectral characteristics of built-up areas and agricultural land were similar. MNDWI can remove built-up noises [70]. An integrated approach consisting of threshold values for EVI and MNDWI was used to create a built-up mask and underpin the agricultural areas. Image segmentation and DEM parameters like slope, aspect, and elevation were also used to create protected area masks. NDBI was used mainly for the built-up areas in tandem with EVI, as some of the built-up features were covered under thick forest cover, and thorough investigation was required with visual inspection and local knowledge of the region.

The spectral characteristics of rivers and built-up areas were also similar, and further, the rivers were covered under thick forest cover. DEM was used to create a drainage network for the rivers in the region.

3.2.2.4 Built-up area distribution trend and direction

LULC built-up maps for the years 2016, 2019, and 2022 were created using MLC, which utilizes the class statistics derived from labelled training samples and assigns each pixel to the most probable class membership given the pixel's spectral values and the statistical information of the classes. Thus, a LULC map consisting of two classes, built-up and non-built-up areas, was created.

The built-up dynamic index (k) measures the degree of change in built-up areas for a certain period [135] and is calculated using the formula in eq. (v)

$$k = \frac{U_b - U_a}{U_a} * \frac{1}{T} * 100 \quad \text{..... (v)}$$

U_b represents the land area of that specific LULC class in the succeeding year

U_a represents the land area of that specific LULC class in the preceding year

T refers to the time between preceding and succeeding year

3.2.2.5 Geo-spatial parameters

DEM comprises a gridded dataset of elevation values, where each pixel represents the height relative to a reference point. Elevation and slope are critical geophysical factors influencing urban sprawl. Elevation influences micro-climate, soil characteristics, and vegetation types, while slope affects settlement patterns [17]. Analyzing slope and elevation alongside satellite imagery offers valuable insights into urban sprawl dynamics. Areas with lower slopes and elevations tend to be more conducive to development and typically experience higher rates of urban sprawl [18].

Slope involves assessing the steepness or inclination of the terrain at each point on the Earth's surface. The inclination of the terrain to the horizontal plane is represented by the slope, which is then expressed as a percentage or in degrees. The slope is classified as gentle if less than and equal to 15%, moderate if it varies from 15-25%, and steep if greater than 25% [126]

Elevation is calculated by measuring the vertical distance between the Earth's surface and a reference point, usually the mean sea level.

3.2.2.6 Spatio-temporal Proximity near Streams

The proximity of built-up to natural streams may become a severe cause of concern in urban flooding scenarios [79]. The situation may become critical in Himalayan cities

due to extreme rainfall-induced flash floods, landslides, and cloud bursts. The built-up activities near the streams impact the geomorphological and hydrological characteristics, making these regions more vulnerable than before [5]. The anthropogenic activities and urbanization have been considered to be major reasons in Dharamshala for constricting the natural drainage of streams, thus causing more damage to life and property [21]. Spatio-temporal proximity analysis around the streams can help monitor and identify areas with such threats.

3.2.2.7 Accuracy assessment

The quality of thematic maps must be assessed qualitatively and meaningfully [2,3]. An optimum sample design for testing data is essential in determining the accuracy of classified maps [42]. The stratified random samples as shown in **Table 3.6** were selected based on the sampling design by Cochran, 1977.

Table 3.6 Sample size for spatiotemporal LULC transitions

	2016	2019	2022
LULC class	Area (km^2)	Area (km^2)	Area (km^2)
PA	232	218	209
AA	57	60	52
BA	38	65	93
BL	30	30	30
WB	20	20	20
Total	377	394	404

3.2.3 Modelling and simulation of LULC maps

3.2.3.1 Inputs

LULC maps for 2016 and 2019, which acted as independent variables for the modelling and simulation of future LULC maps, were used in the study. The approach for image pre-processing of the RS imageries of 2016 and 2019 has been described in **3.2.2.1 Image Pre-processing**. The LULC classification scheme as adopted in **3.2.2.2 LULC classification** was used and shown in **Table 3.5**.

The study utilizes LULC maps corresponding to 2016 and 2019 to examine the LULC transformations within the designated research area. The transition map is generated to depict the percentage variations observed across the five distinct land cover categories from 2016 to 2019.

For the spatial explicit CA model, each pixel must be assigned a particular LULC class. The independent variables used in the study included LULC maps for 2016 and 2019, as illustrated in **Section 3.2.2 Spatio-temporal LULC transitions from 2016 to 2022**. These LULC maps of 2016 and 2019 were used in the CA model. The driving factors included spatial variables and socio-economics variables, which have an essential role in deciding the trend and direction of LULC transitions in the study area [160]. The distance parameters covered under spatial variables encompass measurements from various features relevant to that area and responsible for LULC transitions. The distance parameters are evaluated from Euclidean distance [88,109,144]. Apart from spatial variables, physical attributes, including slope and elevation, derived from DEM can also provide relevant neighbourhood associations to help evaluate the transitional probability surrounding the focal cell. All these driving factors are converted into raster format before being imported into the MOLUSCE plugin of QGIS.

However, the LULC transitions in a particular area are stochastic and generally non-linear [89,100]. The Artificial Neural Network (ANN) model can include non-linear relationships between the driving factors and, subsequently, facilitate the establishment of transition probabilities for the CA model. Thus, physical, spatial and socio-economic variables were included in the learning stage of the ANN model to simulate the impact of driving factors on LULC transitions. Forecasting conversion probabilities from the present LULC to a future state involves considering the present LULC category assigned to a particular pixel and neighbouring cells' state.

With the integration of the CA-ANN model and inclusion of physical, spatial and socio-economic driving factors, the simulation will be conducted to create the LULC map 2022. Subsequently, leveraging the model's performance based on accuracy metrics, the predictions are extrapolated for 2025 and 2040.

3.2.3.2 Evaluating correlation and transition analysis

Different combinations of variables, including distance from built-up areas (DBA), distance from roads (DR), distance from the town centre (DTC), distance from streams (DST), distance from Agricultural areas (DAA), Aspect (AS), elevation (EL) and slope (SL) were performed and their accuracy checked to forecast land LULC map for 2022. **Table 3.7** shows the different combinations performed, and the best accuracy was achieved by considering five driving factors in S. No. 4, indicating substantial agreement between the simulated and LULC map with an accuracy of 86.83%. This suggests that the chosen explanatory variables significantly influenced the prediction of LULC classes.

Table 3.7 Simulation results for different combinations of dependent variables

S. No.	Dependent variables combination	Accuracy (%)	Kappa
1	DBA, DR, EL, SL, AS, DST	86.29	0.77
2	DR, SL, DST, AS, EL	86.77	0.77
3	DAA, AS, DBA, EL, SL, DST, DR	86.62	0.77
4	DBA, DTC, EL, SL, DST	86.83	0.77

The correlation between the dependent variables was assessed using the Cramer Coefficient, which is well-suited for contingency tables larger than 2x2. Results range from 0 to 1, with higher values indicating stronger correlations among the dependent variables. A value exceeding 0.15 signifies significant explanatory power of the variables [110]. The values calculated using this index are shown in **Table 3.8**.

The LULC transitions from 2016 to 2019 that occurred in the study areas using LULC maps of 2016 and 2019 are illustrated in

Table 3.9. As presented in **Table 3.10**, the transition matrix facilitates the analysis and comprehension of temporal changes within the region. Along the diagonal of matrix, the values represent the degree of class stability, indicating how consistently specific land cover categories remain over time. The values near to 1 signify more dominance

of stable class and vice-versa. Similarly, the off-diagonal entries represent magnitude of transitions occurring in the respective classes.

Table 3.8 Dependent variables with Cramer's V

	DBA	DR	DTC	EL	SL	DST
DBA	-	0.3475	0.1284	0.2131	0.314	0.1929
DR	-	-	0.2599	0.006	0.2382	0.3653
DTC	-	-	-	0.2878	0.2321	0.4231
EL	-	-	-	-	0.5143	0.4029
SL	-	-	-	-	-	0.366
DST	-	-	-	-	-	-

Table 3.9 LULC transition from 2016 to 2019

LULC class	2016 (sq km)	2019 (sq km)	Δ (sq km)	2016 (%)	2019 (%)	Δ (%)
PA	29.37	26.26	-3.11	69.1	61.79	-7.31
AA	6.88	6.97	0.09	16.19	16.41	0.22
BA	4.41	7.51	3.10	10.38	17.66	7.28
BL	0.27	0.19	-0.08	0.64	0.45	-0.19
WB	1.57	1.57	0.00	3.69	3.69	0

Table 3.10 Transition Probability matrix

	PA	AA	BA	BL	WB
PA	0.852	0.073	0.073	0.001	0.0000
AA	0.174	0.691	0.133	0.002	0.0000
BA	0.000	0.000	1.000	0.000	0.0000
BL	0.129	0.252	0.106	0.513	0.0000
WB	0.000	0.000	0.000	0.000	0.0000

The explanatory maps/ driving factors so chosen in the study are shown in **Fig. 3.4**. The predictive modelling using the ANN-CA integrated model for future maps of 2025 and

2040 was achieved after undergoing 2 and 7 iterations, respectively.

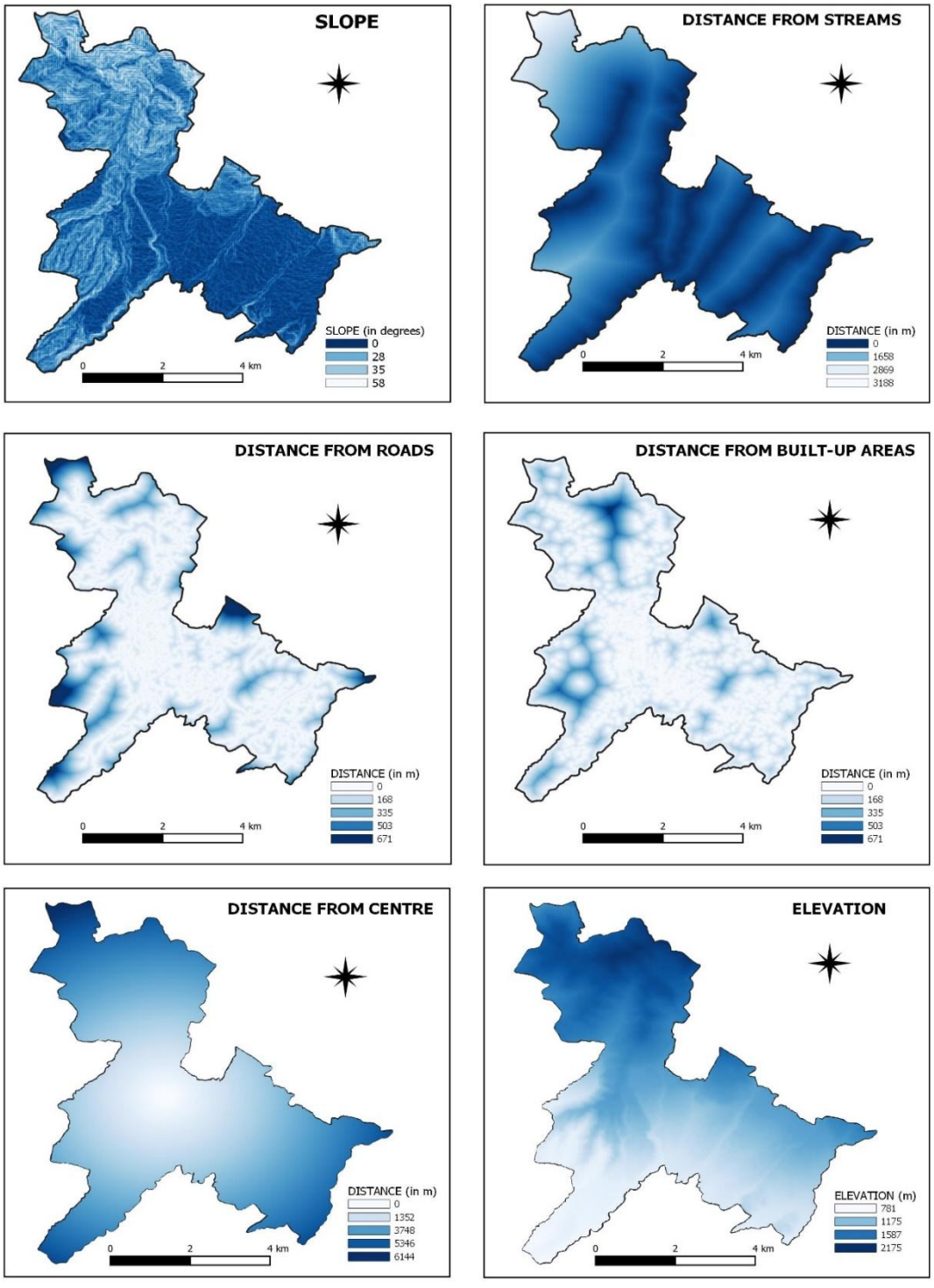

Fig. 3.4 Explanatory Map: Slope, Distance from streams, Distance from roads, Distance from built-up areas, Distance from centre and elevation

3.2.3.3 Transition Potential Modeling

The evolution of any area involves intricate dynamics influenced by both spatial and temporal variations, as well as the driving forces underlying these transformations [34,89]. Although the LULC transitions are complex and dynamic, they also follow a particular pattern [161], and Machine learning algorithms hold significant utility in discerning and identifying these patterns [4,105]. The transition function governing changes in LULC categorizes the association between dependent variables and the likelihood of LULC conversion, determining whether cells will transition to specific classifications. The model employs a multi-layer feed-forward approach trained with Error Back Propagation, where network parameters are adjusted based on output error requirements [109,162,163]. The ANN learning curve is shown in **Fig. 3.5**.

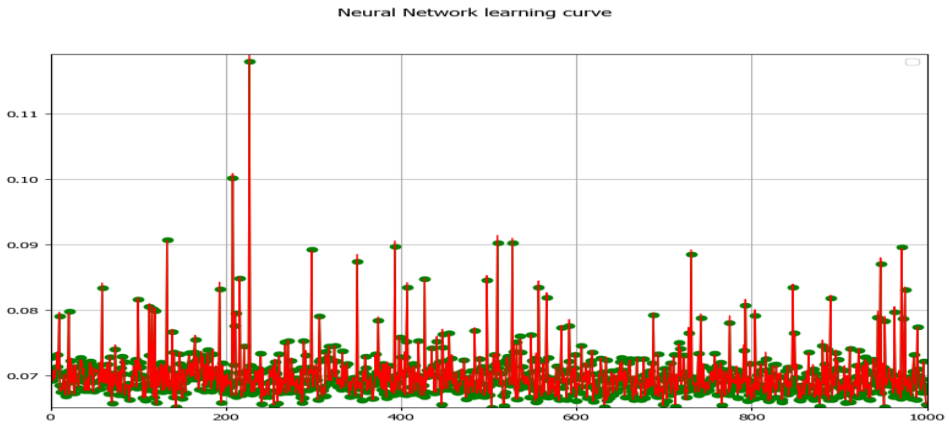

Fig. 3.5 ANN Learning curve

3.2.3.4 Validation

In LULC simulation, an Error matrix is a widely employed method for assessing results [164]. In this matrix, each row represents the predicted category, and each column represents the actual category, highlighting differences in the cells, commonly depicted as errors expressed in percentages or areas [2,88]. OA and kappa hat were used to validate LULC maps. In assessing overall accuracy, only the confusion matrix's diagonal elements are considered. However, the kappa hat extends its consideration to non-diagonal elements, incorporating both omission and commission errors. [2].

CHAPTER 4
RESULTS AND DISCUSSION

4.1 Comparison of satellite data–products

One study objective was to determine which satellite data provided the best results for urbanization studies in Dharamshala. The four land cover types were chosen for this purpose, as these were the major land cover types supposed to be impacted by urbanization. The inconsistency in the thematic maps derived from the different satellites was evident from the classified results. The land cover classification of the three satellites is shown in **Fig. 4.1**. The land cover type, in percentage, is shown in **Fig. 4.2**.

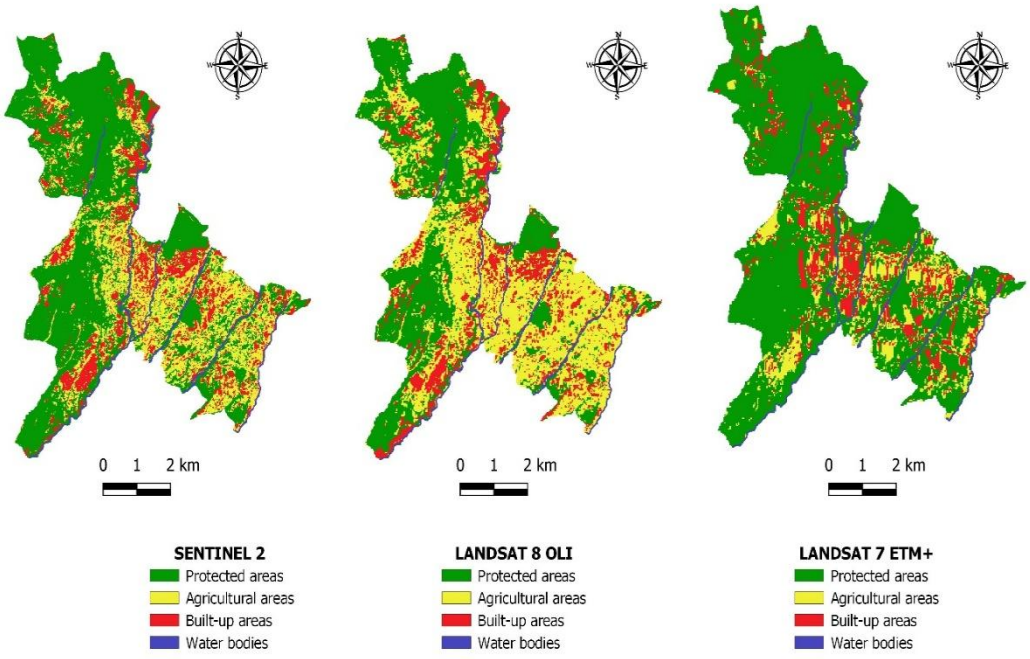

Fig. 4.1 LULC classification results using three satellite data products

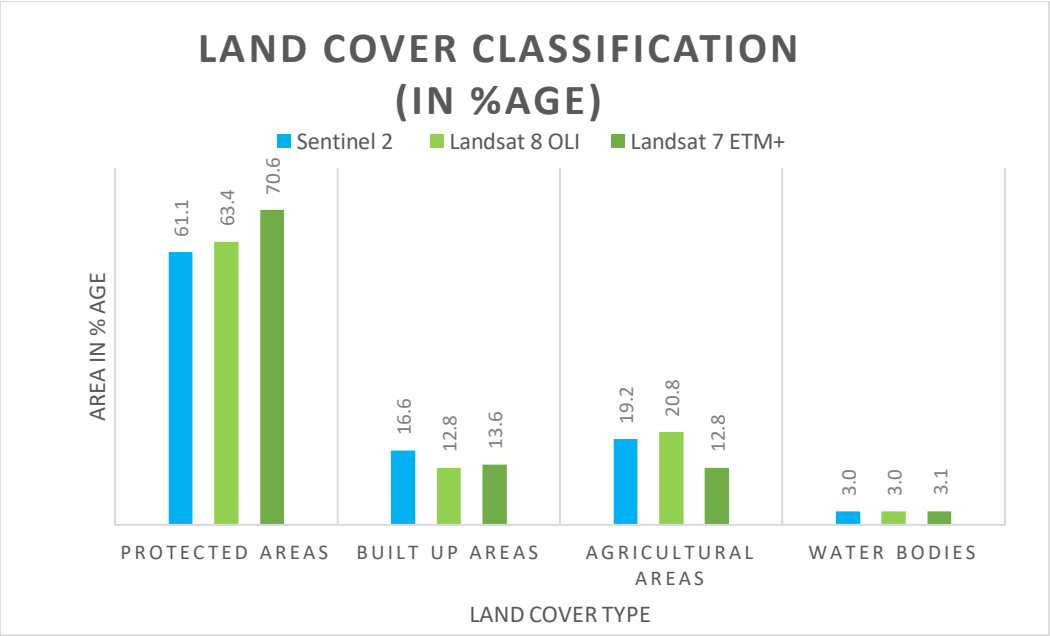

Fig. 4.2 Land cover classification of each land cover type (in %age)

The error matrix for Sentinel 2 classified imagery, Landsat 8 OLI classified imagery, and Landsat 7 ETM+ classified imagery after adopting post-classification correction measures are shown in **Table 4.1**, **Table 4.2** and **Table 4.3,** respectively.

Table 4.1 Error matrix for LULC map using RS imagery from Sentinel 2

	Reference data						
Classified	PA	BA	AA	WB	Total	PrA (%)	UA (%)
PA	205	12	29	1	247	97.6	83.0
BA	3	56	7	1	67	73.7	83.6
AA	2	8	68	0	78	62.8	87.2
WB	0	0	4	8	12	80.4	66.7
Total	210	76	108	10	404		
	Overall accuracy	83.40 %					
	Kappa hat	0.72					

Table 4.2 Error matrix for LULC map using RS imagery from Landsat 8 OLI

	Reference data						
Classified	PA	BA	AA	WB	Total	PrA (%)	UA (%)
PA	204	18	28	0	250	94.6	81.6
BA	2	35	11	0	48	59.0	72.9
AA	8	7	62	1	78	61.7	79.5
WB	1	0	1	9	11	90.2	81.8
Total	215	60	102	10	387		
		Overall accuracy	80.06 %				
		Kappa hat	0.65				

Table 4.3 Error matrix for LULC map using RS imagery from Landsat 7 ETM+

	Reference data						
Classified	PA	BA	AA	WB	Total	PrA (%)	UA (%)
PA	223	32	29	2	286	97.38	77.97
BA	5	31	19	0	55	40.22	56.36
AA	1	13	38	0	52	43.12	73.08
WB	0	1	2	9	12	82.37	75
Total	229	77	88	11	405		
		Overall accuracy [%]	74.32				
		Kappa hat	0.53				

It was evident that there was significant inconsistency in the results. The overall accuracy for Sentinel 2, Landsat 8 OLI, and Landsat 7 ETM+ was 83.40%, 80.06%, and 74.32%, respectively, while Kappa hat was 0.72, 0.65, and 0.53, respectively, as found out in **Table 4.1**, **Table 4.2** and **Table 4.3**, respectively. The study used the same methodology for a similar area but used different satellite data. The inconsistency in classifying the land cover type is evident in the three satellite data chosen for the study. The results indicate significant variation in the thematic maps produced from the different satellite sources.

The OA, Kappa hat, Producer accuracy (PA) and user accuracy (UA) were found to be maximum in Sentinel 2 compared to Landsat 8 OLI and Landsat 7. PA can be used as an indicator of omission error, while UA can be used as an indicator of commission

error. The significant land cover type for urbanisation studies, built-up areas, had the best PA and UA from the Sentinel-2 data product. A substantial variation of 15% in PA and 11% in UA for Built-up areas was found in Sentinel-2 and Landsat 8. The variation was 19% in PA and 27% in UA for the built-up land cover type in the classified maps of Sentinel-2 and Landsat 7, despite employing a consistent methodology for land cover classification across all satellite data products. A similar analysis could be performed for each land cover type depending upon a specific land cover type of interest in a particular study.

The research findings and accuracy metrics indicate that Sentinel-2 satellite imagery is highly suitable for this region's urbanisation studies. The spatial resolution proves especially advantageous in discerning the built-up areas, as the hill architecture promotes vertical expansion rather than lateral expansion due to topographical constraints. In contrast, the coarser spatial resolution of 30m found in Landsat 7 and Landsat 8 may result in mixed land cover classes within a single 30m x 30m grid, leading to a higher potential for errors in classification. Additionally, the Scan Line errors present in Landsat 7 resulted in low accuracy due to the use of interpolation to fill gaps or no-data values. These limitations of Landsat 7 were very significant as the study area was small, leading to misleading results.

Another important finding from the research was that Landsat 7 and Landsat 8 performed better than Sentinel 2 in classifying the water bodies, as evidenced by PA and UA. The reason for this could be attributed to the fact that they both consider a 30x30 m grid and the chances of misclassification being less as the water bodies cover more area laterally. However, in finer spatial resolution, they may be misclassified into other land cover types owing to the finer spatial resolution. The agricultural areas and reserved/ protected areas (illegal encroachments) have more probability of transition into built-up regions; thus, it becomes imperative that the other land cover types (apart from urban areas) are also appropriately classified to understand land cover change dynamics and suggest intervention strategies.

The findings necessitate using multiple satellite data in urban studies, and the best satellite source and a classification algorithm for achieving good classification accuracy and improving the quality and applicability of the produced thematic map are proposed. Satellite imagery having finer spatial resolution may not always give the best results for studying a phenomenon or trend in an area [116]. A significant variance was observed in LULC classification results from the different satellites, justifying the need to choose a reliable satellite data product. The satellite sensor characteristics, spatial, spectral, radiometric and temporal resolution, bandwidth, mode of image acquisition, etc., may differ for the satellites and thus impact the quality of the data product, affecting the image classification.

4.2 Spatio-temporal LULC transitions from 2016 to 2022

The multi-temporal land use land cover classified map for the five land cover types obtained after Post classification corrections are shown in **Fig. 4.3**. Confusion matrix and non-parametric metric kappa hat have been used by the researchers for the accuracy assessment of classified maps [2,42]. The error matrix computed for 2016, 2019, and 2022 is shown in **Table 4.4**, **Table 4.5** and **Table 4.6**, respectively.

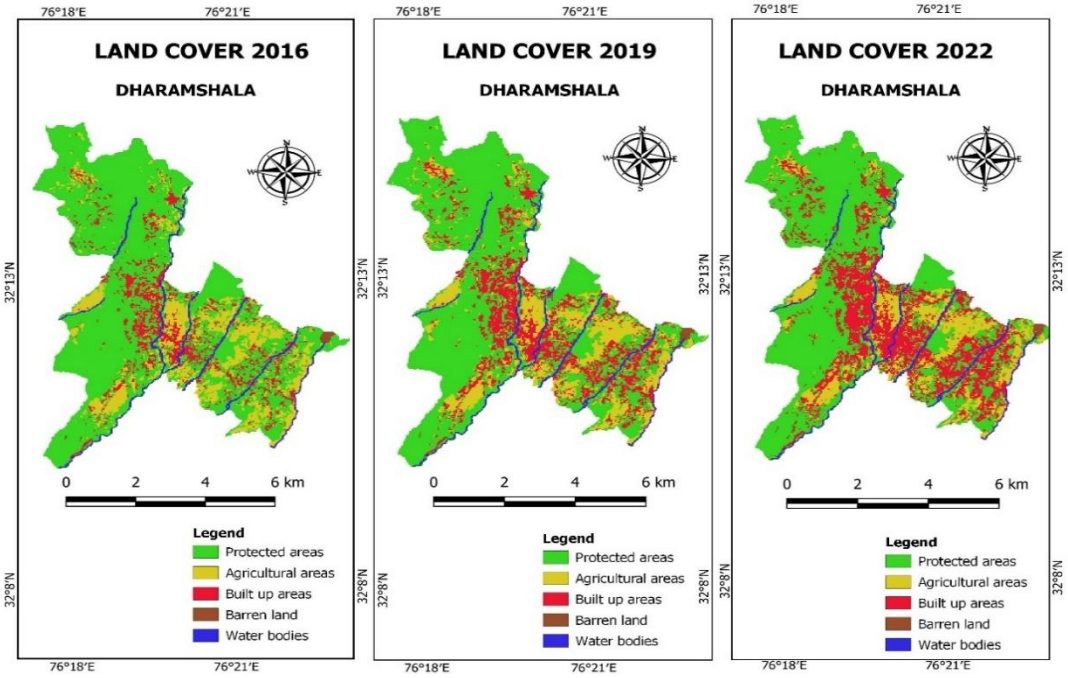

Fig. 4.3 LULC map of Dharamshala city for 2016, 2019 and 2022

Table 4.4 Error matrix of LULC map 2016

	Reference data							
Classified	PA	AA	BA	BL	WB	Total	PrA (%)	UA (%)
PA	204	12	15	1	0	232	97.1	87.9
AA	3	49	4	1	0	57	77.8	86.0
BA	2	1	34	0	1	38	63.0	89.5
BL	1	1	1	27	0	30	93.1	90.0
WB	2	0	0	0	18	20	94.7	90.0
Total	210	63	54	29	19	377		
		Overall accuracy (%)	88.06					
		Kappa hat	80.40					

Table 4.5 Error matrix of LULC map 2019

	Reference data							
Classified	PA	AA	BA	BL	WB	Total	PrA (%)	UA (%)
PA	188	18	12	0	0	218	96.9	86.2
AA	0	56	4	0	0	60	65.9	93.3
BA	3	8	54	0	0	65	77.1	83.1
BL	2	1	0	27	0	30	100.0	90.0
WB	1	2	0	0	17	20	100.0	85.0
Total	194	85	70	27	17	393		
		Overall accuracy (%)	87.02					
		Kappa hat	80.23					

Table 4.6 Error matrix of LULC map 2022

	Reference data							
Classified	PA	AA	BA	BL	WB	Total	PrA (%)	UA (%)
PA	190	11	7	1	0	209	97.4	90.9
AA	1	51	0	0	0	52	72.9	98.1
BA	2	7	82	1	1	93	90.1	88.2
BL	1	0	2	27	0	30	93.1	90.0
WB	1	1	0	0	18	20	94.7	90.0
Total	195	70	91	29	19	404		
		Overall accuracy (%)	91.09					
		Kappa hat	86.67					

4.2.1 LULC statistics from 2016, 2019 and 2022

The LULC change matrix for 2016-2019, 2019-2022, and 2016-2022 is shown in **Table 4.7**, **Table 4.8** and **Table 4.9** respectively. The values in bold indicate no transition or stability in those classes for that period. The LULC distribution of classes, according to elevation, for the years 2016, 2019, and 2022 are shown in **Table 4.10**, **Table 4.11** and **Table 4.12**, respectively. The thematic map showing the from-to conversion of LULC temporally is demonstrated in **Fig. 4.4**.

Table 4.7 LULC transition matrix from 2016 to 2019

2019 (area, in km^2)	2016 (area, in km^2)						
	LULC Class	PA	AA	BA	BL	WB	Grand Total
	PA	**25.03**	2.15	2.15	0.04	0.00	29.36
	AA	1.19	**4.76**	0.92	0.02	0.00	6.88
	BA	0.00	0.00	**4.41**	0.00	0.00	4.41
	BL	0.04	0.07	0.03	**0.14**	0.00	0.27
	WB	0.00	0.00	0.00	0.00	**1.57**	1.57
	Grand Total	26.26	6.97	7.51	0.19	1.57	42.49

Table 4.8 LULC transition matrix from 2019 to 2022

2022 (area, in km^2)	2019 (area, in km^2)						
	LULC Class	PA	AA	BA	BL	WB	Grand Total
	PA	**22.90**	0.83	2.47	0.07	0.00	26.26
	AA	1.41	**4.87**	0.61	0.08	0.00	6.97
	BA	0.00	0.00	**7.51**	0.00	0.00	7.51
	BL	0.02	0.02	0.01	**0.14**	0.00	0.19
	WB	0.00	0.00	0.00	0.00	**1.57**	1.57
	Grand Total	24.33	5.72	10.59	0.29	1.57	42.49

Table 4.9 LULC transition matrix from 2016 to 2022

2022 (area, in km^2)	2016 (area, in km^2)					
	LULC Class	PA	AA	BA	BL	WB	Grand Total
	PA	**23.27**	1.51	4.49	0.09	0.00	29.36
	AA	1.05	**4.16**	1.63	0.05	0.00	6.88
	BA	0.00	0.00	**4.41**	0.00	0.00	4.41
	BL	0.01	0.05	0.06	**0.16**	0.00	0.27
	WB	0.00	0.00	0.00	0.00	**1.57**	1.57
	Grand Total	24.33	5.72	10.59	0.29	1.57	42.49

Table 4.10 Land use/ Land cover distribution elevation-wise in 2016

LULC	<1000m	1000-1500m	1500-2000m	>2000m
Protected areas	2.95	16.30	9.26	0.93
Agricultural areas	0.46	5.77	0.64	0.01
Built up areas	0.14	3.70	0.57	-
Barren land	0.01	0.22	0.04	-
Water bodies	0.21	1.17	0.14	-

Table 4.11 Land use/ Land cover distribution elevation-wise in 2019

LULC	<1000m	1000-1500m	1500-2000m	>2000m
Protected areas	2.94	13.71	8.76	0.93
Agricultural areas	0.40	5.78	0.79	0.01
Built up areas	0.21	6.34	0.95	0.01
Barren land	0.02	0.17	0.004	-
Water bodies	0.21	1.17	0.14	-

Table 4.12 Land use/ Land cover distribution elevation-wise in 2022

LULC	<1000m	1000-1500m	1500-2000m	>2000m
Protected areas	2.84	11.90	8.73	0.92
Agricultural areas	0.35	4.88	0.48	0.01
Built up areas	0.34	9.00	1.25	0.01
Barren land	0.03	0.04	0.04	-
Water bodies	0.21	1.17	0.14	-

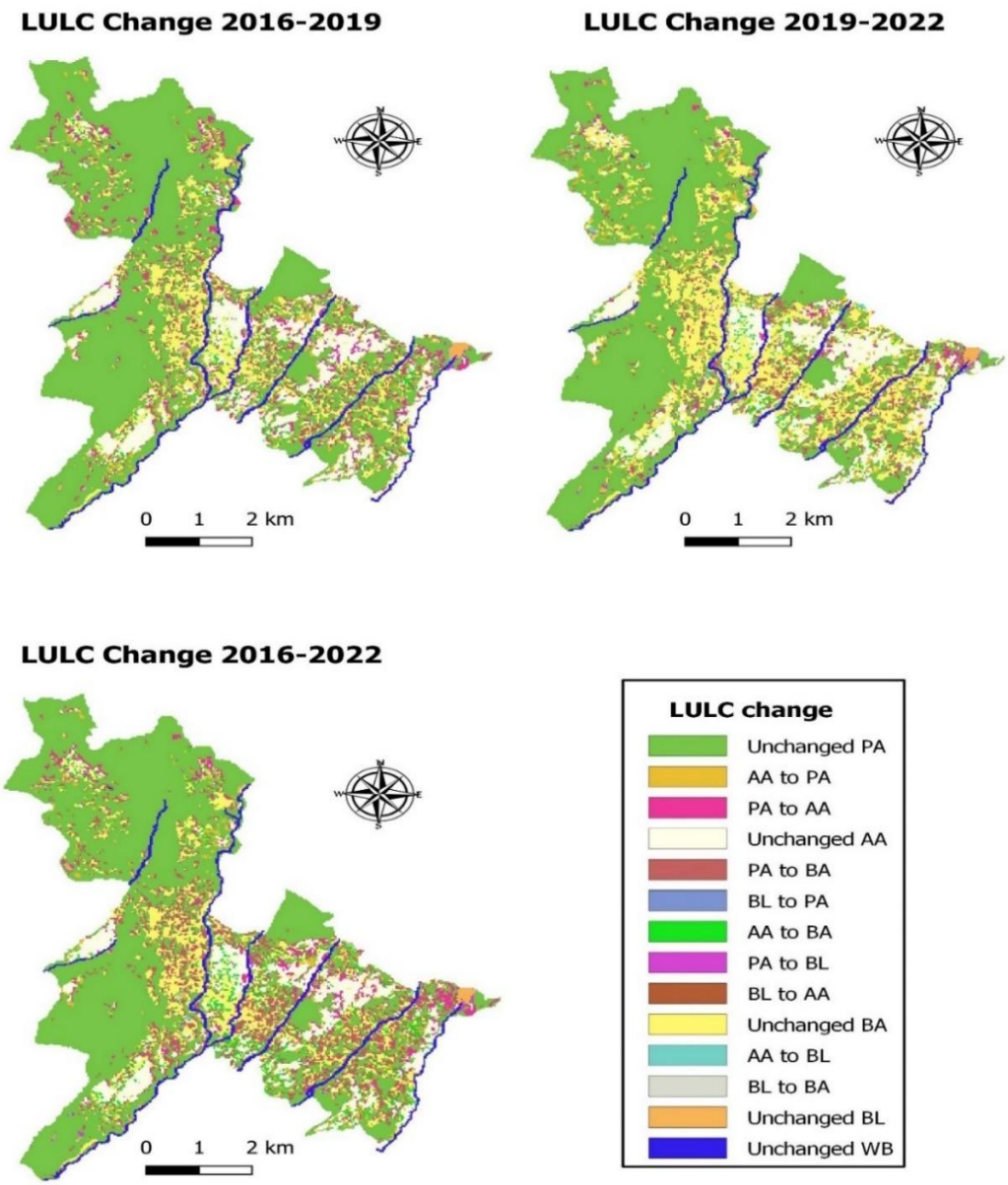

Fig. 4.4 Temporal LULC transitions in the study area

4.2.2 LULC trend from 2016 to 2019

From 2016 to 2019, the maximum transition was observed in Protected Areas. Around 2.15 km^2 of the Protected areas was converted into agricultural and built-up areas. The decrease in protected areas was maximum at 1000-1500m elevation. This signifies the population shift towards higher heights as the region below 1000 m is already stressed

with built-up areas and agricultural areas. The habitation is now moving towards higher heights in search of agricultural land and accommodation; thus, the areas protected by law are seeing encroachments. Around 1.19 km^2 of the agricultural area was converted into protected areas, which could be due to afforestation/ plantation drives and anti-encroachment drives conducted by the Forest Department. The increasing trend of agriculture was witnessed at an elevation of 1500-2000m. Around 0.92 km^2 of the agricultural area was converted into built-up areas. The barren land was predominantly converted into agricultural areas.

4.2.3 LULC trend from 2019 to 2022

Similar to the pattern observed in built-up areas, from 2016 to 2019, around 2.5 km^2 of Protected areas were converted into built-up areas. Elevations of 1000-1500m remained a critical spot for Protected and agricultural areas, with significant transitions occurring in this elevation. The built-up areas increased at an elevation of 1500-2000m, thus justifying the trend of the population shift towards higher areas, as observed from 2016 to 2019. Around 1.4 km^2 of the agricultural area was converted into Protected Areas, while 0.6 km^2 was converted into built-up areas.

4.2.4 Spatio-temporal built-up area Analysis

The increase in built-up areas during the study period is shown in **Fig. 4.5**. The built-up dynamic index calculated using eq. (iv) is shown in **Table 4.13** and was found to be 23.4, 13.7, and 23.3 for 2016-2019, 2019-2022 and 2016-2022, respectively. The study area substantially transformed non-built-up regions into built-up areas from 2016 to 2022. A noticeable reduction from 2019 to 2022 could be attributed to COVID-19-related restrictions, which otherwise might have resulted in a more significant escalation of built-up areas.

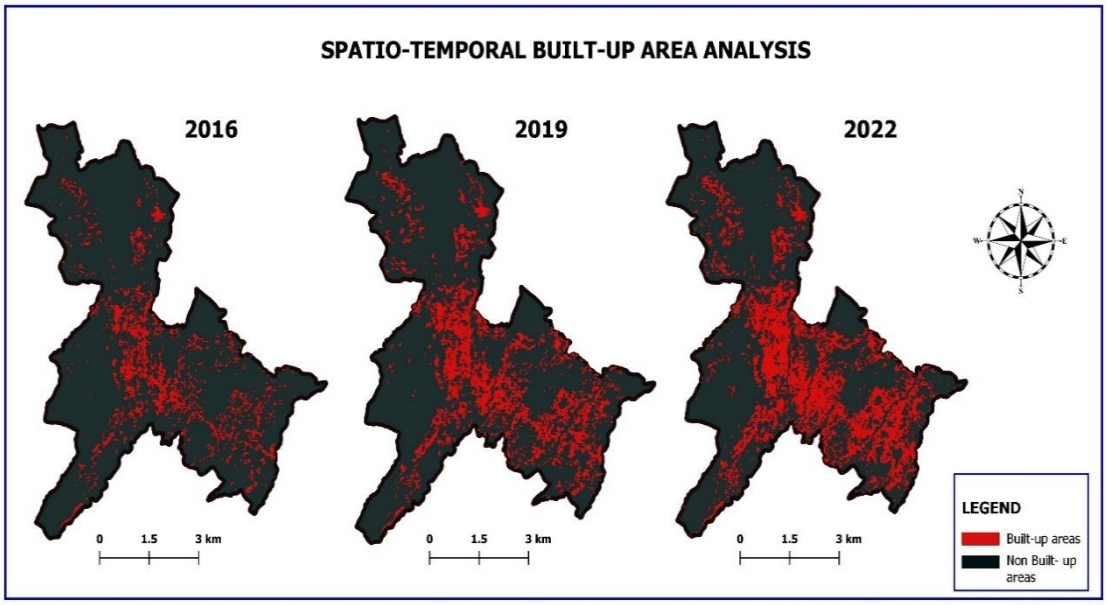

Fig. 4.5 Spatio-temporal built-up area analysis

Table 4.13 Built-up dynamic index calculation for different years

LULC	Area in km^2			Built-up dynamic Index (k)		
Category	2016	2019	2022	2016-2019	2019-2022	2016-2022
Built up areas	4.4	7.5	10.6	23.4	13.7	23.3

4.2.5 Geo-spatial parameters analysis

The urban sprawl during the study period according to elevation and slope is shown in **Fig. 4.6** and **Fig. 4.7**, respectively. The LULC built-up area distribution according to elevation and slope is shown in **Table 4.14** and **Table 4.16**, respectively, signifying a higher concentration of built-up areas at altitudes less than 1500 m and on slopes less than 25%.

The urban sprawl increase in percentage, elevation and slope criteria is shown in **Table 4.15** and **Table 4.17**, respectively. Agricultural areas lying predominantly in lower elevations, less than 1500 m, and slopes less than 25% have been converted into built-up regions with a growth rate of around 140% in each, signifying the shift in occupation of the city-dweller and the study area rapidly turning into a concrete jungle. An increase in built-up areas at higher altitudes (more than 1500m) and steep slopes (>25%) is a

severe cause of concern, given the fact that most of these regions are covered under forests. The urban sprawl in these regions indicates illegal encroachments.

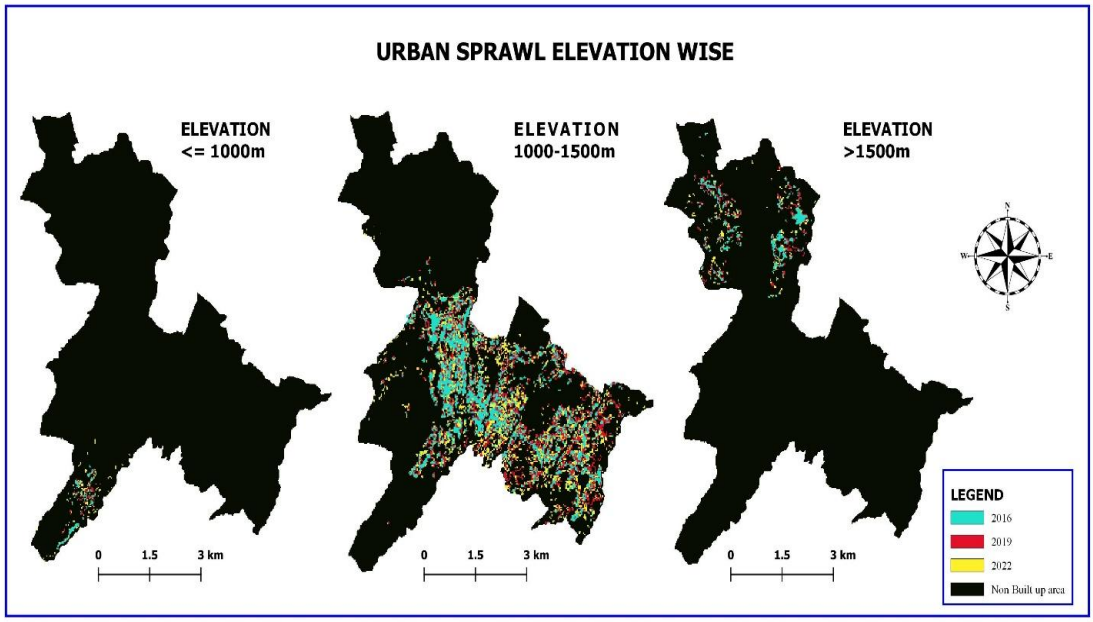

Fig. 4.6 Urban sprawl elevation wise

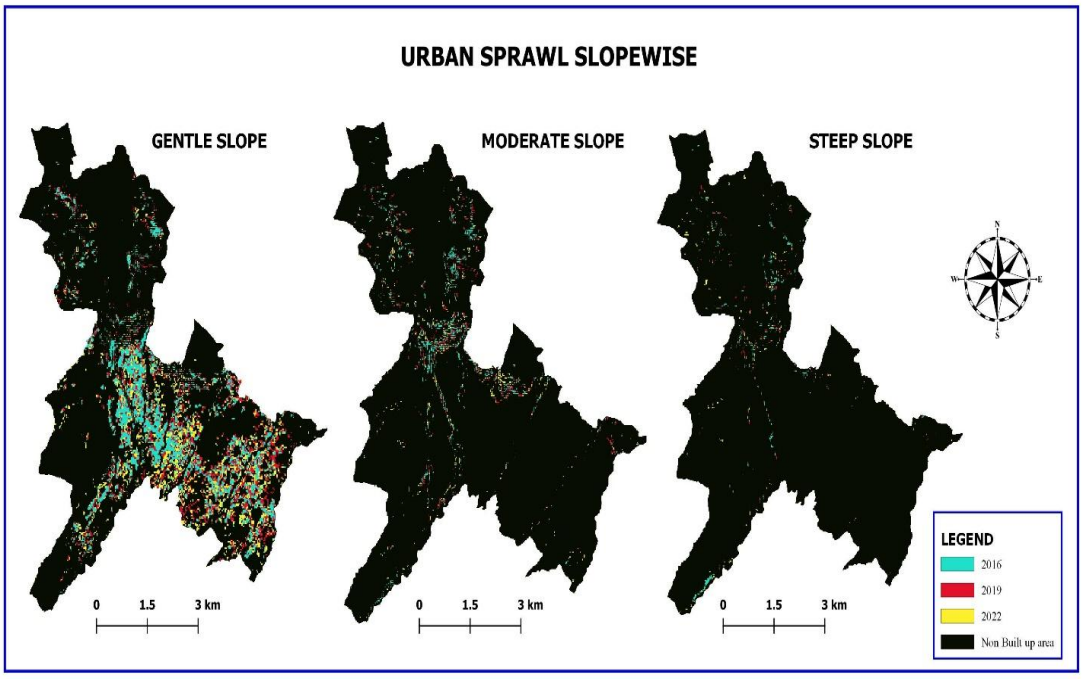

Fig. 4.7 Urban Sprawl slopewise

Table 4.14 LULC built-up area distribution as per elevation

	LULC Built up area distribution as per elevation (in metres)		
Year	≤ 1000m	1000-1500m	> 1500m
2016	0.14	3.70	0.57
2019	0.21	6.34	0.96
2022	0.34	9.00	1.26

Table 4.15 Urban sprawl as per elevation

Year (from-to)	LULC Built up growth rate (%) distribution (Elevation)		
	≤ 1000m	1000-1500m	> 1500m
2016-2019	51.5	71.2	68.2
2019-2022	61.9	42.0	31.3
2016-2022	145.3	143.0	120.8

Table 4.16 LULC built-up area distribution as per slope

	LULC Built up area distribution as per slope (in percentage)		
Year	Gentle Slope	Moderate Slope	Steep Slope
2016	3.66	0.55	0.19
2019	6.23	0.94	0.30
2022	8.72	1.35	0.46

Table 4.17 Urban sprawl as per slope

	LULC Built up growth rate (%) distribution (Slope)		
Year (from-to)	Gentle Slope	Moderate Slope	Steep Slope
2016-2019	70.2	70.9	57.9
2019-2022	40.0	43.6	53.3
2016-2022	138.3	145.5	142.1

4.2.6 Spatio-temporal proximity analysis near Streams

The built-up area distribution at a distance of 100m from the streams is shown in **Fig. 4.8** Built-up distribution near the streams, and the built-up growth rate calculated is shown in **Table 4.18** Urban Sprawl near streams An increase of 23.3% from the year 2016 to 2022 was witnessed in the built-up areas near the streams, indicating a

possibility of a major catastrophe in the future. Increased built-up activities near the streams have severe implications for the aquatic and ecological balance of the region, thus impacting the overall socio-ecological process. The urban sprawl near streams also requires attention from the risk arising due to landslides and loss of life and property on account of cloud-burst conditions in the region.

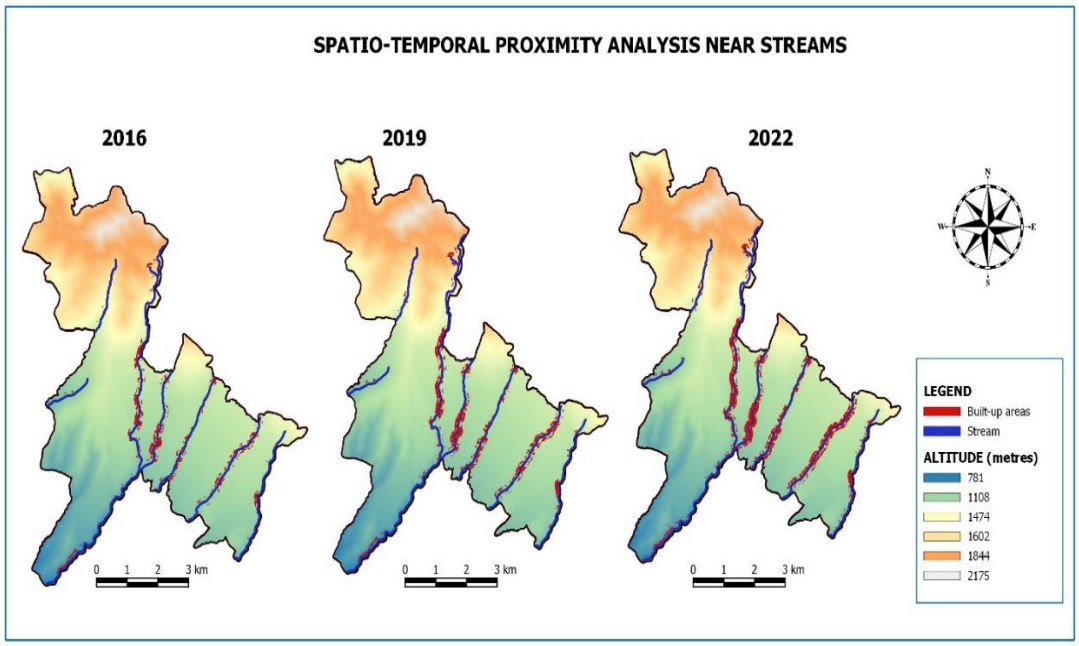

Fig. 4.8 Built-up distribution near the streams

Table 4.18 Urban Sprawl near streams

LULC	Area in km^2			Built up growth rate near streams (Distance ≤ 100m)		
Category	2016	2019	2022	2016-2019	2019-2022	2016-2022
Built-up areas at a distance ≤ 100 m from streams	4.4	7.5	10.6	23.4	13.7	23.3

4.2.7 Overall gain and loss

Table 4.9 indicates the gain and loss for the period 2016 to 2022 in Dharamshala city. The corresponding percentage changes occurring in the study site for the period are

shown in **Fig. 4.9**. The built-up areas increased by 140% from 2016 to 2022. Around 4.5 km^2 of protected areas and 1.6 km^2 of the agricultural areas were converted into built-up areas. Also, an escalation at the rate of 7% has been witnessed in barren land since 2016, and the maximum area of barren land has been transformed into built-up areas. Around 1.5 km^2 of the Protected areas was converted into agricultural areas.

The escalation of built-up areas and expansion of barren land between 2016 and 2022 can be predominantly attributed to the rising human population and the influx of tourists into the city. This surge has amplified the demand for residential and commercial spaces, exerting significant pressure on protected areas and agricultural lands. Consequently, these areas have experienced substantial degradation during this period, reflecting the direct impact of anthropogenic activities on the landscape.

The region below an altitude of 1500 m emerged as the most critical area experiencing significant changes in land use and land cover (LULC) classes. Notably, built-up areas, agricultural lands, and protected areas exhibited the most pronounced transitions within this zone. This phenomenon can be attributed to several factors, including improved transportation infrastructure, enhanced road connectivity, favourable climatic conditions conducive to habitation and agriculture, proliferation of commercial establishments, and higher population density in this region. Conversely, higher altitude areas are less susceptible to urban sprawl due to terrain complexities and geographical constraints.

These changes reflect the influence of human activities and socio-economic factors on the landscape, indicating the rapid urbanization of this hill station. Additionally, the findings suggest widespread encroachment and lax enforcement of regulations. The increased tourist inflow, higher socio-economic activities, and growing population can be the main drivers of the LULC change in Dharamshala city.

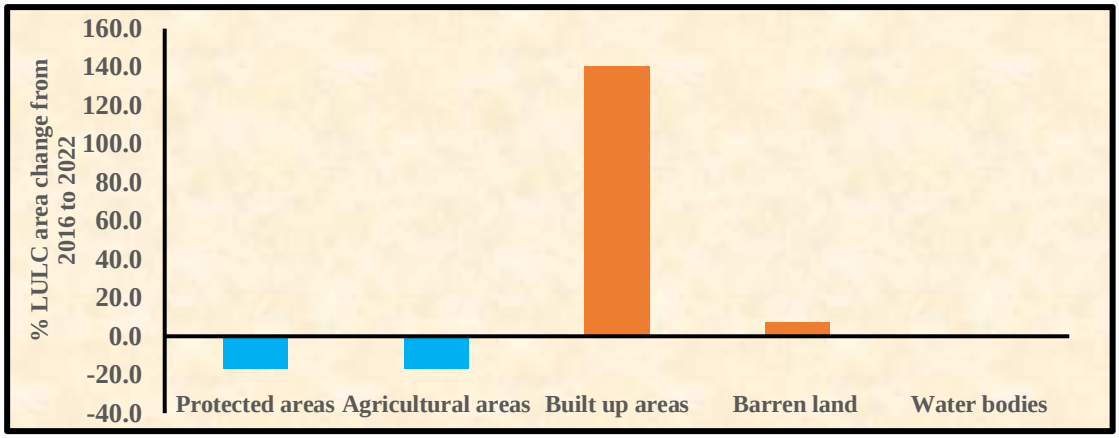

Fig. 4.9 Percentage Change in areas of LU/LC classes of Dharamshala city

4.3 Modelling and simulation of LULC maps

The future LULC maps produced through the integrated use of prediction models can prove helpful in understanding urban sprawl trends. Utilizing CA modelling, LULC maps for 2025 and 2040 were generated, incorporating six key driving factors: DBA, DR, DTC, EL, SL, and DST. **Fig. 4.10** demonstrates the future LULC maps for 2025 and 2040, illustrating the spatial distribution of different LULC classes and can aid informed decision-making and urban planning processes.

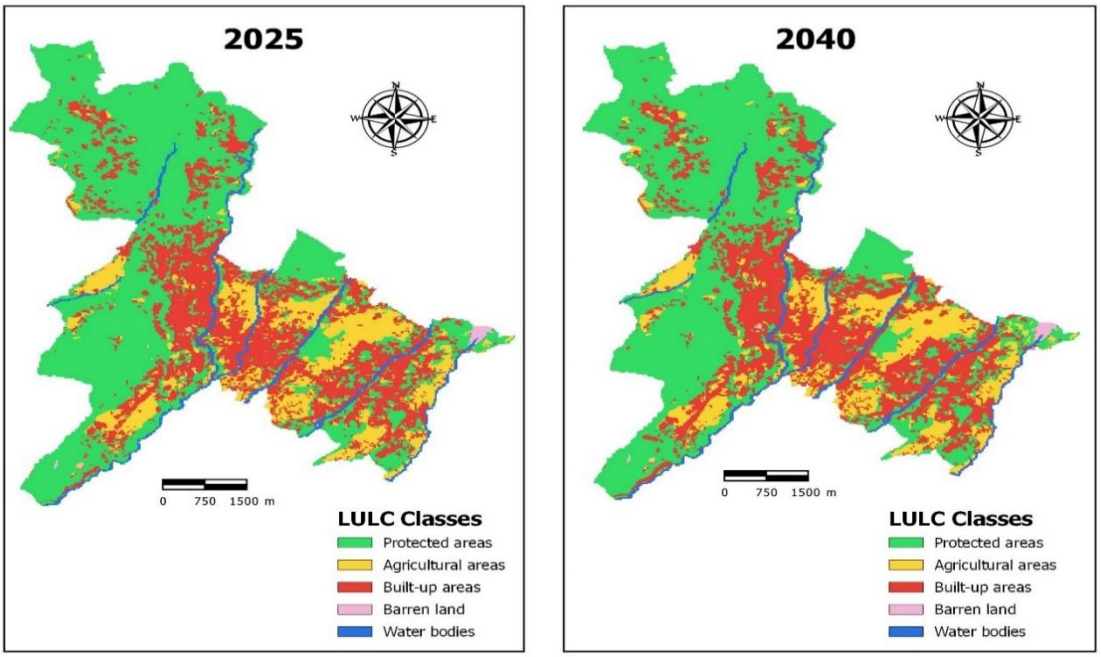

Fig. 4.10 Future LULC maps for 2025 and 2040

The LULC transitions from 2016 to 2025 and 2016 to 2040 are shown in **Table 4.19** and **Table 4.20**, respectively. The findings indicate a consistent trajectory characterized by augmentation and demand of developed areas and decrement in areas designated for conservation measures by 2025. However, the built-up is anticipated to decelerate or saturate after 2025, resulting in a lower percentage increase. This phenomenon can be attributed to the depletion of available and fertile land suitable for construction purposes.

Table 4.19 LULC transition from 2016 to 2025

LULC	2016		2025		Change (2016-2025)	
Category	Area (km^2)	%age	Area (km^2)	%age	Area (km^2)	%age
PA	29.36	69.10	23.10	54.36	-6.27	-14.75
AA	6.88	16.19	5.69	13.39	-1.19	-2.81
BA	4.41	10.38	11.99	28.22	7.58	17.84
BL	0.27	0.64	0.15	0.35	-0.12	-0.29
WB	1.57	3.69	1.57	3.69	0.00	0.00

Table 4.20 LULC transition from 2016 to 2040

LULC	2016		2040		Change (2016-2040)	
Category	Area (km^2)	%age	Area (km^2)	%age	Area (km^2)	%age
PA	29.36	69.10	22.28	52.44	-7.08	-16.66
AA	6.88	16.19	5.72	13.47	-1.16	-2.72
BA	4.41	10.38	12.78	30.07	8.37	19.69
BL	0.27	0.64	0.14	0.33	-0.13	-0.31
WB	1.57	3.69	1.57	3.69	0.00	0.00

Hilly terrains present inherent geographic and topographic limitations for construction activities, favouring mid-altitude locations with moderate slopes. However, these areas often contend with seismic hazards, complicating development endeavours. Consequently, construction efforts may inadvertently concentrate in high seismic and landslide-prone zones, posing significant risks to the safety and well-being of inhabitants. Additionally, the temporal evolution of built-up areas tends to be concentrated primarily in mid and south-eastern regions, indicating a localized pattern of urban sprawl. These regions have experienced a notable expansion in built-up areas, highlighting their ongoing significance as critical areas for future urban development.

The rapid proliferation of urban areas, driven by population growth and increased tourism, underscores the urgent need to adopt sustainable urban planning frameworks. Policymakers and urban planners must prioritize implementing effective management strategies to promote optimal land utilization, mitigate urban sprawl, and safeguard green spaces. These efforts align with the overarching objective of achieving **Sustainable Development Goal (SDG) 11**, which centres on fostering the development of sustainable cities and communities through concerted actions and policies.

The diminishing extent of Protected Areas represents a significant issue, as it jeopardizes biodiversity and ecosystem integrity. Addressing this challenge necessitates rigorous enforcement of legislative measures facilitated through collaborative engagement among environmental stakeholders and policymakers. This initiative is intricately linked to **Sustainable Development Goal (SDG) 15**, which emphasizes preserving and enhancing terrestrial ecosystems and biodiversity.

Effective land-use planning is instrumental in promoting sustainable consumption and production practices. Policymakers can facilitate sustainable resource utilization and minimize the ecological footprint of human endeavours by judiciously allocating land and mitigating encroachment on protected areas. These actions align with the aspirations of **Sustainable Development Goal (SDG) 12**, which seeks to foster responsible consumption and production patterns, thereby advancing the overarching goal of sustainable development.

The reduction in agricultural areas signals a notable shift in agrarian practices, reflecting a recent preference among residents for alternative occupations. Concurrently, the diminishing extent of protected areas underscores persistent encroachments and regulatory non-compliance challenges. Addressing the decline in agricultural land necessitates a concerted effort to promote sustainable farming methodologies and enhance agricultural productivity. This objective can be achieved by adopting innovative agrarian techniques, providing support to small-scale farmers, and ensuring universal access to food security initiatives. These initiatives are integral to advancing the objectives of **Sustainable Development Goal 2 (SDG-2)**, aimed at eradicating hunger and ensuring food security for all.

CHAPTER 5
CONCLUSIONS

5.1 Comparison of satellite data products

The methodology in the thesis touches upon an important aspect: the need to check the suitability of remote-sensing products from different sources. The interpretation of the results shows the disagreement between different satellites in classifying the areas. The study advocates that choosing proper satellite imagery is equally essential as selecting the classification algorithm, ground truth points, and ancillary data. Although many remote sensing data products from different satellites are available freely, an image of a particular date may not always be available from multiple sources. Thus, comparing the datasets from various sources will continue to be a significant challenge, especially regarding phenological effects. Further, the 1970s – 1980s data products may not necessarily be available in most of the satellite missions, which gives a clear advantage to the Landsat mission, with the added benefit of being available free of cost and at moderately good spatial resolution. However, the study advocates comparing multiple satellite data sources, if available (for a particular period), and checks whether their results are significantly different.

Further, temporal and radiometric resolution will also play an essential role in future missions. The study tries to focus on the importance of choosing a proper satellite source for thematic classification (on a micro scale) of smaller regions. It was evident that Sentinel 2 performed better based on overall accuracy and Kappa hat, and also equally suited if a researcher is interested in identifying the built-up areas only. Due to the easy availability of data products (even free) from multiple satellite sources, it is essential to check the suitability of a particular satellite data for studying a specific phenomenon.

However, further spatio-temporal studies in the research area utilized Landsat 8 OLI images since their performance was at par with that of Sentinel 2 satellite images. Furthermore, the Landsat images are adaptable in various software, like the Q-GIS and MOLUSCE plugin used for modelling and simulation of future LULC maps.

5.2 Spatio-temporal LULC transitions from 2016 to 2022

The study assessed and monitored the changes in Dharamshala city from 2016 to 2022 through remote sensing and GIS. The study revealed that the protected areas, primarily forests and agricultural areas, had decreased while the built-up areas had risen dramatically. The results are similar to those observed in other Himalayan cities in the state of Himachal Pradesh [22,164,165,166]. The significant factors contributing to changed land cover are anthropogenic and economic activities, high tourist inflow, illegal encroachments, and increasing population.

A sharp increase in built-up activities has been witnessed in this Himalayan city as it has become the hub of tourism in the state of Himachal Pradesh (HP) with increased demands for commercial complexes and recreational activities. To boost the region's macro-economic activities and promote the tourism and hospital sector, the demand for infrastructural development has risen. Around 55% increase in domestic and foreign tourist footfall has been witnessed in the state of HP from 2008 to 2022, while a rise of 168% from 2021 to 2022 as per the statistics revealed by the Economics & Statistics Department, Government of HP. Around 168 hectares of forest area were lost in HP from 2010 to 2022, equivalent to 78,800 tons of CO2 emissions per Global Forest Watch.

The unregulated tourism activity through the Himachal Pradesh Home Stay Scheme, 2008 has resulted in mushrooming of Homestays and the depletion of land resources. A 27% increase in the bed capacity registered under Himachal Tourism had been witnessed from 2017 to 2019. Further, the recent provisions in the Forest Conservation Amendment Bill, 2023, which mandate the government to utilize forest land and non-classified forest land for non-forestry purposes, will promote environmental degradation in the name of development works and eco-tourism projects. An enormous scope and opportunity lies in hydroelectric power generation and tourism-related service sectors in the Himalayan regions. Still, it should not be due to environmental degradation and ecosystem imbalance. The Amendment Bill seeks exemption on forest land recorded as a “forest” but not notified as a “forest” before 1980. The sustainable development model is the need of the hour, and specific legislative/ administrative

reforms are required to prepare an action plan for managing and conserving land resources.

The research also found that the built-up dynamic index was 23.3% in six years from 2016 to 2022. The situation could have been worse had there not been Covid-related restrictions. It revealed that areas situated above 1500 m altitude with slopes exceeding 25% necessitate meticulous monitoring due to their geographical-seismic attributes, which significantly elevate the vulnerability of built-up structures to heightened risks of loss of life and property. The increased built-up activities at high altitudes indicate possible regional encroachments, as most of these areas are covered under forests. Additionally, the escalating concentration of built-up areas close to streams is projected to severely impede aquatic ecosystems and micro-climatic conditions. Further, an action plan for regulating the built-up activities is required.

The trend of urbanization has now shifted northwards in this region. The transitioned LULC will seriously impact the region's biodiversity and bio-resources. Further, increased urbanisation activities will also affect the region's micro-climate, and the city will lose its relevance as a hill station shortly. Thus, the present study is a clarion call for urban planners and policy-makers to identify the critical areas and frame management/ intervention strategies as soon as possible so that the city can develop smartly and sustainably.

5.3 Modelling and simulation of LULC maps

The study applied a knowledge-based Learning model to create future LULC maps of the region under study. The kappa hat value of 0.77 was achieved, representing a reasonable simulation probability of the model and adequate inclusion and representation of driving factors used in the model. A total of six driving factors were utilised in the study, including socio-economic, spatial and geographical parameters. The findings indicate a projected increase in BA by 7.58 km^2 from 2016 to 2025 and a decline in PA by 6.27 km^2. The area of BA increased by 8.37 km^2, and a decline in the area of PA by 7.08 km^2 was projected from 2016 to 2040.

The swift population growth and burgeoning tourism industry had added pressure to the limited resources of this hill station and resulted in increased demand for urban spaces and commercial activities. There is an inherent need to implement strict

measures involving an efficient land management system with the knowledge based on the LC inventory created in this study. It will enable legislators, administrators, environmentalists, city-dwellers, and other stakeholders to frame management policies aligned with the sustainable development model.

5.4 Proposed Intervention Strategies

The increasing population and change in occupation can have severe implications for the city shortly. Dharmashala City recorded the highest population growth rate of 61% from 2001-2011 in all the Class –III cities (having populations from 20,000 to 50,000) of Himachal Pradesh. The ongoing and projected surge in road construction and recreational pursuits, coupled with the persistent expansion of urban areas into increasingly challenging and complex terrains, is anticipated to render the entire city susceptible to the potential hazards of landslides, earthquakes, and cloud-bursts, leading to significant risks of loss of life and property. Integrating remote sensing and Geographic Information System (GIS) makes it feasible to conduct a comprehensive geospatial evaluation of an urban area, facilitating the formulation of an actionable strategy that effectively harmonizes developmental needs with environmental conservation objectives.

The findings in this research underscore the urgency of formulating an action plan based on a sustainable development model that effectively harmonizes developmental requirements with environmental preservation imperatives. A Sustainable Model that includes various stakeholders in the decision-making process will foster a sense of ownership and encourage collaborative approaches. Engaging local communities and considering their perspectives can lead to more inclusive and equitable land-use planning, ensuring that the benefits and burdens of land-use changes are shared among all members of society. Activities such as afforestation and awareness programmes, enforcement of strict laws to check illegal encroachments, restoration and incentivizing agricultural practices as a measure to check the built-up concentration and ensuring proper drainage in the area to check peak flow conditions as a consequence of increased built-up areas and implementation of effective land use/ resource management strategies need to be implemented in the region.

The escalating expansion of built-up areas, driven by population growth and tourism, and the identification of the vulnerable regions through this research will help in taking into account factors such as infrastructure development, resource efficiency, and the integration of green spaces to foster the creation of urban environment characterized by livability, thereby enhancing the overall quality of life for the resident population. The study advocates environment conservation strategies in the region involving afforestation programs, environment protection campaigns, and identifying areas vulnerable to landslides, earthquakes, and cloudbursts.

BIBLIOGRAPHY

[1] Mehra N, Swain JB. Assessment of land use land cover change and its effects using artificial neural network - based cellular automation. J Eng Appl Sci. 2024;1–17.

[2] Lillesand, Thomas, Ralph W. Kiefer and JC. Remote Sensing and Image Interpretation. 7th Edition. Photogramm Eng Remote Sens. 2015 Aug 1;81(8):615–6.

[3] Foody GM. Status of land cover classification accuracy assessment. Remote Sens Environ. 2002;80:185–201.

[4] Martins VS, Kaleita AL, Gelder BK, da Silveira HLF, Abe CA. Exploring multiscale object-based convolutional neural network (multi-OCNN) for remote sensing image classification at high spatial resolution. ISPRS J Photogramm Remote Sens. 2020;168:56–73.

[5] Belgiu M, Drăgu L. Random forest in remote sensing: A review of applications and future directions. ISPRS J Photogramm Remote Sens. 2016;114:24–31.

[6] Rwanga SS, Ndambuki JM. Accuracy Assessment of Land Use/Land Cover Classification Using Remote Sensing and GIS. Int J Geosci. 2017;08(04):611–622.

[7] Mzava P, Nobert J, Valimba P. Land Cover Change Detection in the Urban Catchments of Dar es Salaam, Tanzania using Remote Sensing and GIS Techniques. Tanzania J Sci. 2019;45(3):315–329.

[8] Rahman MR, Shi ZH, Chongfa C. Soil erosion hazard evaluation—An integrated use of remote sensing, GIS and statistical approaches with biophysical parameters towards management strategies. Ecol Modell. 2009 Jul 17;220(13–14):1724–1734.

[9] Butt A, Shabbir R, Ahmad SS, Aziz N. Land use change mapping and analysis using Remote Sensing and GIS: A case study of Simly watershed, Islamabad, Pakistan. Egypt J Remote Sens Sp Sci. 2015 Dec 1;18(2):251–259.

[10] Jha MK, Chowdary VM. Challenges of using remote sensing and GIS in developing nations. Hydrogeol J. 2007;15(1):197–200.

[11] Singh SP, Singh V, Skutsch M. Rapid warming in the Himalayas: Ecosystem responses and development options. Clim Dev. 2010;2(3):221–232.

[12] Tiwari P, Tiwari A, Joshi B. Urban Growth in Himalaya: Understanding the Process and Options for Sustainable Development. J Urban Reg Stud Contemp India. 2018;4(2):15–27.

[13] Diksha, Kumar A. Analysing urban sprawl and land consumption patterns in major capital cities in the Himalayan region using geoinformatics. Appl Geogr. 2017;89:112–123.

[14] Kumar M, Denis DM, Singh SK, Szabó S, Suryavanshi S. Landscape metrics for assessment of land cover change and fragmentation of a heterogeneous watershed. Remote Sens Appl Soc Environ. 2018;10:224–233.

[15] Nie Y, Sheng Y, Liu Q, Liu L, Liu S, Zhang Y, et al. A regional-scale assessment of Himalayan glacial lake changes using satellite observations from 1990 to 2015. Remote Sens Environ. 2017;189:1–13.

[16] Rawat JS, Kumar M. Monitoring land use/cover change using remote sensing and GIS techniques: A case study of Hawalbagh block, district Almora, Uttarakhand, India. Egypt J Remote Sens Sp Sci. 2015;18(1):77–84.
[17] Deka J, Tripathi OP, Khan ML, Srivastava VK. Study on land-use and land-cover change dynamics in Eastern Arunachal Pradesh, N.E. India using remote sensing and GIS. Trop Ecol. 2019;60(2):199–208.
[18] Hu K, Yang X, Zhong J, Fei F, Qi J. Spatially Explicit Mapping of Heat Health Risk Utilizing Environmental and Socioeconomic Data. Environ Sci Technol. 2017;51(3):1498–1507.
[19] Dong L, Wang W, Ma M, Kong J, Veroustraete F. The change of land cover and land use and its impact factors in upriver key regions of the Yellow River. Int J Remote Sens. 2009;30(5):1251–1265.
[20] Gupta V, Ram BK, Kumar S, Sain K. A Case Study of the 12 July 2021 Bhagsunath (McLeod Ganj) Flash Flood in Dharamshala, Himachal Pradesh: A Warning Against Constricting Natural Drainage. J Geol Soc India. 2022;98(5):607–610.
[21] Sood V, Gupta S, Gusain HS, Singh S. Spatial and Quantitative Comparison of Topographically Derived Different Classification Algorithms Using AWiFS Data over Himalayas, India. J Indian Soc Remote Sens. 2018;46(12):1991–2002.
[22] Sharma S, Mukherjee M, Khare D. Urban growth and water supply system in the hill town, dharamshala, India. Proc Int Conf Archit Sci Assoc. 2019;31–40.
[23] Mishra PK, Rai A, Rai SC. Land use and land cover change detection using geospatial techniques in the Sikkim Himalaya, India. Egypt J Remote Sens Sp Sci. 2020;23(2):133–143.
[24] Weng Q. Remote sensing of impervious surfaces in the urban areas: Requirements, methods, and trends. Remote Sens Environ. 2012;117:34–49.
[25] Bagan H, Wang Q, Yang Y, Yoshifumi Yasuoka, Baod Y. Land cover classification using moderate resolution imaging spectrometer-enhanced vegetation index time-series data and self-organizing map neural network in Inner Mongolia, China. J Appl Remote Sens. 2007;1(1):013545.
[26] Falcucci A, Maiorano L, Boitani L. Changes in land-use/land-cover patterns in Italy and their implications for biodiversity conservation. Landsc Ecol. 2007;22(4):617–631.
[27] Kumar D. Monitoring and assessment of land use and land cover changes (1977 - 2010) in Kamrup district of Assam, India using remote sensing and GIS techniques. Appl Ecol Environ Res. 2017;15(3):221–239.
[28] Yu H, Joshi PK, Das KK, Chauniyal DD, Melick DR, Yang X, et al. Land use/cover change and environmental vulnerability analysis in Birahi Ganga sub-watershed of the Garhwal Himalaya, India. Trop Ecol. 2007;48(2):241–250.
[29] Onur I, Maktav D, Sari M, Kemal Sönmez N. Change detection of land cover and land use using remote sensing and GIS: A case study in Kemer, Turkey. In: International Journal of Remote Sensing. Taylor and Francis Ltd. 2009;1749–1757.

[30] Rahman A, Kumar S, Fazal S, Siddiqui MA. Assessment of Land use/land cover Change in the North-West District of Delhi Using Remote Sensing and GIS Techniques. J Indian Soc Remote Sens. 2012;40(4):689–697.
[31] Rao KS, Pant R. Land use dynamics and landscape change pattern in a typical micro watershed in the mid elevation zone of central Himalaya, India. Vol. 86, Ecosystems and Environment. 2001;86(2):113-124.
[32] Chamling M, Bera B. Spatio-temporal Patterns of Land Use/Land Cover Change in the Bhutan–Bengal Foothill Region Between 1987 and 2019: Study Towards Geospatial Applications and Policy Making. Earth Syst Environ. 2020;4(1):117–130.
[33] Chowdhury M, Hasan ME, Abdullah-Al-Mamun MM. Land use/land cover change assessment of Halda watershed using remote sensing and GIS. Egypt J Remote Sens Sp Sci. 2020;23(1):63–75.
[34] Kafy A Al, Faisal A Al, Shuvo RM, Naim MNH, Sikdar MS, Chowdhury RR, et al. Remote sensing approach to simulate the land use/land cover and seasonal land surface temperature change using machine learning algorithms in a fastest-growing megacity of Bangladesh. Remote Sens Appl Soc Environ. 2021;21:100463.
[35] Mosammam HM, Nia JT, Khani H, Teymouri A, Kazemi M. Monitoring land use change and measuring urban sprawl based on its spatial forms: The case of Qom city. Egypt J Remote Sens Sp Sci. 2017;20(1):103–116.
[36] Singh A. Review Article: Digital change detection techniques using remotely-sensed data. Int J Remote Sens. 1989;10(6):989–1003.
[37] Ahmad A, Quegan S. Analysis of maximum likelihood classification on multispectral data. Appl Math Sci. 2012;6(129–132):6425–6436.
[38] Strahler AH. The use of prior probabilities in maximum likelihood classification of remotely sensed data. Remote Sens Environ. 1980;10(2):135–163.
[39] Otukei JR, Blaschke T. Land cover change assessment using decision trees, support vector machines and maximum likelihood classification algorithms. Int J Appl Earth Obs Geoinf. 2010;12:27–31.
[40] Rimal B, Rijal S, Kunwar R. Comparing Support Vector Machines and Maximum Likelihood Classifiers for Mapping of Urbanization. J Indian Soc Remote Sens. 2020;48(1):71–79.
[41] Congalton RG. A review of assessing the accuracy of classifications of remotely sensed data. Remote Sens Environ. 1991;37(1):35–46.
[42] Olofsson P, Foody GM, Herold M, Stehman S V., Woodcock CE, Wulder MA. Good practices for estimating area and assessing accuracy of land change. Vol. 148, Remote Sensing of Environment. Elsevier Inc.; 2014. p. 42–57.
[43] Saha AK, Arora MK, Csaplovics E, Gupta RP. Land cover classification using IRS liss III image and DEM in a rugged terrain: A case study in Himalayas. Geocarto Int. 2005;20(2):33–40.
[44] Liping C, Yujun S, Saeed S. Monitoring and predicting land use and land cover changes using remote sensing and GIS techniques—A case study of a hilly area, Jiangle, China. PLoS One. 2018;1:13(7).

[45] Sharma S, Mahajan AK. Comparative evaluation of GIS-based landslide susceptibility mapping using statistical and heuristic approach for Dharamshala region of Kangra Valley, India. Geoenvironmental Disasters. 2018;5(1):1–16.
[46] Krishna Bahadur KC. Improving landsat and irs image classification: Evaluation of unsupervised and supervised classification through band ratios and dem in a mountainous landscape in Nepal. Remote Sens. 2009;1(4):1257–1272.
[47] Thakkar AK, Desai VR, Patel A, Potdar MB. Post-classification corrections in improving the classification of Land Use/Land Cover of arid region using RS and GIS: The case of Arjuni watershed, Gujarat, India. Egypt J Remote Sens Sp Sci. 2017;20(1):79–89.
[48] Das S, Angadi DP. Land use land cover change detection and monitoring of urban growth using remote sensing and GIS techniques: a micro-level study. GeoJournal. 2022;87(3):2101–2123.
[49] Dwivedi RS, Sreenivas K, Ramana K V. Land-use/land-cover change analysis in part of Ethiopia using Landsat Thematic Mapper data. Int J Remote Sens. 2005;26(7):1285–1287.
[50] Shalaby A, Tateishi R. Remote sensing and GIS for mapping and monitoring land cover and land-use changes in the Northwestern coastal zone of Egypt. Appl Geogr. 2007;27(1):28–41.
[51] Debnath J, Das N, Ahmed I, Bhowmik M. Channel migration and its impact on land use/land cover using RS and GIS: A study on Khowai River of Tripura, North-East India. Egypt J Remote Sens Sp Sci. 2017;20(2):197–210.
[52] Meshesha TW, Tripathi SK, Khare D. Analyses of land use and land cover change dynamics using GIS and remote sensing during 1984 and 2015 in the Beressa Watershed Northern Central Highland of Ethiopia. Model Earth Syst Environ. 2016;2(4).
[53] Gupta M, Srivastava PK. Integrating GIS and remote sensing for identification of groundwater potential zones in the hilly terrain of Pavagarh, Gujarat, India. Water Int. 2010;35(2):233–245.
[54] Weidinger JT. Predesign, failure and displacement mechanisms of large rockslides in the Annapurna Himalayas, Nepal. Eng Geol. 2006;83(1–3):201–216.
[55] Srivastava P, Tripathi JK, Islam R, Jaiswal MK. Fashion and phases of late Pleistocene aggradation and incision in the Alaknanda River Valley , western Himalaya , India. 2008;70:68–80.
[56] Passy P, Théry S. The Use of SAGA GIS Modules in QGIS. QGIS Generic Tools. 2018;1:107–49.
[57] Pella H, Ose K. Network Analysis and Routing with QGIS. QGIS Appl Water Risks. 2018;4:105–44.
[58] Strahler A. Quantitative Analysis of Watershed Geomorphology, Transactions of the American Geophysical Union. Trans Am Geophys Union. 1957;38(6):913–20.
[59] Chopra R, Dhiman RD, Sharma PK. Morphometric analysis of sub-watersheds in Gurdaspur district, Punjab using remote sensing and GIS techniques. J Indian Soc Remote Sens. 2005;33(4):531–539.

[60] Narendra K, Nageswara Rao K. Morphometry of the Meghadrigedda watershed, Visakhapatnam district, Andhra Pradesh using GIS and resourcesat data. J Indian Soc Remote Sens. 2006;34(2):101–110.
[61] Magesh NS, Chandrasekar N. GIS model-based morphometric evaluation of Tamiraparani subbasin, Tirunelveli district, Tamil Nadu, India. Arab J Geosci. 2014;7(1):131–141.
[62] Mehra N, Swain JB. Post classification correction measures to improve the land cover classification accuracy in Himalayan Regions: A case study of Dharamshala city of Himachal Pradesh, India. In 2024. p. 030012.
[63] Huete AR. Vegetation Indices, Remote Sensing and Forest Monitoring. Geogr Compass. 2012;6(9):513–532.
[64] Xue J, Su B. Significant remote sensing vegetation indices: A review of developments and applications. J Sensors. 2017;2017(1):1353691.
[65] Mehra N, Swain JB. Use of enhanced vegetation index (EVI) as a land cover classification tool and its suitability in urban development studies. AIP Conf Proc. 2023;2852(1).
[66] Xu H. A new index for delineating built-up land features in satellite imagery. Int J Remote Sens. 2008;29(14):4269–4276.
[67] Zha Y, Gao J, Ni S. Use of normalized difference built-up index in automatically mapping urban areas from TM imagery. Int J Remote Sens. 2003;24(3):583–594.
[68] Tarboton DG. A new method for the determination of flow directions and upslope areas in grid digital elevation models. Water resources research. 1997;33(2):309-319.
[69] Gleyzer A, Denisyuk M, Rimmer A, Salingar Y. A fast recursive GIS algorithm for computing strahler stream order in braided and nonbraided networks. J Am Water Resour Assoc. 2004;40(4):937–946.
[70] Xu H. Modification of normalised difference water index (NDWI) to enhance open water features in remotely sensed imagery. Int J Remote Sens. 2006;27(14):3025–3033.
[71] Gaigbe-Togbe V, Bassarsky L, Gu D, Spoorenberg T, Zeifman L. World Population Prospects 2022;1–54 p.
[72] Jat MK, Garg PK, Khare D. Monitoring and modelling of urban sprawl using remote sensing and GIS techniques. Int J Appl Earth Obs Geoinf. 2008;10(1):26–43.
[73] Mondal I, Thakur S, Ghosh P, De TK, Bandyopadhyay J. Land use/land cover modeling of Sagar Island, India using remote sensing and GIS techniques. In: Advances in Intelligent Systems and Computing. Springer Verlag; 2019. p. 771–785.
[74] Mushtaq F, Pandey AC. Assessment of land use/land cover dynamics vis-à-vis hydrometeorological variability in Wular Lake environs Kashmir Valley, India using multitemporal satellite data. Arab J Geosci. 2014;7(11):4707–4715.
[75] Fazal S. Urban expansion and loss of agricultural land - a GIS based study of Saharanpur City, India. Environ Urban. 2000;12(2):133–149.

[76] Aithal BH, Ramachandra T V. Visualization of Urban Growth Pattern in Chennai Using Geoinformatics and Spatial Metrics. J Indian Soc Remote Sens. 2016;44(4):617–633.
[77] Ghosh S, Sen KK, Rana U, Rao KS, Saxena KG. Application of GIS for Land-Use/Land-Cover Change Analysis in a Mountainous Terrain. Vol. 24, Journal of the Indian Society of Remote Sensing. 1996;24:193-202.
[78] Bisht BS, Kothyari BP. Land-Cover change analysis of garur Ganga watershed using GIS/Remote Sensing technique. J Indian Soc Remote Sens. 2001 Sep;29(3):137–41.
[79] Hegazy IR, Kaloop MR. Monitoring urban growth and land use change detection with GIS and remote sensing techniques in Daqahlia governorate Egypt. Int J Sustain Built Environ. 2015;4(1):117–124.
[80] Berberoglu S, Akin A. Assessing different remote sensing techniques to detect land use/cover changes in the eastern Mediterranean. Int J Appl Earth Obs Geoinf. 2009;11(1):46–53.
[81] Zhao S, Liu S, Zhou D. Prevalent vegetation growth enhancement in urban environment. Proc Natl Acad Sci U S A. 2016;113(22):6313–6318.
[82] Muhammad R, Zhang W, Abbas Z, Guo F, Gwiazdzinski L. Spatiotemporal Change Analysis and Prediction of Future Land Use and Land Cover Changes Using QGIS MOLUSCE Plugin and Remote Sensing Big Data: A Case Study of Linyi, China. Land. 2022;11(3).
[83] Mathew A, Chaudhary R, Gupta N. Study of Urban heat Island Effect on Ahmedabad City and Its Relationship with Urbanization and Vegetation Parameters. Int J Comput Math Sci. 2015;4:126–135.
[84] Wang SW, Gebru BM, Lamchin M, Kayastha RB, Lee WK. Land use and land cover change detection and prediction in the kathmandu district of nepal using remote sensing and GIS. Sustain. 2020;12(9).
[85] Gharaibeh A, Shaamala A, Obeidat R, Al-Kofahi S. Improving land-use change modeling by integrating ANN with Cellular Automata-Markov Chain model. Heliyon. 2020;6(9):e05092.
[86] Bhattacharya RK, Das Chatterjee N, Das K. Land use and Land Cover change and its resultant erosion susceptible level: an appraisal using RUSLE and Logistic Regression in a tropical plateau basin of West Bengal, India. Vol. 23, Environment, Development and Sustainability. Springer Netherlands; 2021. 1411–1446 p.
[87] Nagendra H, Munroe DK, Southworth J. From pattern to process: Landscape fragmentation and the analysis of land use/land cover change. Vol. 101, Agriculture, Ecosystems and Environment. Elsevier; 2004. p. 111–115.
[88] Buğday E, Erkan Buğday S. Modeling and simulating land use/cover change using artificial neural network from remotely sensing data. Cerne. 2019;25(2):246–254.
[89] Aburas MM, Ho YM, Ramli MF, Ash'aari ZH. The simulation and prediction of spatio-temporal urban growth trends using cellular automata models: A review. Int J Appl Earth Obs Geoinf. 2016;52:380–389.

[90] Buğday E, Erkan Buğday S. Modeling and simulating land use/cover change using artificial neural network from remotely sensing data. Cerne. 2019;25(2):246–254.
[91] Al-doski J, Mansor SB, Zulhaidi H, Shafri M. Image Classification in Remote Sensing. 2013;3(10):141–148.
[92] Bruzzone L, Serpico SB. Classification of imbalanced remote-sensing data by neural networks. Pattern Recognit Lett. 1997;18(11–13):1323–1328.
[93] Wolfarm S. Cellular automata: a model of complexity. Nature. 1984;31:419–424.
[94] Batty M, Xie Y. Research article modelling inside gis: Part 1. model structures, exploratory spatial data analysis and aggregation. Int J Geogr Inf Syst. 1994;8(3):291–307.
[95] Batty M, Xie Y, Sun Z. Modeling urban dynamics through GIS-based cellular automata. Comput Environ Urban Syst. 1999 May 1;23(3):205–233.
[96] Santé I, García AM, Miranda D, Crecente R. Cellular automata models for the simulation of real-world urban processes: A review and analysis. Landsc Urban Plan. 2010;96(2):108–122.
[97] Sarkar P. A brief history of cellular automata. ACM Comput Surv. 2000;32(1):80–107.
[98] Leao S, Bishop I, Evans D. Simulating Urban Growth in a Developing Nation's Region Using a Cellular Automata-Based Model. J Urban Plan Dev. 2004;130(3):145–158.
[99] Lagarias A. Urban sprawl simulation linking macro-scale processes to micro-dynamics through cellular automata, an application in Thessaloniki, Greece. Appl Geogr. 2012 May 1;34:146–160.
[100] Kamaraj M, Rangarajan S. Predicting the future land use and land cover changes for Bhavani basin, Tamil Nadu, India, using QGIS MOLUSCE plugin. Environ Sci Pollut Res. 2022;(0123456789).
[101] Atef I, Ahmed W, Abdel-Maguid RH. Future land use land cover changes in El-Fayoum governorate: a simulation study using satellite data and CA-Markov model. Stoch Environ Res Risk Assess. 2023; 38(2):651-664.
[102] Asori M, Adu P. Modeling the impact of the future state of land use land cover change patterns on land surface temperatures beyond the frontiers of greater Kumasi: A coupled cellular automaton (CA) and Markov chains approaches. Remote Sens Appl Soc Environ. 2023;29:100908.
[103] Saputra MH, Lee HS. Prediction of land use and land cover changes for North Sumatra, Indonesia, using an artificial-neural-network-based cellular automaton. Sustain. 2019;11(11):1–16.
[104] Gupta N, Vaya N, Mishra B. Artificial Neural Network. Eastern pharmacist. 1997;40(475):39-41.
[105] Wu X, Liu X, Zhang D, Zhang J, He J, Xu X. Simulating mixed land-use change under multi- label concept by integrating a convolutional neural network and cellular automata : a case study of. GIScience Remote Sens. 2022;59(1):609–632.

[106] Wagh AKKVM, Umrikar AAMBN. Prediction of water quality index using artificial neural network and multiple linear regression modelling approach in Shivganga River basin , India. Model Earth Syst Environ. 2019;5:951-962.
[107] Shafizadeh-moghadam H, Tayyebi A, Helbich M. Transition index maps for urban growth simulation : application of artificial neural networks , weight of evidence and fuzzy multi-criteria evaluation. 2017;189:1-4.
[108] Tayyebi A, Pijanowski BC. International Journal of Applied Earth Observation and Geoinformation Modeling multiple land use changes using ANN , CART and MARS : Comparing tradeoffs in goodness of fit and explanatory power of data mining tools. Int J Appl Earth Obs Geoinf. 2014;28:102–116.
[109] Atkinson PM, Tatnall ARL. Introduction neural networks in remote sensing. Int J Remote Sens. 1997;18(4):699–709.
[110] Hakim AMY, Baja S, Rampisela DA, Arif S. Spatial dynamic prediction of landuse / landcover change (Case study: Tamalanrea sub-district, makassar city). IOP Conf Ser Earth Environ Sci. 2019;280(1).
[111] Bai Y, Feng M, Jiang H, Wang J, Zhu Y, Liu Y. Assessing consistency of five global land cover data sets in China. Remote Sens. 2014;6(9):8739–8759.
[112] Grekousis G, Mountrakis G, Kavouras M. An overview of 21 global and 43 regional land-cover mapping products. Int J Remote Sens. 2015;36(21):5309–5335.
[113] Fritz S, See L. Comparison of land cover maps using fuzzy agreement. Int J Geogr Inf Sci. 2005;19(7):787–807.
[114] Hansen MC, Reed B. A comparison of the IGBP DISCover and university of maryland 1 km global land cover products. Int J Remote Sens. 2000;21(6–7):1365–1373.
[115] Cohen WB, Maiersperger TK, Yang Z, Gower ST, Turner DP, Ritts WD, et al. Comparisons of land cover and LAI estimates derived from ETM+ and MODIS for four sites in North America: A quality assessment of 2000/2001 provisional MODIS products. Remote Sens Environ. 2003;88(3):233–255.
[116] Kumar B, Patra KC, Lakshmi V. Error in Digital Network and Basin Area Delineation using D8 Method: A Case Study in a Sub-basin of the Ganga. Vol. 89, J Geol Soc. of India. 2017;89, pp.65-70.
[117] Verburg PH, Neumann K, Nol L. Challenges in using land use and land cover data for global change studies. Glob Chang Biol. 2011;17(2):974–989.
[118] Tchuenté ATK, Roujean JL, de Jong SM. Comparison and relative quality assessment of the GLC2000, GLOBCOVER, MODIS and ECOCLIMAP land cover data sets at the African continental scale. Int J Appl Earth Obs Geoinf. 2011;13(2):207–219.
[119] Civco DL, Hurd JD, Wilson EH, Song M, Zhang Z. 2002 ASPRS-ACSM Annual Conference and FIG XXII Congress A Comparison Of Land Use And Land Cover Change Detection Methods. InASPRS-ACSM Annual Conference. 2002;21:18-33.
[120] Gong Jianyaa, Sui Haiganga MG and ZQ. A review of multi-temporal remote sensing data change detection algorithms A Review Of Multi-Temporal Remote Sensing Data Change Detection. 2014;757–762.

[121] Lu D, Mausel P, Brondízio E, Moran E. Change detection techniques. Int J Remote Sens. 2004;25(12):2365–2401.
[122] Mas JF. Monitoring land-cover changes: A comparison of change detection techniques. Int J Remote Sens. 1999;20(1):139–152.
[123] Tewkesbury AP, Comber AJ, Tate NJ, Lamb A, Fisher PF. A critical synthesis of remotely sensed optical image change detection techniques. Remote Sens Environ. 2015;160:1–14.
[124] O'Callaghan JF, Mark DM. The extraction of drainage networks from digital elevation data. Computer vision, graphics, and image processing. 1984;28(3):323-344.
[125] Du Y, Teillet PM, Cihlar J. Radiometric normalization of multitemporal high-resolution satellite images with quality control for land cover change detection. 2002;82(1):123-134.
[126] Zaz SN, Romshoo SA. Assessing the geoindicators of land degradation in the Kashmir Himalayan region, India. Nat Hazards. 2012;64(2):1219–1245.
[127] Viana CM, Oliveira S, Oliveira SC, Rocha J. Land Use/Land Cover Change Detection and Urban Sprawl Analysis. Spatial Modeling in GIS and R for Earth and Environmental Sciences. Elsevier Inc.; 2019. 621–651 p.
[128] Nazarnia N, Harding C, Jaeger JAG. How suitable is entropy as a measure of urban sprawl. Landsc Urban Plan. 2019;184:32–43.
[129] Dhanaraj K, Angadi DP. Land use land cover mapping and monitoring urban growth using remote sensing and GIS techniques in Mangaluru, India. GeoJournal. 2022;87(2):1133–1159.
[130] Thanh Son N, Thi Thu Trang N, Bui XT, Thi Da C. Remote sensing and GIS for urbanization and flood risk assessment in Phnom Penh, Cambodia. Geocarto Int. 2022;37(22):6625–6642.
[131] Dimyati M, Mizuno K, Kobayashi S, Kitamura T. An analysis of land use/cover change using the combination of MSS landsat and land use map—a case study in yogyakarta, indonesia. Int J Remote Sens. 1996;17(5):931–944.
[132] Alphan H. Land-use change and urbanization of Adana, Turkey. L Degrad Dev. 2003 Nov;14(6):575–586.
[133] Li A, Wang A, Liang S, Zhou W. Eco-environmental vulnerability evaluation in mountainous region using remote sensing and GIS - A case study in the upper reaches of Minjiang River, China. Ecol Modell. 2006 Feb 15;192(1–2):175–87.
[134] Xiao J, Shen Y, Ge J, Tateishi R, Tang C, Liang Y, et al. Evaluating urban expansion and land use change in Shijiazhuang, China, by using GIS and remote sensing. Landsc Urban Plan. 2006 Feb 28;75(1–2):69–80.
[135] Sharma L, Pandey PC, Nathawat MS. Assessment of land consumption rate with urban dynamics change using geospatial techniques. J Land Use Sci. 2012;7(2):135–148.
[136] El-Asmar HM, Hereher ME, El Kafrawy SB. Surface area change detection of the Burullus Lagoon, North of the Nile Delta, Egypt, using water indices: A remote sensing approach. Egypt J Remote Sens Sp Sci. 2013;16(1):119–123.
[137] Hassan Z, Shabbir R, Ahmad SS, Malik AH, Aziz N, Butt A, et al. Dynamics of land use and land cover change (LULCC) using geospatial techniques: a case study of Islamabad Pakistan. Springerplus. 2016;5(1).

[138] Negi V, Irfan M. Land Use/Cover Mapping and Change Detection Using Remote Sensing Techniques: A Case of Upper Kullu Valley, Himachal Pradesh. Current World Environment. 2022;17(2):417-26.
[139] Chowdhury MS. Comparison of accuracy and reliability of random forest, support vector machine, artificial neural network and maximum likelihood method in land use/cover classification of urban setting. Environmental Challenges. 2024 Jan 1;14:100800.
[140] Kumar A, Uniyal SK, Lal B. Stratification of forest density and its validation by NDVI analysis in a part of western Himalaya, India using Remote sensing and GIS techniques. Int J Remote Sens. 2007;28(11):2485–2495.
[141] Shi, Qi, Liu, Niu, Zhang. Urban Land Use and Land Cover Classification Using Multisource Remote Sensing Images and Social Media Data. Remote Sens. 2019;11(22):2719.
[142] Xu Y, Du B, Zhang L, Cerra D, Pato M, Carmona E, et al. Advanced multi-sensor optical remote sensing for urban land use and land cover classification: Outcome of the 2018 ieee grss data fusion contest. IEEE J Sel Top Appl Earth Obs Remote Sens. 2019;12(6):1709–1724.
[143] Pech-May F, Aquino-Santos R, Rios-Toledo G, Posadas-Durán JPF. Mapping of Land Cover with Optical Images, Supervised Algorithms, and Google Earth Engine. Sensors. 2022;22(13):1–19.
[144] Kumar S, Singh V, Saroha J. Interpretation of land use/land cover dynamics with the application of geospatial techniques in sarbari khad watershed of Himachal Pradesh, India. GeoJournal. 2023 Jun;88(3):2623-33.
[145] Li X, Yeh AGO. Zoning land for agricultural protection by the integration of remote sensing, GIS, and cellular automata. Photogramm Eng Remote Sensing. 2001;67(4):471–477.
[146] Myint SW, Wang L. Multicriteria decision approach for land use land cover change using Markov chain analysis and a cellular automata approach. Can J Remote Sens. 2006;32(6):390–404.
[147] Thota LS, Changalasetty SB. Optimum Learning Rate for Classification Problem With Mlp in Data Mining. Int J Adv Eng Technol. 2013;6(1):35–44.
[148] Deep S, Saklani A. Urban sprawl modeling using cellular automata. Egypt J Remote Sens Sp Sci. 2014;17(2):179–187.
[149] Mohammady S, Delavar MR, Pahlavani P. Urban growth modeling using an Artificial Neural Network a case study of Sanandaj city, Iran. Int Arch Photogramm Remote Sens Spat Inf Sci - ISPRS Arch. 2014;40(2W3):203–208.
[150] Das S, Sarkar R. Predicting the land use and land cover change using Markov model: A catchment level analysis of the Bhagirathi-Hugli River. Spat Inf Res. 2019;27(4):439–452.
[151] Ramachandran RM, Roy PS, Chakravarthi V, Joshi PK, Sanjay J. Land use and climate change impacts on distribution of plant species of conservation value in Eastern Ghats, India: a simulation study. Environ Monit Assess. 2020;192(2).
[152] Tariq A, Shu H. CA-Markov chain analysis of seasonal land surface temperature and land use landcover change using optical multi-temporal satellite data of Faisalabad, Pakistan. Remote Sens. 2020;12(20):1–23.

[153] Phinzi K, Ngetar NS, Pham QB, Chakilu GG, Szabó S. Understanding the role of training sample size in the uncertainty of high-resolution LULC mapping using random forest. Earth Sci Informatics. 2023;16(4):3667–3677.
[154] Jain M. Future land use and land cover simulations with cellular automata-based artificial neural network: A case study over Delhi megacity (India). Heliyon. 2024 Jul 30;10(14).
[155] Weng Q, Fu P. Modeling annual parameters of clear-sky land surface temperature variations and evaluating the impact of cloud cover using time series of Landsat TIR data. Remote Sens Environ. 2014 Jan 1;140:267–278.
[156] Lu GY, Wong DW. An adaptive inverse-distance weighting spatial interpolation technique. Comput Geosci. 2008 Sep 1;34(9):1044–1055.
[157] Gong P, Wang J, Yu L, Zhao Y, Zhao Y, Liang L, et al. Finer resolution observation and monitoring of global land cover: First mapping results with Landsat TM and ETM+ data. Int J Remote Sens. 2013;34(7):2607–54.
[158] Arora MK, Mathur S. Multi-source classification using artificial neural network in a rugged terrain. Geocarto Int. 2001;16(3):37–44.
[159] Sisodia PS, Tiwari V, Kumar A. Analysis of Supervised Maximum Likelihood Classification for remote sensing image. Int Conf Recent Adv Innov Eng ICRAIE 2014. 2014;9–12.
[160] Deng Z, Zhang X, Li D, Pan G. Simulation of land use/land cover change and its effects on the hydrological characteristics of the upper reaches of the Hanjiang Basin. Environ Earth Sci. 2015;73(3):1119–1132.
[161] Yeh AGO, Li X. Sustainable land development model for rapid growth areas using GIS. Int J Geogr Inf Sci. 1998;12(2):169–189.
[162] Chettry V, Surawar M. Delineating Urban Growth Boundary Using Remote sensing, ANN-MLP and CA model: A Case Study of Thiruvananthapuram Urban Agglomeration, India. J Indian Soc Remote Sens. 2021;49(10):2437–2450.
[163] Bozkaya AG, Balcik FB, Goksel C, Esbah H. Forecasting land-cover growth using remotely sensed data: a case study of the Igneada protection area in Turkey. Environ Monit Assess. 2015;187(3).
[164] Tong X, Feng Y. A review of assessment methods for cellular automata models of land-use change and urban growth. Int J Geogr Inf Sci. 2020;34(5):866–898.
[165] Singh RB, Hietala R eds. Livelihood Security in Northwestern Himalaya: Case Studies from Changing Socio-economic Environments in Himachal Pradesh, India. Advances in Geographical and Environmental Sciences. New York and Heidelberg: Springer. 2014. viii, 258
[166] Singh U, Upadhyay SP, Jha I. The co-production of space in a tourist city: A case of Dharamshala. Cities. 2022;131:103998.

LIST OF PUBLICATIONS

[1] Mehra, N., & Swain, J. B. (2024). Assessment of land use land cover change and its effects using artificial neural network-based cellular automation. Journal of Engineering and Applied Science, 71(1), 70. https://doi.org/10.1186/s44147-024-00402-0

[2] Mehra, N., & Swain, J. B. (2024). Suitability of Satellite Data for Urbanization Study: A Comparative Analysis. Journal of The Institution of Engineers (India): Series A, 105(4), 865-874. https://doi.org/10.1007/s40030-024-00832-2

[3] Mehra, N., & Swain, J. B. (2025). GIS and remote sensing based analysis for monitoring urban growth dynamics in Western Himalayan city of Dharamshala, India. Urban Lifeline, 3(1), 4. https://doi.org/10.1007/s44285-024-00033-0

LIST OF CONFERENCES

[1] Mehra, N., & Swain, J. B. (2023, August). Use of enhanced vegetation index (EVI) as a land cover classification tool and its suitability in urban development studies. In AIP Conference Proceedings (Vol. 2852, No. 1). AIP Publishing. https://doi.org/10.1063/5.0164422

[2] Mehra, N., & Swain, J. B. (2024, January). Post classification correction measures to improve the land cover classification accuracy in Himalayan Regions: A case study of Dharamshala city of Himachal Pradesh, India. In AIP Conference Proceedings (Vol. 3010, No. 1). AIP Publishing. https://doi.org/10.1063/5.0193278

[3] Mehra, N., & Swain, J. B. (2024, April). Geospatial Assessment Of Urban Sprawl Using Remote Sensing And GIS: A Case Study of Western Himalayan City of Dharmashala, Himachal Pradesh, India. In IOP Conference Series: Earth and Environmental Science (Vol. 1327, No. 1, p. 012031). IOP Publishing. 10.1088/1755-1315/1327/1/012031